Geothermal Resources in Southern Thailand: Integrated Geoscientific Investigations and Assessments

Wipada Ngansom

A Thesis Submitted in Fulfillment of the Requirements for the Degree of Doctor of Philosophy in Geophysics

Prince of Songkla University

2018

Geothermal Resources in Southern Thailand: Integrated Geoscientific Investigations and Assessments

Wipada Ngansom

A Thesis Submitted in Fulfillment of the Requirements for the Degree of Doctor of Philosophy in Geophysics

Prince of Songkla University

2018

Thesis Title	Geothermal Resources in Southern Thailand: Integrated Geoscientific Investigations and Assessments
Author	Miss Wipada Ngansom
Major Program	Geophysics

Major Advisor

……
(Asst. Prof. Dr. Helmut Dürrast)

Examining Committee:

……Chairperson
(Prof. Dr. Sheng-Rong Song)

…….Committee
(Assoc. Prof. Dr. Yutthana Tirawanichakul)

…….Committee
(Asst. Prof. Dr. Nararak Leesakul)

…….Committee
(Asst. Prof. Dr. Helmut Dürrast)

…….Committee
(Dr. Aranya Fuangswasdi)

The Graduate School, Prince of Songkla University, has approved this thesis as fulfillment of the requirements for the Doctor of Philosophy Degree in Geophysics

…….....
(Prof. Dr. Damrongsak Faroongsarng)
Dean of Graduate School

This is to certify that the work here submitted is the result of the candidate's own investigations. Due acknowledgement has been made of any assistance received.

.....Signature
(Asst. Prof. Dr. Helmut Dürrast)
Major Advisor

.....Signature
(Miss Wipada Ngansom)
Candidate

I hereby certify that this work has not been accepted in substance for any degree, and is not being currently submitted in candidature for any degree.

.....Signature

(Miss Wipada Ngansom)

Candidate

ชื่อวิทยานิพนธ์ แหล่งพลังงานใต้พิภพบริเวณภาคใต้ของประเทศไทย: การบูรณาการสำรวจและการประเมินศักยภาพแหล่งทรัพยากร
ผู้เขียน นางสาววิภาดา งานสม
สาขาวิชา ธรณีฟิสิกส์
ปีการศึกษา 2561

บทคัดย่อ

การใช้ประโยชน์แหล่งพลังงานความร้อนใต้พิภพด้านพลังงานทดแทนมีแนวโน้มสูงขึ้นช่วงทศวรรษที่ผ่านมา สืบเนื่องจากผลกระทบด้านการเปลี่ยนแปลงสภาพภูมิอากาศโลก สำหรับบริเวณภาคใต้ของประไทย พบแหล่งน้ำพุร้อนธรรมชาติ มากกว่า 30 แห่ง อุณหภูมิพื้นผิวระหว่าง 40 ถึง 80°C โดยผลการประเมินศักยภาพเบื้องต้น พบว่า แหล่งน้ำพุร้อนธรรมชาติจำนวน 7 แหล่ง มีอุณหภูมิพื้นผิวตั้งแต่ 60°C และอุณหภูมิของแหล่งกักเก็บตั้งแต่ 100°C ขึ้นไป ซึ่งนำไปสู่การศึกษาขั้นรายละเอียดโดยอาศัยคุณสมบัติด้านปัจจัยเชิงบวก ประกอบ ปัจจัยด้านสถานที่ ข้อมูลการศึกษา ศักยภาพของแหล่งกักเก็บพลังงานความร้อนใต้พิภพ และปัจจัยด้านการตลาด พบว่า แหล่งน้ำพุร้อนจังหวัดระนอง (RN1) และแหล่งน้ำพุร้อนจังหวัดพังงา (PG1) มีศักยภาพเพียงพอต่อการส่งเสริมด้านการผลิตกระแสไฟฟ้าได้ในอนาคต โดยผลการศึกษาเชิงลึกของโครงสร้างทางธรณีวิทยาและคุณสมบัติของแหล่งกักเก็บความร้อนใต้พิภพของแหล่งน้ำพุร้อนจังหวัดพังงา (PG1) พบว่า แหล่งกำเนิดความร้อนของระบบน่าจะได้รับอิทธิพลจากกระบวนการแปรสัณฐานของรอยเลื่อนระดับลึก นอกจากนี้ ได้ดำเนินการศึกษาและสำรวจแหล่งน้ำพุร้อนเค็มคลองท่อม (KB4) จังหวัดกระบี่ พบว่า เกิดจากการผสมผสานระหว่างการรุกล้ำของน้ำทะเลกับแหล่งกักเก็บน้ำร้อนธรรมชาติระดับตื้น ส่งผลให้แหล่งน้ำพุร้อนแห่งนี้มีรสเค็ม ทั้งนี้ผลการบูรณาการองค์ความรู้ด้านธรณีวิทยา การสำรวจธรณีฟิสิกส์ และการวิเคราะห์ทางธรณีเคมี สามารถอนุมานได้ว่ามวลน้ำร้อนจากแหล่งกำเนิดระดับลึก เคลื่อนตัวผ่านรอยเลื่อนภายในพื้นที่เข้าสู่ชั้นน้ำบาดาลท้องถิ่น ซึ่งถูกรุกล้ำด้วยน้ำทะเลระดับตื้น ก่อนเคลื่อนตัวสู่ผิวโลก

Thesis Title	Geothermal Resources in Southern Thailand: Integrated Geoscientific Investigations and Assessments
Author	Miss Wipada Ngansom
Major Program	Geophysics
Academic Year	2018

ABSTRACT

Utilization of geothermal energy resources has increased over the last decades due to climate change concerns. Southern Thailand is hosts 30 hot major springs with the surface discharge temperatures varying between 40 and 80 °C. From all, seven were selected in the first stage using a 60 °C surface discharge temperature and 100°C reservoir temperature of silica geothermometer cutoff value. In a second stage a quantitative potential assessment applying positive attitude factors technique was applied using numerical scores. A final ranking shows that two hot springs sites, in RN1 hot spring of Ranong geothermal system and PG1 hot spring of PhangNga Province, have a good potential for further developed. For the PG1 site was possibility of the origin of the hot spring is derived from deep circulation and which is controlled by faults that are associated either with the igneous bodies. A regional forced convective-circulation model for geothermal area is suggested, reflecting deep structural controls of the fluid pathways in the area, which has limited the degree of mixing. On the other hand, Saline Hot Spring Khlong Thom (KB4) of Krabi geothermal system is an active hot spring site, making it a real saline hot spring, in comparison to hyper saline hot spring water, which can be found worldwide often. It was found that the salinity of the hot spring water is from saline groundwater intrusion into the shallow to intermediate deep aquifers. Hot water is coming from the depth via open faults and fractures and geochemical data suggest a possible recharge of the geothermal system by meteoric water. Mixing of the hot water and the brackish water is considered in the shallow subsurface, acting also as a geothermal reservoir. Shallow, mainly vertical faults separating this reservoir in small compartments thus making groundwater flow very localized.

ACKNOWLEDGEMENTS

The thesis project was partly supported by a Thesis Grant for Doctoral Degree Student (FY2016) for W.N. from the National Research Council of Thailand and the PSU-Ph.D. Scholarship-2014.

The completion of a thesis project is rarely the result of an individual effort, which the project was completed through the assistance and support of many.

First, my deepest gratitude goes to Asst. Prof. Dr. Helmut Dürrast, my adviser for his supervision and efforts for steering me towards the right direction during this research until this thesis project was completed.

Thanks are also due to Prof. Dr. Sheng-Rong Song, Assoc. Prof. Dr. Yutthana Tirawanichakul, Asst. Prof. Dr. Nararak Leesakul and Dr. Aranya Fuangswasdi for their committees and assistance in reviewing this thesis.

During the field work, many assistants contributed time and effort, many thanks are due them. I am especially indebted to Ms. Maytipa Phalakarn, Mr. Kraipat Petrit, Mr. Kritsakorn Pothaworn and Ms. Jinjutar Saisakares for their countless volunteer hours in the field.

And last, but not least, I wish to express my gratitude to my family, without whose support and understanding this thesis project would not have been possible.

Wipada Ngansom

CONTENTS

CONTENTS (CONTINUED)

CONTENTS (CONTINUED)

LIST OF TABLES

LIST OF TABLES (CONTINUED)

LIST OF FIGURES

LIST OF FIGURES (CONTINUED)

LIST OF FIGURES (CONTINUED)

LIST OF FIGURES (CONTINUED)

LIST OF FIGURES (CONTINUED)

LIST OF FIGURES (CONTINUED)

LIST OF FIGURES (CONTINUED)

CHAPTER 1
INTRODUCTION

1.1 Background and rationale

At present, geothermal energy is the firm position that part of the renewable energy mix, which is replacing more and more traditional fossil fuel sources that are mainly responsible for the climate change. Some countries already have been developed geothermal resources to such a degree that resulting energy share displays the main part of energy productions, e.g. Iceland (Stober and Bucher, 2013; Barkaoui et al., 2016; Younas et al., 2016). However, also has been shown that a heat inside the earth feeding and recharging geothermal resources is not reaching a shallow crust equally indicated by different geothermal gradients found at different locations. Higher geothermal gradients can often be found at active volcanic areas as well as extensional tectonic settings, where crustal thickness is lower than average (e.g. Stober and Bucher, 2013; Stelling et al., 2015; Chena and Chiang, 2016). However, as in general for the earth temperature increases with depth geothermal resources can actually be found everywhere depending on depths, but might be economically and/or technically not feasible (Tsuchiya and Yamada, 2017).

Geothermal hot springs is one of the surface expressions of geothermal systems at depth exist. As results of the delicate and unique interplay are between heat, water, and rocks at the certain location. Hot springs themselves are often famous as spas for their contribution to human health (Lund and Boyd, 2016). However, electricity can be generated by tapping deeper aquifers below such hot spring systems, which have temperatures of around 200 °C or more depending on their plate tectonics locations (Stelling et al., 2015). Generally, geothermal hot spring systems can be divided into two main groups, (1) the high-temperature resources with reservoir temperatures greater than 150 °C, which are suitable for electricity production using conventional techniques (Barkaoui et al., 2016) and (2) the low-temperature resources with temperatures less than 100 °C, which can be used for direct applications or electricity generating utilizing low-enthalpy technology (Craig et al., 2013; Awaleh et al., 2015).

Numerous geothermal hot spring sites in Thailand are representing surface discharge temperatures in a range from 35 °C to 100 °C from the northern to the southern region. A serious exploration for geothermal systems in Thailand had been done in the 1970s at the Fang geothermal system of Northern Thailand that resulted in the first and only geothermal power plant of the country (Wanakasem and Takabut, 1986; Apollaro et al., 2015). Although the Fang geothermal plant is the small scale project it is the important cornerstone representing the beginning of geothermal energy production in Thailand and neighboring countries (e.g. Praserdvigai, 1986; Chuaviroj, 1988). For the southern region there are at least 30 natural hot spring sites with surface discharge temperatures in the range from 40 to 80 °C. Preliminary investigations had been showed that all hot geothermal spring sites can be classified according to low-enthalpy geothermal systems (Ngansom et al., 2016).

One of the first steps of geothermal developments is to understand the site specifics of the plate tectonics location, as heat flux can vary accordingly (Stober and Bucher, 2013). In the following steps then the variety of the geoscientific and geoengineering methods are applied, including, geology, geophysics, geochemistry, and hydrogeology, as well as geothermal drilling, in order to characterize the geothermal system. Geological and geophysical data help to identify and narrow down areas, locations, and depths, where geothermal resources might exist, while geochemical data can provide already information about heat source and pathways. However, in order to generate electrical power from the subsurface heat source, the certain potential of the geothermal reservoir has to be established. In most countries, geothermal energy is not well-known, and only extrapolates about their resources are available.

1.2 Review of literature

1.2.1 Topography and climate

The climate of Southern Thailand is intermediate between equatorial and tropical monsoon type and is favored by constant higher temperature without extremes of heat. A high rainfall is mainly from the NE monsoon in the eastern part

and from the SW monsoon in the western part; and a dry season is of moderate severity (TMD, 2015). The topography of the region is shaped by mountain chains running almost parallel along the peninsula, which has a considerable effect on the rainfall distribution (Trisurat et al., 2011). Dry season is generally experienced in February and March on both the east and west coast. In April, rainfall was started on the west coast due to the southwest monsoon and lasts from June to September. Then, the winter or northeast monsoons dry conditions prevailed until February. Rainfall on the east coasts is moderate at about 100 mm/month until the onset of the northeast monsoon in September. Precipitation intensifies up to 500 mm around November (Promprou et al., 2005). Although the rainfall patterns of Krabi and Phuket province are of west coast-type (Lange et al., 2019), precipitation is considerably lower than the average of Ranong and Phang Nga province. Especially in April, monthly temperature ranges from 29 up to 39 °C inland, usually in the wettest month of about 33 to 35 °C. In January temperatures may fall down to an average of 20 °C and rarely get lower (TMD, 2015). Therefore, for Southern Thailand no winter heating is required, which is different in the northern and northeastern part, where temperatures can be significantly lower.

1.2.2 General geology in Southern Thailand

During either the Late Triassic or the Permo-Triassic, Thailand and adjoining countries have occupied both major blocks joined together, which played by continent-continent collision shown in Figure 1.1 (Garson et al. 1975; Bunopas 1982). A Sundaland covered Southern Thailand is part of the geologically stable area, where it has only the experience of very slow vertical crustal movement (Charusiri et al., 2000; Watkinson et al., 2008; Ridd, 2012). Faults are the main geological structure in Southern Thailand that related to the coastal zone (Bunopas, 1982; Bunopas and Vella, 1992). For the Three Pagoda Fault (TPF) is trending from NW to SE direction, and extending from Western mountain range of Thai-Burmese border to Western Gulf of Thailand coast (Bunopas, 1982; Chinoroje, 1993; Watkinson et al., 2008) (Figure 1.1).

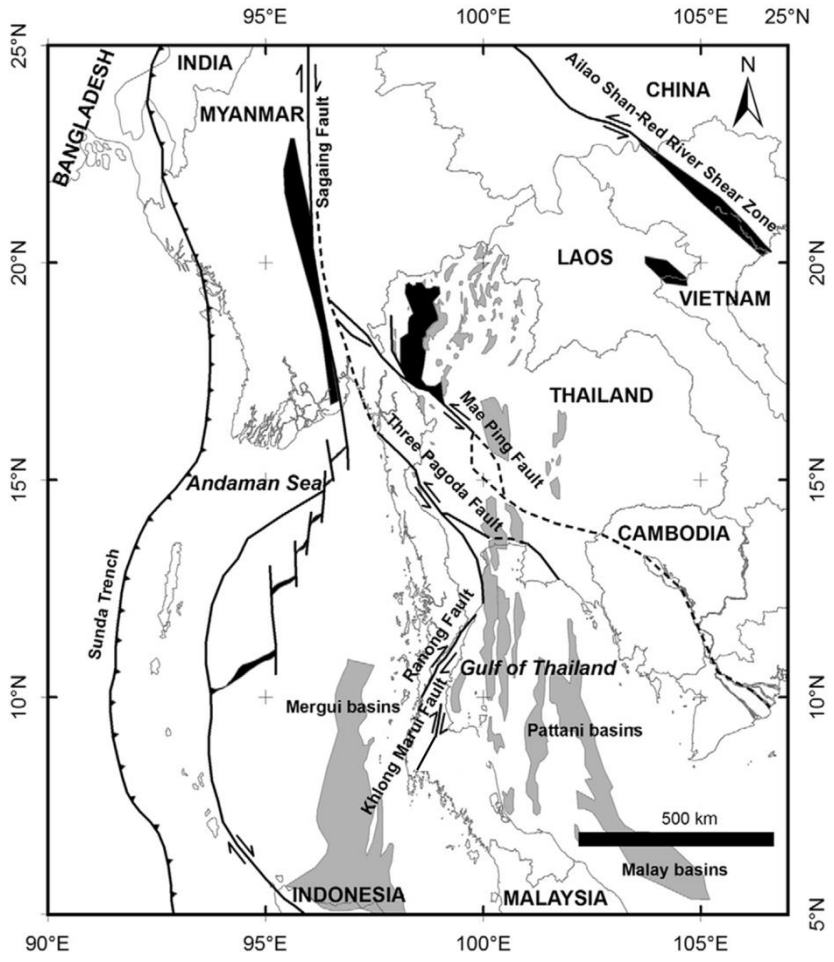

Figure 1.1 Tectonic framework of Thailand and surrounding area including major faults and related structures (after Morley, 2002; and Polachan and Sattayarak, 1989).

Southern Thailand comprises the northern part of the Malay Peninsula, bounded by the Andaman Sea in the west and the Gulf of Thailand in the east, and with a political boundary to Malaysia in the south (Figure 1.1). Peninsular Thailand has been a complex geological history (e.g. Bunopas, 1982; Chinoroje, 1993; Watkinson et al., 2008). All of the folds and faults activity have resulted in the series of roughly parallel NE-SW trending mountain ranges running down the middle of the entire peninsula (Garson et al. 1975; Polachan et al., 1991; Ridd and Watkinson, 2013). Major strike-slip faults zones crossing through the peninsula from west to east are the Ranong Fault (RF) Zone and further south the Khlong Marui Fault (KMF) Zone (e.g. Watkinson et al., 2008; Ridd, 2012). Both fault zones have been interpreted to be conjugates to the Three Pagodas Fault (TPF) Zone and Mae Ping

Fault (MPF) Zone in the central part of Thailand (Polachan et al., 1991; Kanjanapayont, 2014; Shi et al., 2015). All fault zones have been entrenched and subsequently referenced to the Cenozoic deformation of SE Asia (Polachan et al., 1991; Kanjanapayont et al., 2012). Granites have been intruded into shale, sandstone, and limestone formations as major lithologies in the area (e.g. Watkinson et al., 2008; Ridd, 2012) and they often form the mountain ranges, which can rise to a height of 1,500 meters (Ridd and Watkinson, 2013). Vertical cliffs and rugged terrain were developed on the limestone outcrops found over the whole peninsula (Ridd, 2009); some of them are famous tourist places.

On the other hand, the geologic setting of the Krabi Province was constructed and later modified by DMR (2010), partly shown in Figure 1.2. A significant geological feature in the area is the Tertiary Krabi basin of possible late Eocene or Oligocene age, which appears north of KB4 site (Morley and Racey, 2011; Figure 1.2). Although according to Ridd (2009) the basin has been shown no clear evidence of major bounding faults, the estuary south of the basin can be assumed as one, as the geological setting south of it appears considerably different. Outcrops of Permian-Carboniferous (CP) sand- and mudstones, Permian (P) limestone karsts, Triassic (TR) sand- and siltstones, as well as Cretaceous-Jurassic (JK) sandstones are aligned in NW-SE direction, including the study site. From the combination of the locations with the stratigraphic positions of the outcrops NW-SE trending faults and fold axis (latter not depicted) might be introduced as a result of compressional tectonics. These faults are assumed to be older than the basin bounding fault described above. Folds with NW-SE axis were already described by Teerarungsigul et al. (1999) further northeast of the area presented in Figure 1.2, in Khlong Thom, Lam Thap, and Bang Khan.

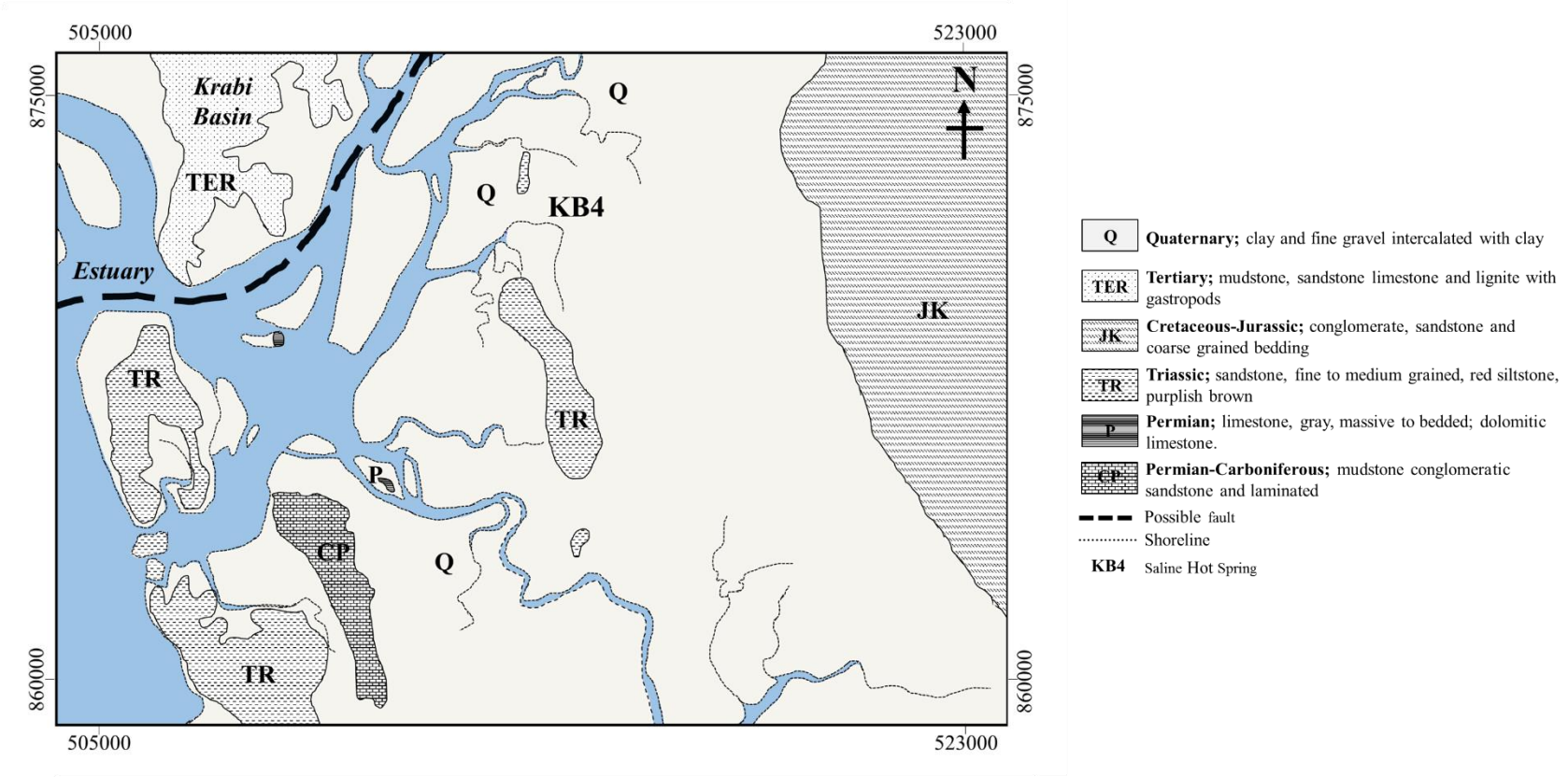

Figure 1.2 Geological setting of the Krabi Province after DMR (2010) was showing the location map of the Saline Hot Spring Khlong Thom (KB4).

1.2.3 Hot springs and geothermal reservoirs

Summarized a relation between hot springs and geothermal reservoirs given by Yasukawaet al. (2018), can be schematically categorized into five types shown in Figure 1.3. Briefly described of each geothermal system type as followed; Type 1, geothermal reservoirs and hot spring aquifers are identical systems, only well depths are different, Type 2, caprocks between spring aquifers and geothermal reservoirs are rather permeable so that hot spring water is partly supplied from deep reservoirs, Type 3, waters cannot permeate caprocks but steam and gas can so that gas content in hot springs is supplied from the deep reservoir, Type 4, caprocks are so impermeable that only heat conducts from deep reservoirs, and Type 5, geothermal reservoirs and hot spring aquifers are spatially separated, independent systems.

Possibility to planning of a geothermal development for each geothermal system are followed; Type 1 and Type 2 may interfere with the hot spring systems, Type 3 and Type 4 may not cause serious affect and Type 5 should not have any affect for development at all.

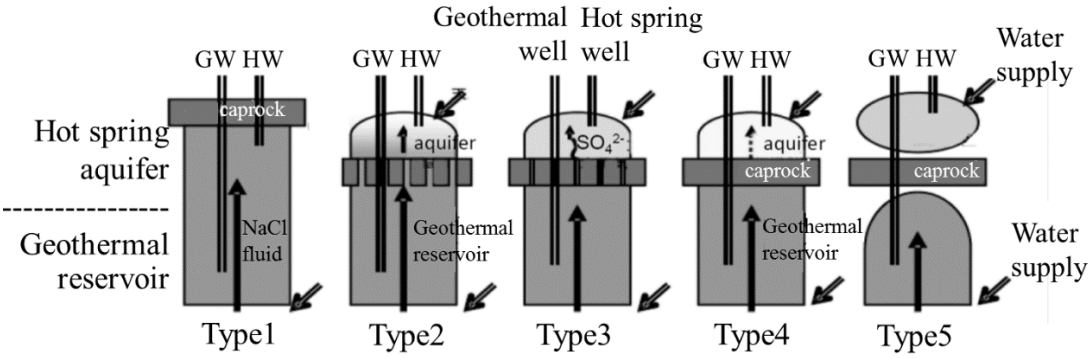

Figure 1.3 Types of geothermal hot spring aquifers in relation to geothermal reservoirs (modified from Yasukawa et al., 2018).

1.2.4 General geothermal setting in Southern Thailand

Although hot springs can be found from the northernmost to the southernmost part of Thailand a gap in hot spring locations can be found between Ratchaburi province WSW of Bangkok and Chumphon and Ranong province much further south (Figure 1.4); however it is not clear yet whether this has any geological or geothermal significance.

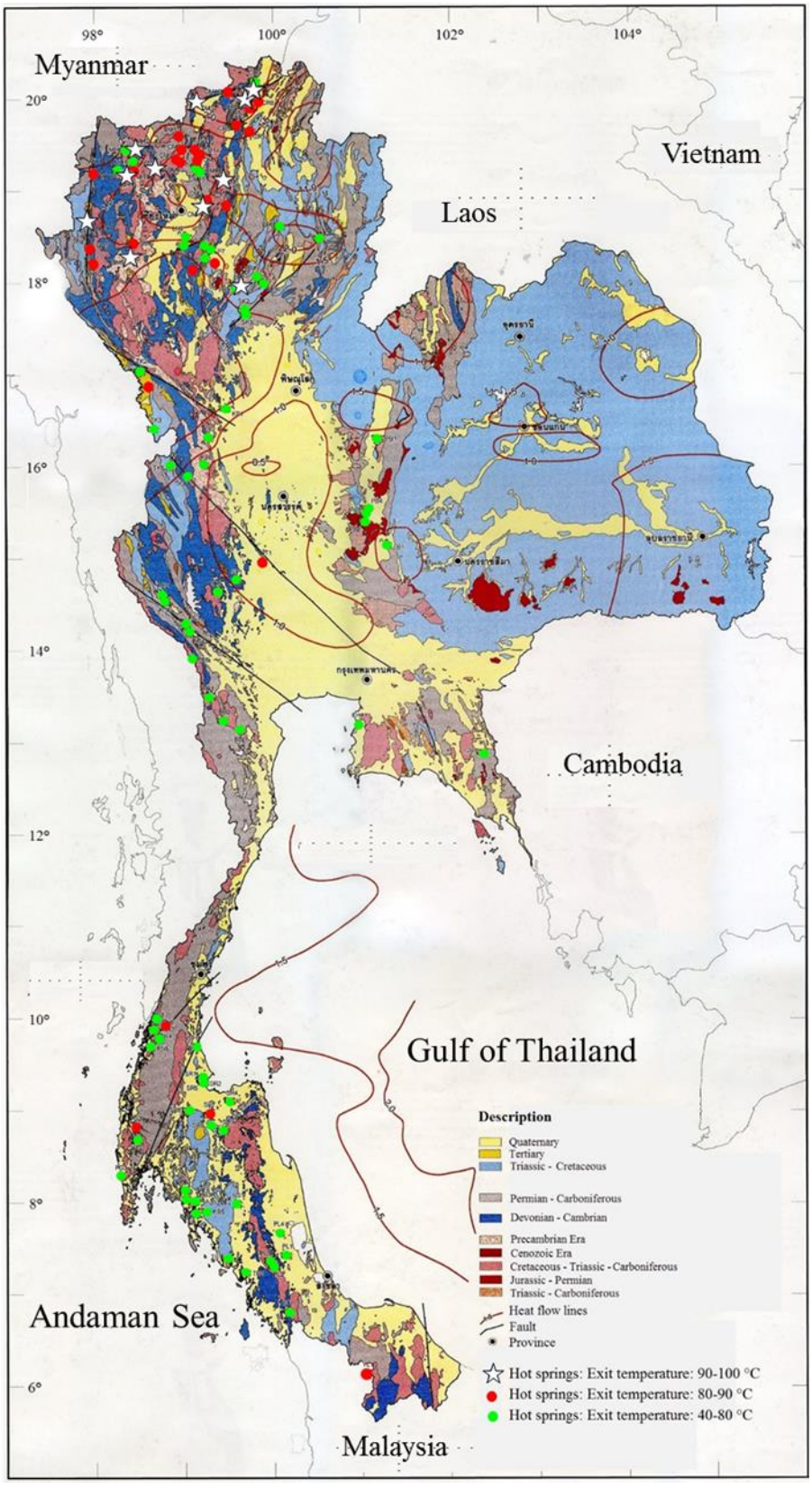

Figure 1.4 Location of hot springs in Thailand (modified from Groundwater Technology Service Center, Chiang Mai University, GTSC, 2007 and DMR, 1975).

Geothermal hot spring systems in Southern Thailand in general can be separated into three groups according, for example, to Raksaskulwong (2008): Group 1 is characterized by a general granitic setting of geothermal systems, with a lesser extent of sedimentary rocks, and with the surface discharge temperature of more than 60 °C, such as in Phang Nga and Ranong (e.g. Duerrast et al., 2016) represented by Figure 1.4 and Figure 1.5a.The sediment cover is relatively thin. Cold water is flowing down and hot water moves up to the surface along open fractures likely to be associated with the emplacement and cooling down of igneous bodies. Group 2 hot springs are associated with a sedimentary or metamorphic rock setting represented by Figure 1.4 and Figure 1.5b, with the surface discharge temperature of about 60 °C or less, such as the Surat Thani, Krabi, and Phatthalung geothermal systems (Khawdee et al., 2007). The sediment cover here is much thicker compared to Group 1 as these hot springs often found along faults and fractures related to basin tectonics where cold water flows down and hot water up. However, as these faults usually are not fully developed up into the shallower subsurface the uprising hot water is mixing with near surface groundwater bodies shown Figure 1.5b (Duerrast et al., 2016), thus resulting in lower a surface discharge temperature of the hot springs water (Khoonphunnarai al., 2007) and also in multiple hot springs at the surface discharge temperature, e.g Surat Thani. In Group 3 hot springs are classified, which are associated or in the vicinity of major fault zones, in Southern Thailand the KMFZ and RFZ. These hot springs are directly or indirectly affected by the fluid flow along and related to these fault zones (Khawtawan et al., 2004).

For all hot springs in Southern Thailand the real heat sources are not known. It can be either an igneous body where radioactive decay produces heat or a higher heat flow during basin development onshore. One exception is the Ranong hot springs as geophysical investigations hint a possible igneous (magmatic) body at larger depth as the possible heat source (Khoonphunnarai et al., 2007).

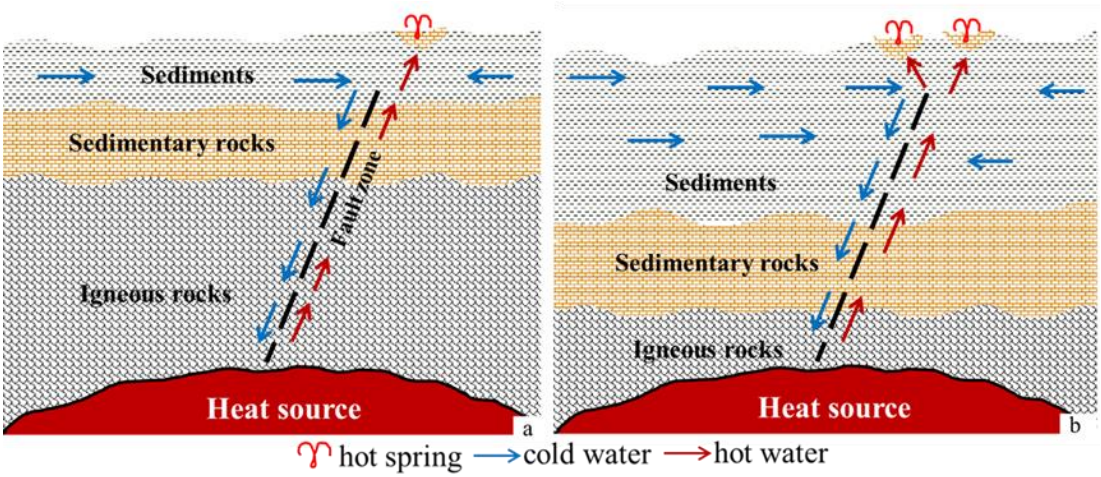

Figure 1.5 Schematic drawing of the reservoir characteristics of geothermal hot springs in Southern Thailand (modified from Raksaskulwong, 2008) related to origin and circulation, which (a) granitic setting and (b) in sedimentary or metamorphic settings.

1.2.5 Surface chemical characteristics in Thailand

Preliminary analysis of a chemical composition of hot spring waters in Thailand was represented in Table 1.1. Altogether 114 water samples from northern to southern regions have been analyzed (e.g. Chaturongkawanich and Leevongchareon, 2000; Subtavewung et al., 2005; Ngansom and Durrast 2016; Ngansom et al., 2017) mainly focused on major cations and anions e.g. Ca^{2+}, Cl^{-}, K^{+}, Mg^{2+}, Na^{+}, F^{-}, Fe^{2+}, Mn^{-}, NH_3, SiO_2, HCO_3^{-} and SO_4^{2-} contents. Physical properties of hot spring waters such as pH, and TDS contents have been done on sites. Results shown most of hot spring waters are relatively transparent, colorless and their composition is sodium bicarbonate. Although water samples from northern region generally exhibit high SiO_2 content and strong smell of sulfur, which different from waters in southern region. In addition, hot springs located next to the sea of southern region are showing a high concentration of Cl^{-}, Ca^{2+}, Na^{+}, K^{+} and Mg^{2+} represented in Table 1.1. Subsurface temperatures were estimated by a silica geothermometer range from 70 to 200 °C (Subtavewung et al., 2005; Ngansom and Durrast 2016; Ngansom et al., 2017).

Table 1.1 Summarized chemical analysis of hot spring waters in Thailand

List of analysis	**Content**	**Unit**	**Remark**
pH	6.35 - 9.5	-	the most of water samples are weak alkaline
TDS	130 - 20,000	mg/L	KB4 site of Krabi system in southern region is the highest content
Calcium, Ca^{2+}	1 - 1,000	mg/L	high Ca content that was affected by gypsum deposits is one of the reasons; Surat-Thani system in southern region
Chlorine, Cl^{-}	1 - 12,000	mg/L	KB4 site of Krabi system in southern region is the highest content
Potassium, K^{+}	1- 300	mg/L	KB4 site of Krabi system in southern region is the highest content
Magnesium, Mg^{2+}	0.01-375	mg/L	the average is about 25 mg/L
Sodium, Na^{+}	4 - 5,500	mg/L	KB4 site of Krabi system in southern region is the highest content
Fluorine, F^{-}	0.01 - 21	mg/L	contents more than 15 mg/L are probably near fluorite deposit in northern part
Iron, Fe^{2+}	0 - 2.5	mg/L	two samples from Mea Hong Son province of northern part show higher Fe than 1 mg/L
Manganese, Mn^{-}	0 - 0.58		the average is about 0.1 mg/L
Ammonia, NH_3	4 - 5,479	mg/L	the average is about 446.7 mg/l
Silica, SiO_2	2 - 273	mg/L	the most of water samples from northern part are higher contents than southern part, except PG1 and YL sites are quite similar
Alkalinity, HCO_3^{-}	47- 608	mg/L	the most of water samples from northern part are indicated HCO_3 higher than the average value that might be effects from the chemical reaction during hot waters flow through limestone
Sulfate, SO_4^{2-}	2 - 1,328	mg/L	the most of water samples from Surat-Thani, Phang Nga, Krabi and Trang systems are higher SO_4 than others

1.2.6 Geothermal exploration and development in Thailand

Due to the energy crisis in 1980's, Thailand was started and sated up the renewable energy committee for work on the issue (Chuaviroj, 1988; Praserdvigai, 1986). One of alternative energy sources is geothermal resources that their explorations are carried out to a preliminary evaluation step on hot spring systems. First collaboration began with working group comprised Chiang Mai University (CMU), Electricity Generating Authority of Thailand (EGAT) and Department of Mineral Resources (DMR) signed contract in 1977 (Chuaviroj, 1988; Coothongkul and Chinapongsanond, 1985; Hirukawa, et al., 1987). Second collaborations also supported by other Thai organizations e.g. National Energy Department and Prince of Songkla University (PSU) preliminarily explored geothermal in Southern Thailand. Furthermore, Meteorological Department, Hydrographic Department, Royal Thai Navy is supported for the earthquake data both inside and neighboring countries (Raksaskulwong and Thienprasert, 1995; Ratanasthien, et al., 1985). A summary of organizations that are worked during the past of 30 years represented in Table 1.2.

Table1.2 Previous activities in geothermal exploration and development of Thailand

Periods	**Activities**	**Organizations**
1973	a reconnaissance survey in possibility for geothermal utilizations	NEA and KAZ
1979-1981	geothermal working group formed and potential studied in 30 well-known hot springs	EGAT, DMR and CMU
1982	additional areas for geothermal potential studied	CMU and DEDP
1982-1988	pre-feasibility study on the development in San Kamphaeng geothermal system	EGAT and JICA
1982-1992	a geothermal energy for the electricity generation in the Fang hot spring system	EGAT and ADEME
1983-1986	a geological, geophysical and geochemical prospecting of more than 50 sites in northern part are including drilled well data evaluated	DMR, UNDP and GIS

Table 1.2 Continued

Periods	**Activities**	**Organizations**
1989	a geothermal power plant was established with the capacity of 0.3 MW in the Fang system	EGAT and FAEM
1992-1996	at least 9 geothermal systems in northern region have been investigated for developed as the small scale direct use project	DEDP
1994-1998	a geothermal investigation and drilling exploration in Mae Hong Son	EGAT and CMU
1997-1999	an investigation of hydrology of Fang geothermal system by isotope and chemical tools	CMU, DMR and IAEA
2001-2003	digital compilation of groundwater and geothermal database in Thailand	CCOP and DMR
2005	potential of geothermal resources by means of the geochemical analysis	DEDE and CMU
2011-2016	a new phase of geothermal exploration for a power plant comprise of geological, geophysical and geochemical investigation	PTT, DEDE, DMR and DGR

NEA	National Energy Administration of Thailand
KAZ	Kingston Reynoldsthom & Allardice Ltd. Of New Zealand
EGAT	Electricity Generating Authority of Thailand
DMR	Department of Mineral Resources
CMU	Chiang Mai University
DEDP	Department of Energy Development and Promotion
JICA	Japan International Cooperation Agency
UNDP	United Nation Development Program
FAEM	French Agency for Energy Management
IAEA	International Atomic Energy Agency
CCOP	Coordinating Committee for Geoscience Programmes in East and Southeast Asia
PTT	PTT Public Company Limited
DGR	Department of Groundwater Resources

1.2.7 Fang Geothermal Power Plant

A project cooperation agreement between the Bureau de Recherches Géologiques et Minières (BRGM) of France and Electricity Generating Authority of Thailand (EGAT) was formulated during 1981-1984 at the Fang geothermal system of Northern Thailand. (Wanakasem and Takabut, 1986; Wood et al., 2018). The purposes of the project are to characterize geothermal reservoirs and to appraise geothermal enthalpy targeting for an electrical generation (Wanakasem and Takabut, 1986; Praserdvigai, 1986). Fang Geothermal Power Plant is classified into the suitable possibilities for the small scale power plant, in the range 1 to 10 MW with binary technology (Chuaviroj, 1988; Coothongkul and Chinapongsanond, 1985; Ramingwong et al., 2000). Subsurface temperature varies between 110 and 130 °C, at the shallow well about 100 m and drilling program produced about 22 L/s of 125 °C water, and two wells to 500 m produced about 10 L/s (Coothongkul and Chinapongsanond, 1985). Characteristics of Fang geothermal system are hot water dominated type, high pH, with sodium bicarbonate species and is associated with granitic rocks (Wood et al., 2018; Apollaro et al., 2015). Geochemical data of hot fluids indicate the water contains very low concentration in most of elements and the heavy metals are not detectable (Ratanasthien et al., 1985). An isotopic study has investigated on tritium, deuterium and oxygen-18. The deuterium and oxygen results suggest the origin of water may have been derived from local precipitation, possibly from somewhat higher altitudes (Hirukawa et al., 1987; Takashima and Jarach, 1987). Small numbers of tritium present in this water indicates a short circulation period of these hot waters as groundwater.

On the other hand, Fang power plant is one of a predominantly agricultural producing in the Chiang Mai province. After harvesting, many crops can be stored at a room temperature for a short time and many percentages of crops have to throw away due to sprouting and spoliation. Major cultivations are garlic, onion, rice, chili, tobacco, potato, soybean, maize, cotton, etc. Moreover, after using the hot water in the Fang geothermal power plant it can be exploited downstream for agricultural-industrial, spa, bathing, and other purposes (Ratanasthien et al., 1985; Chuaviroj, 1988). Concepts to extract the released thermal water for agricultural-industrial utilization are considered into two categories.

1.2.8 Geothermal resource evaluation

For an assessment of the geothermal potential of a certain geothermal site, first reliable estimations have to be made of the resource temperature, heat source, and reservoir characteristics. According to Muffler and Cataldi (1978), sufficient information for a detailed reservoir characterization is available when using well data. Further, Muffler and Cataldi (1978) described four groups where different assessment methodologies can be separated into: (1) assessment of the thermal heat flux; it determined the amount of thermal energy transferred from sediments to the atmosphere by conductive heat transport and the amount of convective heat transferred to the surface by fluids over the same unit of time, (2) the assessment of planar fracture is based on a model, which has planar fractures in an otherwise impermeable rock. If the initial rock temperature, recharge temperature, and minimum outflow temperature are known, then the recoverable thermal energy can be determined, (3) the volume assessment is based on a calculation of the amount of heat energy, related to the mean annual surface temperature, stored in a defined volume of rock, and (4) the assessment of the magmatic heat budget (magma) estimates the size, position, and age of an intrusion, and it is used to estimate the accessible resource base associated with an magmatic intrusion (Muffler and Cataldi, 1978).

Extended and modified version of the methodological approach described by Bignall and Sanders (2016) was used in the geothermal hot spring in Southern Thailand, especially wells and well data are often missing. A set of parameters, selection criteria has been established to determine which sites have a good potential and thus should be further characterized in detail. Following common geothermal resource parameters have been considered: (1) area extent estimated from geophysical surveys, (2) reservoir depth defined as mean depth from a ground surface to a top of the reservoir; reservoir thickness at depth; and reservoir volume as the resource area multiplied by reservoir thickness, (3) temperatures consist of a maximum surface discharge temperature, a reservoir temperature (geothermometry), and an enthalpy, (4) fluid acidity, gas content and scaling as they might have an impact on resource utilization, (5) reservoir related effects include subsidence and ingress of groundwater, and (6) geological hazards involve site-specific geotechnical factors thus avoiding having facilities on a risk locations.

Further, the approach has been extended for social factors. Several factors of a geothermal power development play a part of both the land use and the marketing relationships of its development. For example, bankable geothermal power projects require extra road between construction site or owner of strongly agree. Moreover, the geomorphology of many geothermal hot spring sites varies, ranging from flat areas, over hilly environments, to limited accessibility. The approach has been applied for two reasons; the first it is based on the series of geological, geochemical and geophysical factors, which can be determined for the specific area and the second it is similar to methods used in the assessment of institutional/environmental analysis. A main weakness is associated with the estimation of reservoir depth, thickness, and volume, as only a broad indication can be given in the absence of well data; however, estimates can be given based on the overall geological setting. In Southern Thailand well data are mostly not available.

In the case of Thailand, geothermal energy is non-traditional resources. A few research links have been presented upon to base resources and reserve estimates. Consequently, there is an important role for classification and assessment of geothermal resources, particularly in hot spring systems, both toward characteristics of reservoir and in institutional or environmental availability.

1.3 Objective

The research is providing an assessment and subsequent ranking of hot spring systems in Southern Thailand using a variety of different factors in order to support any decision making process for future geothermal power stations. Subsequently, a site characterization was carried out for one of the highest ranking sites, and based on all available information and data power production calculations were done. Outline possible scenarios for the use of geothermal energy, including choices of technology for the geothermal power plants in southern region. On the other hand, the geothermal system of the Saline Hot Spring Khlong Thom (KB4) has been investigated to better understand the subsurface structure, at least in the shallower part of the first few hundred meters for an understanding of the geological and hydrogeological setting.

1.4 Study area

For this research at least 30 hot spring sites in Southern Thailand were used, which are located in eight geothermal systems which consist of Chumphon (CP), Ranong (RN), Surat Thani (SR), Phang Nga (PG), Krabi (KB), Trang (TR), Phatthalung (PL), and Yala (YL) shown in Figure 1.6, Figure 1.7 and Table 1.3. Surface discharge temperatures are between 40 and 80 °C. A focus is on the PG1 site as it is the one of higher surface temperature and the saline hot spring KB4 as a unique hot spring system. A summary of information for each geothermal system in the southern region is briefly given as followed.

Chumphon Geothermal System (CP)

CP system is located in Chumphon Province, northern part of Surat-Thani geothermal system represented by Figure 1.6, 1.7a and Table 1.3. Natural hot springs of more than three pools developed for tourist attractions have surface discharge temperatures ranging from 45 and 50 °C. Local geology at the hot spring and surrounding area is represented dolomitic limestone (Bhongsuwan and Auisui, 2015).

Ranong Geothermal System (RN)

RN system as one of the larger geothermal systems in the southern region is located in Ranong Province and famed for natural hot springs, thus drawing attention to local visitors and foreign tourists as shown in Figure 1.6, 1.7b and Table 1.3. Altogether seven hot spring sites are located in the RN system, which have the surface discharge temperatures between 40 and 75 °C (Khoonphunnarai, et al., 2007; Chaturongkawanich and Leevongchareon, 2000). RN1 and RN6 sites have the highest temperature of this system. RN1 site is praised as a famous landmark of Ranong City, also providing spa and hot massage therapy nearby. RN6 site was discovered in deep forest of Kapoe District located about 60 km south of Ranong City; the site is protected by the Ranong Forest Preservation and Protection Division. All hot spring sites of the RN system are located close to the Ranong Fault Zone, a major strike-slip fault (Khoonphunnarai, et al., 2007; Sanmuang, et al., 2007).

Surat Thani Geothermal System (SR)

SR system is located in the western part of the southern region with altogether nine hot spring sites recorded. The surface discharge temperatures range from 40 to 70 °C; while SR3, SR7, and SR9 sites show the highest surface discharge temperature of this system as presented in Figure 1.6, 1.7c and Table 1.3. SR3 is in Tha Chang District located on public land in close proximity to the main railway line from Bangkok to HatYai, and also relatively close to the Gulf of Thailand. For SR7 is in Phunphin District and it is already developed for tourism; its larger pond is already visible from the main road. While SR9 in Khian Sa District is located in a national park area. A general geology surrounding the SR system is characterized by isolated steep sided hills of Permian limestone tower karsts and granitic mountains on western margins (Khawdee, et al., 2007).

Phang Nga Geothermal System (PG)

PG system is located on the western side of the southern region, about 100 km north of Phuket City represented by Figure 1.6, 1.7d and Table 1.3. At least three hot spring sites can be found in this system, with surface discharge temperatures recorded from 45 to 78 °C (Ngansom et al., 2016; Ngansom et al., 2017) with only one site, PG1, has the surface discharge temperature of up to 78 °C. PG1 site can be found close to and at the banks of the Pai Phu River. Rocks in and around the PG1 site are dominantly granites, which are distributed in the southeastern part and sedimentary/metamorphic rock unit, which covers other parts (Duerrast et al., 2016; Ngansom et al., 2017).

Krabi Geothermal System (KB)

KB system was located in western part of southern region and connected to Andaman Sea, which consist of at least five hot spring sites located in the system shown in Figure 1.6, 1.7e and Table 1.3. Surface discharge temperatures are recorded from 40 to 46°C. Most of the hot spring sites are famous around the world for their natural beauty such as Saline Hot Spring Khlong Thom (KB4), the Hot Spring Waterfall (KB5), and also Krabi Hot Spring (KB3). The one of a unique geothermal

system as KB4 site has been identified for its complex geothermal setting (Ngansom and Durrast 2016). It has both saline and hot waters represented in one system.

Trang Geothermal System (TR)

TR system was located in southern part of Krabi geothermal system about 140 km shown in Figure 1.6, 1.7f and Table 1.3. Natural hot springs at least three pools can visit as developed for tourist attractions and integrated for the Thai Massage School supported by the Local Administration Organization. Surface discharge temperatures range from 45 to 50 °C (Ramingwong et al., 2000). A surface geological survey discovered sandstone outcrops both inside and outside the hot spring area.

Phatthalung Geothermal System (PL)

PL system was located in Phatthalung Province, about 84 km east of Trang geothermal system represented by Figure 1.6, 1.7g and Table 1.3. There are four hot spring sites with surface discharge temperatures between 41 and 57 °C have recorded in this system. A general geological setting is exposed range from Cambrian to Quaternary. For Cambrian rocks comprise white to light gray colored fine grained sandstone and quartzite and Ordovician rocks compose of mainly gray colored, finely crystalline to coarse grain limestone (Jonjana et al., 2012).

Yala Geothermal System (YL)

Yala system is located in the southernmost part of Thailand near the border to Malaysia represented by Figure 1.6, 1.7h, and Table 1.3. Detailed investigations of this site have been affected by continuous armed conflicts in this area since 2004; therefore geological and geophysical surveys data are limited. However, YL site is a famous tourist attraction, mainly for Malaysian guests; the surface discharge temperature is above 80°C (Ramingwong et al., 2000).

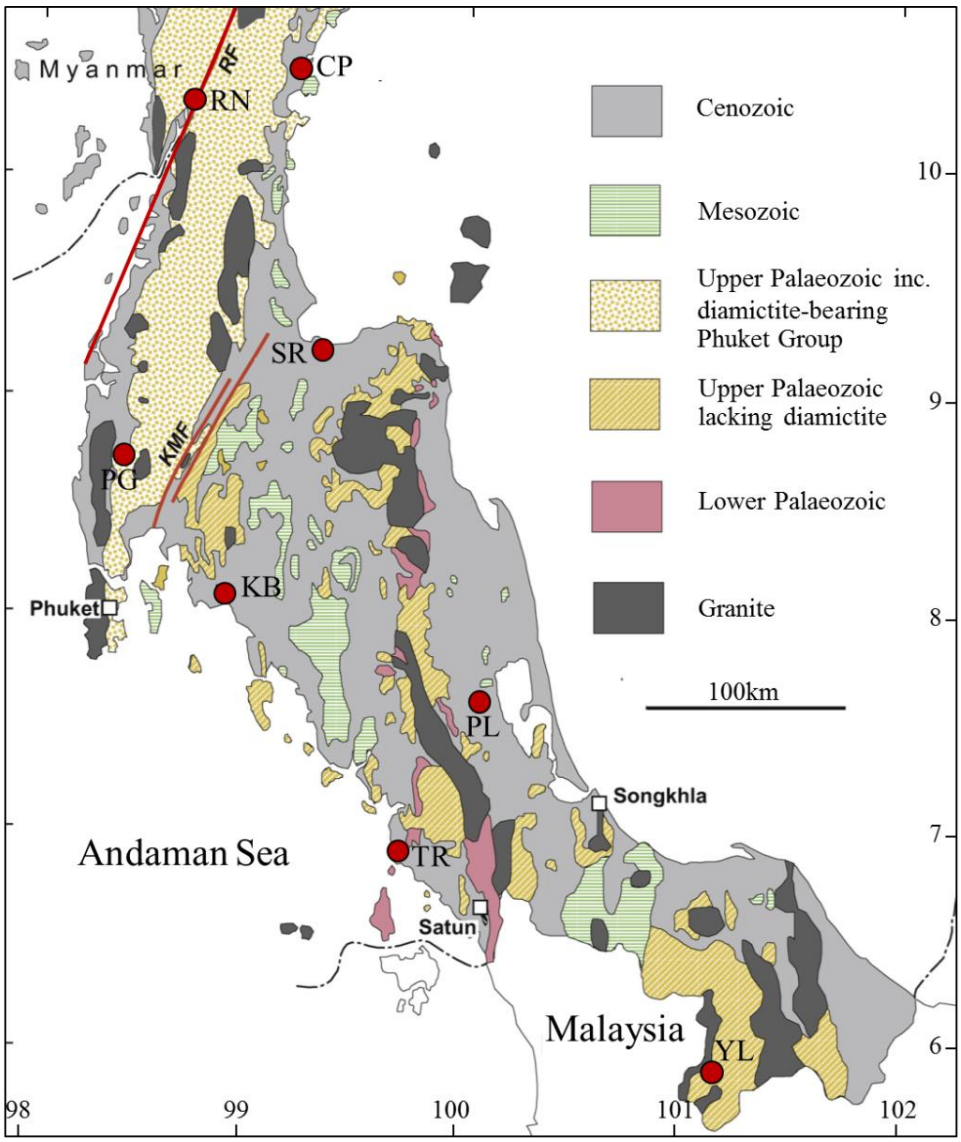

Figure 1.6 Simplified geological map and location of geothermal hot spring systems part of Southern Thailand (modified from DMR, 1975; Ridd and Watkinson, 2013); CP – Chumphon Geothermal System, RN –Ranong Geothermal System, SR – Surat Thani Geothermal System, PG – Phang Nga Geothermal System, KB – Krabi Geothermal System, TR – Trang Geothermal System, PL – Phatthalung Geothermal System, YL – Yala Geothermal System, RF – Ranong Fault, and KMF – Khlong Marui Fault.

Figure 1.7 Geothermal hot springs in Southern Thailand; (a) Chumphon hot spring, (b) RN1 site of Ranong system, (c) SR7 site of Surat Thani system, (d) PG1 site of Phang Nga system, (e) KB4 site of Krabi system, (f) Trang hot spring, (g) PL1 site of Phatthalung system and (h) Yala hot spring.

Table 1.3 Locations and surface discharge temperatures of geothermal hot spring systems in Southern Thailand

Hot spring system	**UTM (WGS-84), Zone 47**		**Surface Temp. (°C)**
	East (m)	North (m)	
Chumphon: CP	512222	1075014	50
Ranong			
RN1	462169	1100516	65
RN2	460000	1094700	40
RN3	461030	1093400	45
RN4	462290	1094275	50
RN5	456192	1080300	46
RN6	470810	1060430	75
Surat Thani			
SR1	521107	1034893	45
SR2	520518	1033905	40
SR3	522412	1031459	60
SR4	555129	1009502	41
SR5	545897	972938	42
SR6	503522	979890	53
SR7	529417	991895	70
SR8	530806	991094	56
SR9	524947	977116	62
Phang Nga			
PG1	441455	960807	78
PG2	437870	975306	55
PG3	420496	918037	45
Krabi			
KB1	499622	900439	45
KB2	500183	891731	47
KB3	510462	888220	45
KB4	512329	873475	47
KB5	523171	876867	47
Trang: TR	551391	818787	52
Phatthalung			
PL1	625096	823266	57
PL2	608944	810077	46
PL3	604490	816432	50
PL4	615661	850513	41
Yala: YL	729730	646758	80

1.5 Conceptual framework

A framework for this research was represented by Figure 1.8. The first step was started with the detailed literature research and summary of all available data of the study area, thus followed by the second steps are planned and carried out geophysical, geological and geochemical explorations on the hot spring sites. Various geophysical, geological and geochemical methodologies will be applied depending what data are needed and what data are not available and what surveys are feasible. For geological investigations will provide information about rock types, stratigraphic setting, as well as structural features, like faults and folds. Geophysical investigations can comprise a number of different methods as followed; (a) gravity and magnetic investigations will provide data about possible igneous rocks as sources for geothermal reservoirs as well as providing data for possible large scale faults and folds in the subsurface, (b) near surface resistivity and seismic investigations can reveal shallow structures as well as the distribution of fluids in the shallow subsurface, and (c) magnetotelluric survey can provide such information for a deeper subsurface down to several hundred meters or even some kilometer. While the geochemical composition of hot spring waters can provide information about the source of the hot water, especially when using isotope analysis. For the various geoscientific investigations at hot springs sites conclusions can be drawn about possible heat sources as well as fluid pathways from the depth to the surface, as well as possible mixing with ground or seawater. Parallel information from public sources will retrieved about the technological choices in geothermal energy production for regional energy demand.

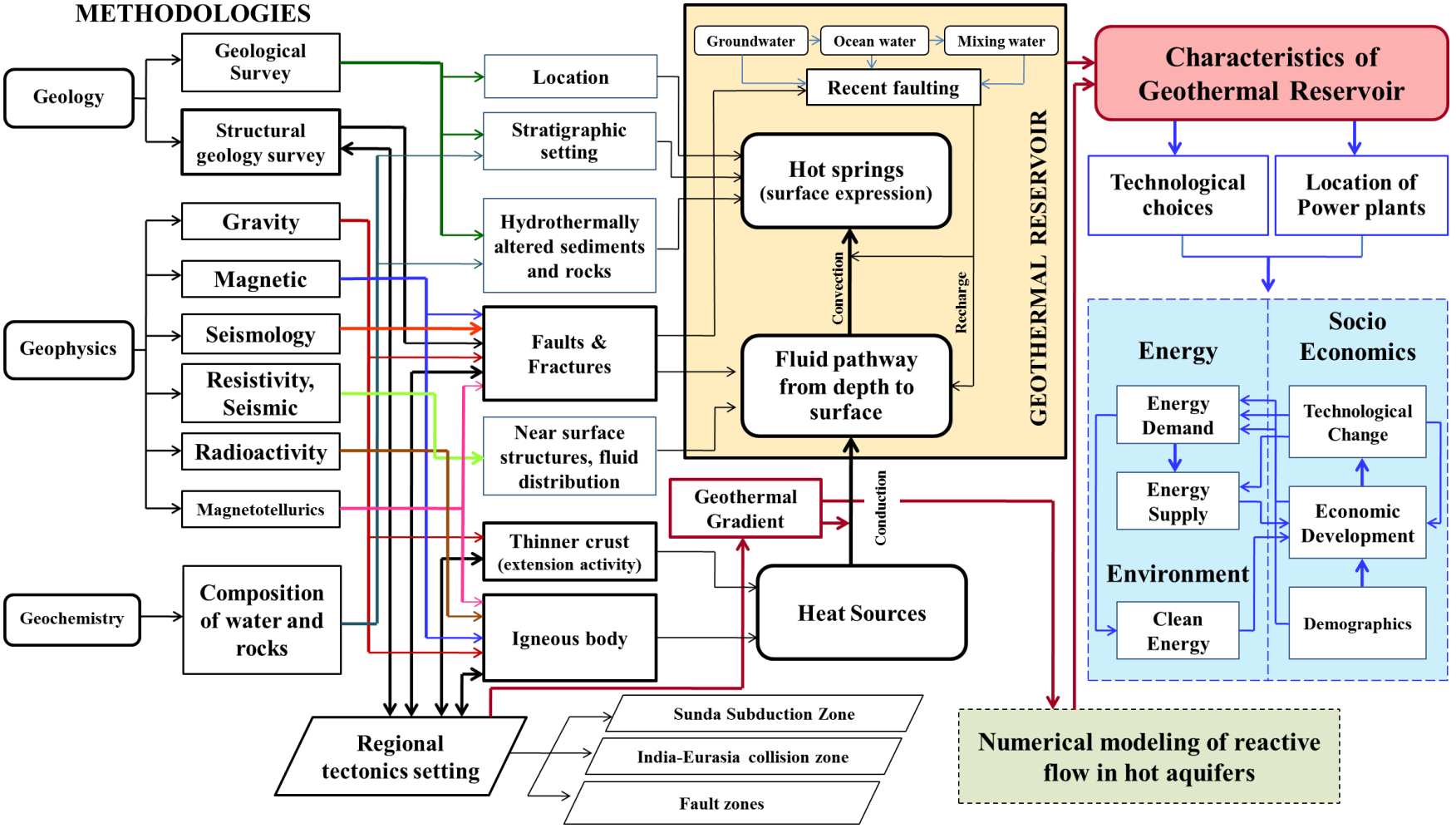

Figure 1.8 Conceptual framework of the research. Dashed line indicates parts which are not covered by this research.

CHAPTER 2
RESEARCH METHODOLOGY

2.1 Geological survey

Geological surveys are significant for the understanding of the subsurface structural setting of geothermal hot spring areas (Faulds et al., 2006). All available data of literature and geological studies including reports of fieldwork, which have been carried out both at regional and local level, have been utilized for the geothermal reservoir characterization. Initial geological fieldwork focused on an overall geological setting and identification of the most prominent features, including pathways, which allows hot fluids from the deepest parts moving to shallow parts of the geothermal system. Main areas of geological survey investigations can be briefly described as following (see also Faulds et al., 2006):

1) Surface manifestations of geothermal resources, as well as measured water temperature, flow rate and water samples for geochemical analysis.

2) All available data of local geologic structures, geologic controls, physical environment and a rate of fluid discharge.

3) Geothermal hot spring sites located on geological maps for further examination of particular rock types.

4) Field reconnaissance, such as geothermal wells, groundwater wells, outcrops and mountains (e.g. limestone, sandstone) which indicate a potential geothermal resource, and estimating of boundaries of geothermal hot springs.

An analysis of the geometry of fault systems and discrete steps in fault zones can be used to map promising areas of possible geothermal areas or to understand the structural setting of existing hot spring sites. Features indicative of fault zones in geothermal systems are summarized by Faulds et al. (2006) and shown in Figure 2.1:

(a) Hard linking between two major faults is provided by a step over between two overlapping normal fault segments and multiple minor faults,

(b) Faults have been broken up into multiple displays indicating the termination of major normal faults,

(c) Multiple fault intersections in subsurface as the result of overlapping and oppositely dipping normal fault systems, and

(d) Delusional fault intersection between oblique-slip normal faults.

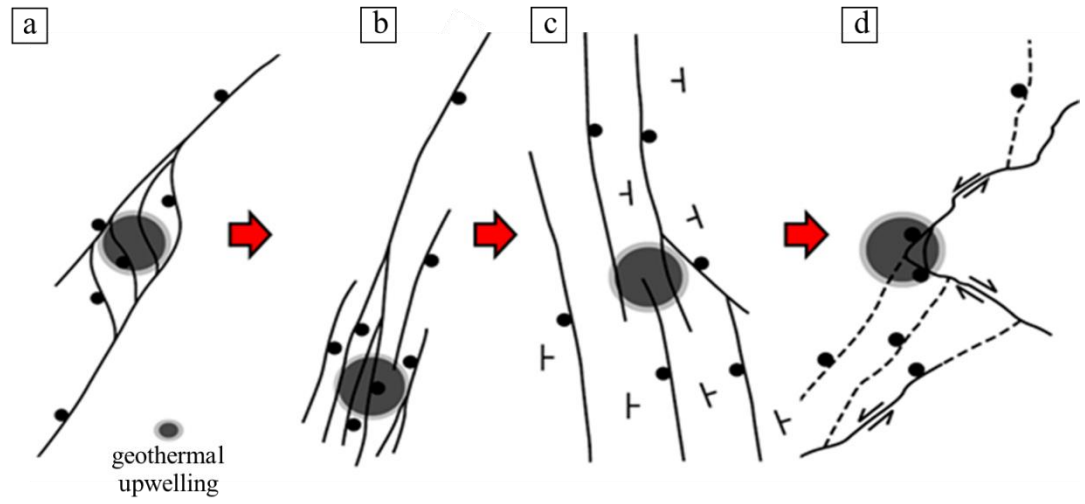

Figure 2.1 Examples of favorable structural settings for geothermal systems (modified from Faulds et al., 2006).

2.2 Geochemical exploration

Geochemistry can be a useful tool in the exploration of hot spring geothermal systems of Southern Thailand to explain reservoir characteristics and to answer production questions (e.g. Nicholson, 1993). All available data are used to determine the reservoir characteristics of hot spring system, with an estimation of the minimum temperature at depth; with a prediction of the homogeneity of water supply; to infer the chemical character of waters at depth and determine the source of recharge water. Moreover, in order to understand the origin of geothermal waters a close correlation or similarity of geothermal waters to local groundwater was represented by isotope studies (e.g. Nicholson, 1993). For this research, the steps for geochemical exploration can briefly described as followed.

2.2.1 Collection and preparation of samples

At the sampling site, the surface discharge temperature and the salinity of all water samples were measured at sampling points using a standard glass thermometer (max. 100 °C) and the Atago Master refractometer, respectively. In all cases, water samples for geochemical analysis were collected in a 500 mL well cleaned airtight polypropylene bottle (with good chemical resistance), after it was rinsed at least three times with the same water prior to final collection (Ármannsson and Ólafsson, 2007; Huang et al., 2012). Bottles, labeled accordingly, indicating date, number, purpose of analysis, and location, were cooled down naturally to ambient temperatures (30-35°C) as thermal contraction is reasonably small (around 0.5% and smaller, Arnórsson et al., 2006), and then send to the laboratory. Parameters have been analyzed in a few days after samples were taken.

2.2.2 Qualitative inorganic analysis

The major cation and anion concentrations of all hot spring water samples were analyzed anions at the Central Equipment Division, Faculty of Science, Prince of Songkla University, Thailand, using standard procedures outlined in Eaton et al. (2005). The accuracy and precision of the laboratory measurements were computed by analyzing using certified reference materials and by performing several replicas and dilutions of collected samples. The methods of analysis and detection limits of elements are summarized in Table 2.1. For the pH was measured with a standard pH meter, resistivity with a standard laboratory resistivity meter, Ca^{2+}, Mg^{2+}, Na^{+}, K^{+}, and SiO_2 concentrations were determined by ICP-OES and HCO_3^{-} concentration was determined by standard titration method. Although determination of bicarbonate concentration is preferable on site, it is also possible in the laboratory if time between sampling and analysis is not prolonged (Nicholson, 1993).

Table 2.1 Methods applied at the Central Equipment Division, Faculty of Science, Prince of Songkla University, Thailand and detection limits of analyzed cations and anions

Parameters	Method used	Detection limits (mg/L)
Fluoride, F^-	Photometric	0.1
Chloride, Cl^-	Argentometric	0.1
Iron, Fe^{2+}	Inductively Couple Plasma (ICP)-OES	0.005
Calcium, Ca^{2+}	Inductively Couple Plasma (ICP)-OES	0.01
Magnesium, Mg^{2+}	Inductively Couple Plasma (ICP)-OES	0.01
Potassium, K^+	Inductively Couple Plasma (ICP)-OES	0.01
Sodium, Na^+	Inductively Couple Plasma (ICP)-OES	0.005
Sulfate, SO_4^{2-}	Photometric	1
Bicarbonate, HCO_3^-	Titration	1
Dissolve silica, SiO_2	Inductively Couple Plasma (ICP)-OES	1

2.2.3 Isotopes

Stable isotopes (δD and $\delta^{18}O$)

Non-acidified water samples taken from the hot spring systems for stable isotopes (δD and $\delta^{18}O$) measurement were analyzed using a Liquid Scintillation Counter (Tricarb 3180 TR/SL) (Swart et al., 1991; Cid-Andres, 2015). After an electrolytic enrichment major anions were measured by Dionex, ICS-3000 at Thailand Institute of Nuclear Technology (TINT). Relevant to research is an isotopic composition of hot spring waters associated with mineralization in granitic and related sedimentary rocks. The stable isotope work has delineated two main types of waters, magmatic and meteoric, important in case closely related to mixing occurring within a reservoir system. Magmatic water is very important in the earliest stage in an evolution of deposit, followed by increasing meteoric water contribution accompanied by cooling of an igneous intrusion. A brief summary of isotopic characteristics of magmatic and meteoric waters of the study area presented below.

1) Magmatic water depends on equilibrated igneous rocks and released from magmatic temperatures. $\delta^{18}O$ value for ultramafic (>5 and <7%) agree with presumed mantle origin. More siliceous rocks are progressively enriched in ^{18}O for sequence from basalt and gabbro (5.5 to <8%), through andesite and granodiorite (6 to 13%). Generalized trend is compatible with observed fractionations between a common rock-forming mineral wherein the $\delta^{18}O$ values are largest in quartzes, carbonates and

alkali feldspars; intermediate in plagioclase feldspars, micas and ferromagnesian minerals.

2) Meteoric water varies in a systematic way with respect to latitude and elevation, which a very close approximation follow Craig (1961); $\delta D = 8\delta^{18}O + 10$. A linear relationship exists with equilibrium fractionation processes during condensation of water from the Earth's atmosphere, and D/H fractionation is proportional to $^{18}O/^{16}O$ fractionation. A coupled depletion of ^{18}O and D in meteoric waters relative to SMOW (Figure 2.2) reflects a lower vapor pressure of HDO and $H_2{}^{16}O$, and a consequent preferential tendency of heavy water molecule to condense. A fractionation increases proportionately with decreasing temperature, resulting in a factor of eight in the slope of Meteoric Water Line (MWL). Thus, water condensed from atmospheric vapor in air mass will be richer in ^{18}O and D than vapor, and any subsequent precipitation from the same air mass must be lower in ^{18}O and D than this initial condensate.

3) A water-rock exchange at elevated temperatures can cause larges in the isotopic composition of waters. A magnitude of these changes depends on the initial isotopic composition of fluid, on the temperature of exchange as reflected by the water-rock fractionation factor, on the ratio of exchanged oxygen and hydrogen atoms in water to those in rock, on the degree of approach to isotopic equilibrium, and on the boundary condition. For the general statement has been represented here; (a) exchanged meteoric water is enriched in ^{18}O and D under most geologic conditions, whereas exchanged magmatic water is enriched in deuterium but may be either depleted in ^{18}O through exchange with igneous rock, or enriched in ^{18}O through exchange with sedimentary rocks, (b) the magnitude of isotopic enrichment or depletion varies inversely with a water-rock mass ratio, (c) the change in fluid $\delta^{18}O$ values is more significant than of δD values at high water-rock mass ratio but the reverse is true at low rations, and (d) at equivalent temperatures and water-rock mass rations, fluids that have equilibrated with sedimentary rock are isotopically heavier than those that have equilibrated with igneous rock because the former is enriched in ^{18}O and D and contains a greater quantity of hydrogen relative to the latter.

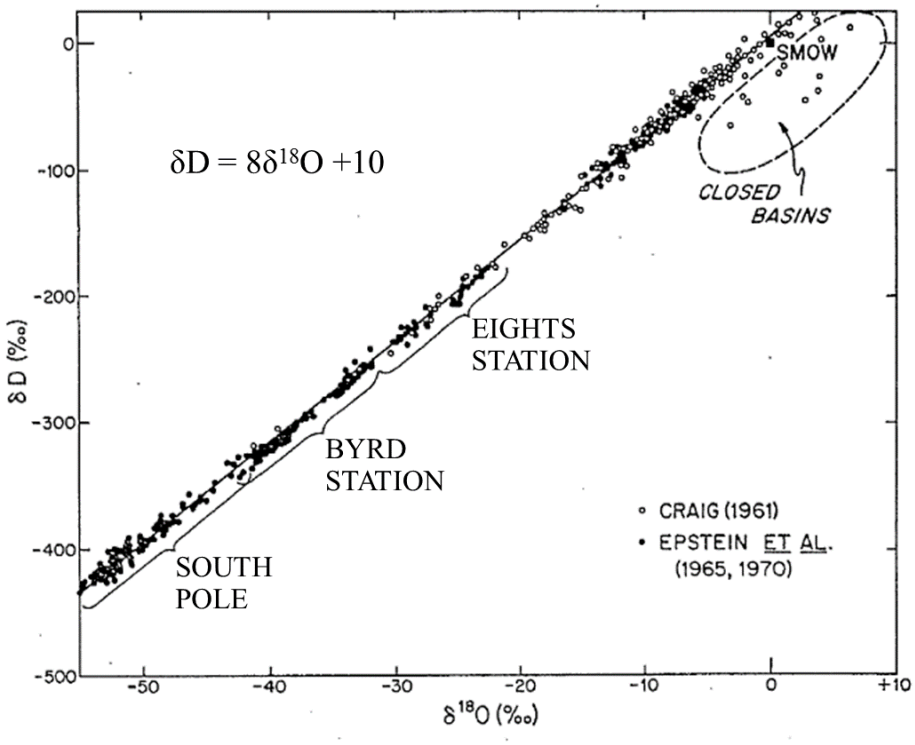

Figure 2.2 Isotopic compositions of meteoric waters, relative to standard mean ocean water (S.M.O.W.) (Craig, 1961).

Strontium isotopes (Sr and $^{87}Sr/^{86}Sr$)

Sr concentrations of geothermal hot spring water samples were determined on a Thermo-Finnigan Triton© TIMS, at the Geoscience Centre at University of Göttingen (GZG, Germany). Prior to digestion, all water samples were mixed with the tracer solution enriched in ^{87}Rb-^{84}Sr (Krabbenhöft et al., 2010; Takashima and Jarach, 1987). Detailed descriptions for all analytical procedure for water samples are given in Wiegand et al. (2001), Tütken et al. (2002), and Klaus et al. (2007). For this study a value of 0.710259±0.000076 (2σ) for the NBS 987 (n=4) was determined. For instrumental mass fractionation a correction with $^{88}Sr/^{86}Sr$ of 0.1194 was applied using exponential law.

A quantity of elements is measured from a change produced in its isotopic composition by addition of known quantity of the stable isotope of that element. For the strontium determination, known quantity of the spike solution enriched in Sr^{86} is added to solution containing the known quantity of the water samples to be analyzed and measurement of the resulting Sr^{86}/Sr^{88} ratio is made, followed Equation 2.1.

$$\frac{Sr^{86}}{Sr^{88}} = \frac{Ab^{86}_{N}N + Ab^{86}_{S}S}{Ab^{88}_{N}N + Ab^{86}_{S}S} \quad \text{.....(2.1)}$$

where the N is a total number of Sr atoms in the known amount of water, the S is a total number of Sr atoms in the spike solution, the $Ab^{86}{}_{N}/Ab^{88}{}_{N}$ is abundances of the Sr^{86} and Sr^{88} in waters, and the $Ab^{86}{}_{S}/Ab^{88}{}_{S}$ is an abundances of the Sr^{86} and Sr^{88} in the spike solution.

For the N/S atomic ratio is converted in to the weight ratio by multiplication with the ratio, the weight ratio is solved for N, and the weight of strontium in samples for S. Therefore, the concentration of the strontium spike solution was determined by isotope dilution, using a standard of normal isotopic composition.

2.2.4 Rare-earth elements

All water samples were analyzed the REEs by ICP-MS on the PerkinElmer DRC II (Sciex, Canada) at the department of Geochemistry (Geoscience Centre, University of Göttingen, Germany). Geochemical classification of the REEs is largely determined for commoner cations on the basis of their high reactivity in the metallic state. For the research has focused on the use of REEs in understanding the water-rock interactions in hot spring systems. Thought the water-rock interaction imparts the comparable REE signature to the hot spring water that is related to that of the rocks through which the hot water flows.

For all REEs consist of cerium (Ce), dysprosium (Dy), erbium (Er), europium (Eu), gadolinium (Gd), holmium (Ho), lanthanum (La), lutetium (Lu), neodymium (Nd), praseodymium (Pr), promethium (Pm), samarium (Sm), scandium (Sc), terbium (Tb), thulium (Tm), ytterbium (Yb), and yttrium (Y) with are also known as the lanthanide series elements. The elements are divided into two major groups based on mass; the light REEs (LREEs) La through Eu, and the heavy REEs (HREEs) Gd through La (Taylor and McLennan, 1988). Fractionation between HREEs and LREEs may result from the geologic processes, as the consequence of the differences in ionic radii between individual REEs and REEs bonding capacities with anions (Fee et al., 1992).

For REE patterns in part acquired from hot spring water samples of Southern Thailand are possible applying normalizing procedure to differentiation products might expect three types; (a) horizontal line for materials having the same REE distributions as the chondritic meteorites, (b) positive slope for the normalized curve denotes the material enriched in heavier lanthanides, and (c) negative slope for normalized curve indicates enrichment in lighter lanthanides.

2.2.5 Geothermometers

Silica geothermometer

A silica geothermometer measurement is based on the solubility of quartz and chalcedony, which is widely used to estimate the subsurface temperature of geothermal systems (Fournier and Rowe, 1966). A solubility of minerals generally changes as the function of temperature shown in Table 2.2.

Table 2.2 Equations for the silica geothermometer (after Fournier and Rowe, 1966)

Silica geothermometer	Equation
Quartz-no steam loss	$t°C = \frac{1309}{5.19 - \log S} - 273.15$
Quartz-maximum steam loss at 100°C	$t°C = \frac{1522}{5.75 - \log S} - 273.15$
Chalcedony	$t°C = \frac{1032}{4.69 - \log S} - 273.15$
α-Cristobalite	$t°C = \frac{1000}{4.78 - \log S} - 273.15$
β- Cristobalite	$t°C = \frac{781}{4.51 - \log S} - 273.15$
Amorphous silica	$t°C = \frac{731}{4.52 - \log S} - 273.15$

Cation geothermometers

The cation geothermometers are widely used to calculate the subsurface temperature of the waters collected from the hot springs and wells. They are based on the ion exchange reaction with the temperature-dependent equilibrium constant. Equations for the various geothermometers are given in Table 2.3

Table 2.3 Equations for the cation geothermometers

Geothermometer	Equation	Source
Na-K	$t°C = \frac{856}{0.857 + \log(Na/K)} - 273.15$	Truesdell, 1976
	$t°C = \frac{933}{0.993 + \log(Na/K)} - 273.15$ (25-250°C) $t°C = \frac{1319}{1.699 + \log(Na/K)} - 273.15$ (250-350°C)	Arnorsson, 1983
	$t°C = \frac{1217}{1.483 + \log(Na/K)} - 273.15$	Fournier, 1983
	$t°C = \frac{1390}{1.750 + \log(Na/K)} - 273.15$	Giggenbach, 1988
Na-Mg	$t°C = \frac{4410}{14.00 + \log(K/\sqrt{Mg})} - 273.15$	Giggenbach, 1988
Na-Li	$t°C = \frac{1590}{0.779 + \log(Na/Li)} - 273.15$	Kharaka et al., 1982
Na-Li (Cl<0.3M)	$t°C = \frac{1000}{0.389 + \log(Na/Li)} - 273.15$	Fouillac and Michard, 1982
Na-Li (Cl>0.3M)	$t°C = \frac{1195}{0.130 + \log(Na/Li)} - 273.15$	Fouillac and Michard, 1982
Na-Ca	$t°C = \frac{1096.7}{2.370 - \log(Na/\sqrt{Ca})} - 273.15$	Tonani, 1980
K-Ca	$t°C = \frac{1930}{2.920 - \log(K/\sqrt{Ca})} - 273.15$	Tonani, 1980
Na-K-Ca	$t°C = \frac{1647}{\log(Na/K) + \beta[\log(\sqrt{Ca}/Na) + 2.06] + 2.47} - 273.15$ $\beta = 4/3$ for t<100°C; $\beta = 1/3$ for t>100°C	Fournier and Truesdell, 1973

2.3 Geophysical exploration

Vertical electrical sounding (VES) surveys and electrical resistivity tomography (ERT) were carried out for investigations of the shallow subsurface. Shallow seismic reflection (SSR) profiles were done to image deeper sections. Magnetotellurics (MT) is planned to delineate hot spring water down to a depth of a few kilometers. All the steps are briefly described as following.

2.3.1 Electrical resistivity surveys

Based on the principles of electrical resistivity survey assumes the isotropic and homogeneous ground. As the electricity flows in all directions from the point source; all points equidistant from the source will show the same electrical potential, which the generally factors include elementary and mineral composition; granularity, porosity, pore fluids, and temperature. For the variations in the size, shape, location and conductivity of the subsurface materials alter the distribution of the electric potential are consisted. It is possible to obtain information about the subsurface from the potential measurements made at the surface. Hence, the possibility of the subsurface structure of the study area was included; (a) the surface conditions and depth to water table, (b) the abrupt deviations in apparent resistivity, and (c) the substantial vertical or horizontal resistivity contrasts in subsurface layers. For the general steps of the resistivity processes were represented in Figure 2.3.

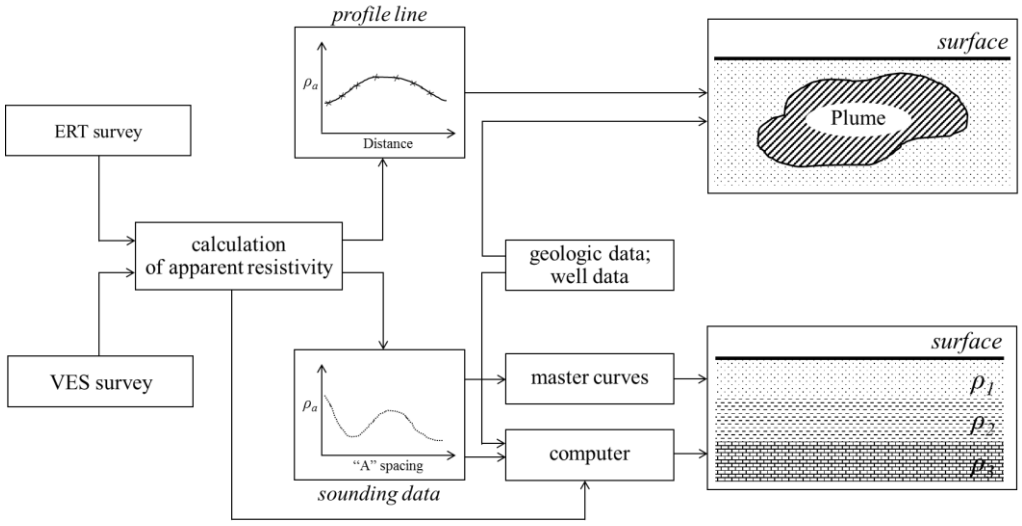

Figure 2.3 Schematic diagram of electrical resistivity processes.

Vertical electrical soundings (VES) survey

All VES surveys have been recorded by ABEM Terrameter SAS 1000 using the Schlumberger array with the minimum AB/2 of about 100 m, which is adequate for investigations of the shallow hot spring systems (Kearey et al., 2002). The VES method is carried out by keeping the center point stationary and successively moving the current electrodes farther apart, the apparent resistivity is measured at each spacing. In the field, the electrodes are usually arranged in the straight line with the potential electrodes placed inside the current electrodes and symmetrically arranged with respect to the center of the configuration (Kearey et al., 2002).

The Schlumberger electrode configuration was employed for this research (see Figure 2.4), in which the current electrodes of A and B are moved apart while keeping the potential electrodes of M and N at a relatively close spacing. A distance between A and B is successively increased logarithmically, the exact interval desired is dependent upon the geological setting in the survey area. During the course of each sounding, the potential electrodes spacing (MN) is kept as small as possible - very small compared to the AB spacing. If the MN spacing is not increased, then the potential difference becomes too small to measure accurately. When the potential electrode spacing is increased, the current electrodes are kept at the same spacing for one overlap reading to facilitate the detection of any surface inhomogeneity in the area around the potential electrodes (Kearey et al., 2002).

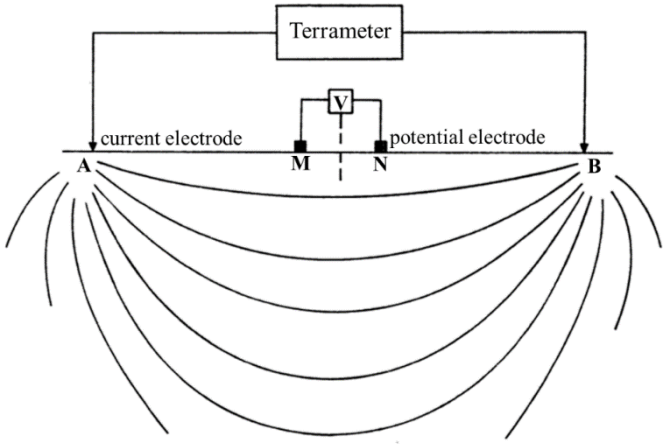

Figure 2.4 Arrangement of apparatus for the Schlumberger electrical soundings, showing the form of current flow in a semi-infinite earth.

Considering, if the direct current of strength I is introduced into the homogeneous isotropic earth at the two current electrodes, A and B; the potential difference V measured between M and N is given by the Equation 2.2 (Kearey et al., 2002).

$$V = \frac{I\rho}{2\pi}\left[\left(\frac{1}{AM} - \frac{1}{BM}\right) - \left(\frac{1}{AN} - \frac{1}{BN}\right)\right] \quad \text{..... (2.2)}$$

Thus, the apparent resistivity (ρ_a) for each electrode position was calculated;

$$\rho_a = \frac{\pi}{4}\left[\frac{(AB)^2 - (MN)^2}{MN}\right]\frac{\Delta V}{I} \quad \text{..... (2.3)}$$

where the V is the potential between M and N, measured with voltmeter (mV) and the I is the current into ground at A and B, generated by DC transmitter (mA); see Kearey et al. (2002).

The series of successive apparent resistivity are measured at the each VES point giving the weighted average resistivity at the specific current electrode spacing. When the VES point is completed, each apparent resistivity (ρ_a) is plotted, AB/2 on semi-log graphs, from which the quantitative solution may be interpreted.

Electrical resistivity tomography (ERT) survey

The ERT surveys were carried out with the ABEM Terrameter SAS 1000 with ABEM Lund Imaging System (Lund University, Lund, Sweden) using the dipole–dipole configuration by applying different layouts. Maximal electrode spacing was 25 m and with the n-factor of 8. For the RES2DINV version 3.4 (Loke and Barker, 1996; Loke and Dahlin, 2002) was used for the inversion of two-dimensional spatial distribution of resistivity values from ERT.

The surveys focused on the dipole-dipole configuration that refer to the number of the four-electrode configurations in which the potential electrodes P1 and P2 are outside the current electrodes C1 and C2, each pair or dipole having a constant mutual separation ‘a’ shown on Figure 2.5 (Kearey et al. 2002). Various arrangements

are possible depending on the relative orientation of the pairs. The distance between the electrode pairs is normally greater than their individual spacing and in the ideal case it is considerably larger. In the latter case measurements are made of the curvature of a potential field. For the apparent resistivity (ρ_a) is given by Equation 2.4.

$$\rho_a = \pi \frac{\Delta V}{I} n(n+1)(n+2)a \quad \text{.....(2.4)}$$

where the C1 and C2 are the current electrodes; the P1 and P2 are the potential electrodes, the a is the spacing between electrodes used for each measurement and the n is the expansion factor (Kearey et al. 2002).

Sounding part is done by increasing n in steps and profiling part is done by moving along the ground surface the whole system without altering the interelectrode distances.

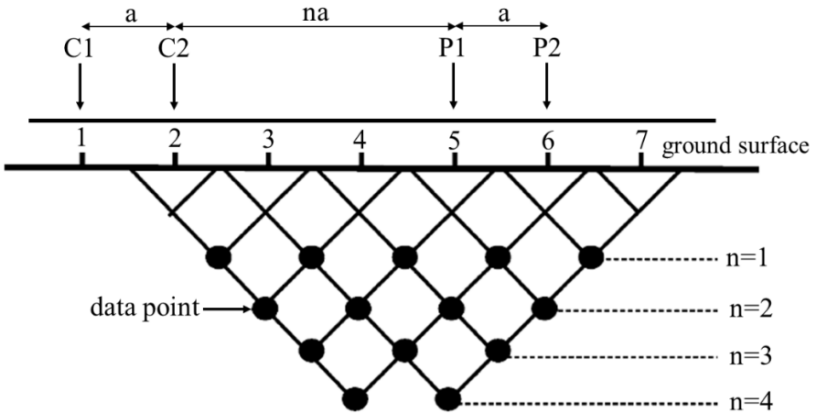

Figure 2.5 Configuration of the dipole–dipole array used for ERT surveys.

As mentioned above the polar dipole configuration has been used widely for induced polarization and in particular frequency domain measurements. A usual field procedure is to make series of measurements with a fixed dipole length (Loke and Barker, 1996; Loke and Dahlin, 2002), while dipoles are being separated by the variable integral number of dipole lengths ‘na’ (Figure 2.5). Since the larger ‘n’ values are associated with depths of investigation (Loke and Barker, 1996; Loke and

Dahlin, 2002). Consequently, the data can be arranged in the two-dimensional "pseudosection" plot which gives the simultaneous display of both horizontal and vertical variations in apparent resistivity.

2.3.2 Shallow seismic reflection survey

The SSR surveys have been recorded with the Geometrics Smartseis S-24 (Geometrics Inc., San Jose, CA, USA) with following parameters: (a) 10 kg sledgehammer source, 5-10 shots per source point, 5 m shot spacing, (b) vertical geophones with 14 Hz natural frequency (single), 5 m geophone spacing, (c) 20 m/135 m min/max offset, maximum fold 12, distance between CMP 2.5 m, and (d) record length 1,024 ms, and sampling interval 0.5 ms. Data processing was done with Globe Claritas software (Ravens 2007) following normal shallow seismic reflection processing steps, including a 20-40-150-250 Hz band path filter and NMO correction.

In the part of the reflection data was analyzed by means of the arrival time versus offset distance plots, with the events typically arrive in a timing window, bounded by the first arrival refracted waves and the later air wave arrival (Kearey et al. 2002). The reflection events are recognized by their hyperbolic curvature on the time-distance plot whereas refraction, air and surface waves plot as straight lines. By virtue of their linear character, refraction events provide the means with which to calculate the velocity (V_n) and the thickness (ΔZ) of underlying units by the fitting hyperbolas to each reflection event (t_n, V_n^{rms}) for n = 1, 2,... is represented by Equations below (Kearey et al. 2002):

$$V_n \approx \left[\frac{\left(V_n^{RMS}\right)^2 t_n - \left(V_{n-1}^{RMS}\right)^2 t_{n-1}}{t_n - t_{n-1}} \right]^{1/2} \quad \text{.....(2.5)}$$

$$\Delta Z = Z_n - Z_{n-1} = \left(\frac{t_n - t_{n-1}}{2} \right) V_n \quad \text{.....(2.6)}$$

For the equations 2.5 and 2.6, the interval velocity and thickness of the n^{th} layer are directly obtainable from the definition of V_n^{rms} given by Equations 2.7.

$$V_n^{RMS^2} = \frac{\sum_{i=1}^{n} v_i^2 \tau_i}{\sum_{i=1}^{n} \tau_i} \quad \text{.....(2.7)}$$

where v_i is velocity of the i^{th} layer, and τ_i is one-way travel time through the i^{th} layer (Kearey et al. 2002).

The accuracy of the layer velocities and depths calculated from the reflection method is dependent upon the error associated with arrival time interpretations and in the measuring offset distances. Determining the specific accuracy of calculated velocities and depths is impossible because of the difficulty in estimating the precision of graphical methods employed.

2.3.4 Magnetotellurics survey

The MT survey was designed by using a grid profile with interval stations ranged from 500 m to 1,000 m. The distance between stations was depending on available spaces of the study area. A series of audio-magnetotelluric surveys was carried out with hardware from KMS Technologies–KJT Enterprises Inc., Houston, Texas, consisting of two components of an electric field in x- and y-directions and two components of a magnetic field in x-, y- and z-direction. Frequency ranges from 10 kHz to 0.001 Hz were recorded simultaneously by an analogue data recorder for about twenty hours. All MT data recorded on an internal hard disk were downloaded through the connection to the field laptop. Power was supplied by a 12 V external battery. The data was processed with using the KMS processing software based on a robust multiple-station technique. A parallel version of WSINV3DMT (Siripunvaraporn and Egbert, 2009; Siripunvaraporn et al., 2005) was used to invert selected impedance tensor.

MT surveying method has considered a coordinate system at Earth's surface, with axes aligned having x-north, y-east, and z-down (Siripunvaraporn and Egbert, 2009; Siripunvaraporn et al., 2005). A plane wave generated by a source in an ionosphere is given by Equation 2.8 (Chave and Jones, 2012).

$$Z = \frac{E_x}{H_y} \quad \text{.....(2.8)}$$

where Z is a characteristic impedance, E_x is an electric field intensity (north) in mV/km and H_y is a magnetic field intensity (east).

Assumption made that the Earth's is homogeneous and isotropic then all true resistivity values are related to the characteristic impedance (surge impedance) through the relation represented by the Equation 2.9 (Chave and Jones, 2012).

$$\rho = 0.2T|Z|^2 \quad \text{.....(2.9)}$$

where the ρ is the resistivity (ohm-m) and the T is the period (sec.).

In case of the horizontally layered earth, the equation 2.9 become the apparent resistivity (ρ_a) represented by the Equation 2.10 (Chave and Jones, 2012),

$$\rho_a = 0.2T\left|\frac{E_x}{H_y}\right|^2 \quad \text{.....(2.10)}$$

A slightly more complicated situation exists between electric and magnetic fields in regions where the Earth's has a more complicated structure than simple plane layers (Cagniard, 1953; Everett and Hyndman, 1967). A lateral discontinuity of each point in the vicinity is affected on a linear coupling between electric field component and a combination of both magnetic field components represented by the Equation 2.11 (Chave and Jones, 2012).

$$E_x = aH_x + bH_y \quad \text{.....(2.11)}$$

where 'a and b' are called coupling coefficients. Both parameters depend on position, coordinate directions, period, geometry and electrical properties of a lateral

inhomogeneity (Cagniard, 1953; Everett and Hyndman, 1967). Defining the impedance tensor in Equation 2.12 (Chave and Jones, 2012):

$$[Z] = \begin{bmatrix} Z_{xx} & Z_{xy} \\ Z_{yx} & Z_{yy} \end{bmatrix} \quad \text{.....(2.12)}$$

Generalized the equation 2.11 to relation of the form $E = [Z] \cdot H$ or represented by the Equation 2.13 (Chave and Jones, 2012).

$$E_x = Z_{xx}H_x + Z_{xy}H_y \text{ , and } E_y = Z_{yx}H_x + Z_{yy}H_y \quad \text{..... (2.13)}$$

However, Maxwell's equations are separated into two modes for a strictly two-dimensional geometry. The first mode explained the E-parallel to strike that depends only on H-perpendicular to strike (Cagniard, 1953; Everett and Hyndman, 1967). The second mode focuses on the E-perpendicular to strike depending only on H-parallel to strike of the tensor decouples (Cagniard, 1953; Everett and Hyndman, 1967) represented by the Equation 2.14 (Chave and Jones, 2012).

$$E'_x = Z'_{xy}H'_y \text{ , and } E'_y = Z'_{yx}H'_x \quad \text{.....(2.14)}$$

where prime indicates that the measuring axes X and Y are parallel aligned and perpendicular to the strike of the two-dimensional lateral inhomogeneity.

2.4 Assessment and ranking

As the potential of geothermal hot spring systems in Southern Thailand might vary an evaluation and ranking was necessary. Significant information of heat source and reservoir characteristics have required from detailed study of hot spring sites. Detailed investigations are including heat flow and hydrology, geochemistry of fluids, exploration technology and reservoir mechanics as well as land use and marketing (Muffler and Christiansen, 1978/79; Pasqualetti, 1981). In case well data for a site would be available, a relatively straightforward and established methodology

is available to develop these estimates (e.g. Muffler and Christiansen, 1978/79). But for geothermal hot spring sites in Southern Thailand well or subsurface data, like temperature gradient and hot water flow rates, for example, is often not available.

A set of parameters, selection criteria utilizing positive attitude factors, has been established for this study to determine which sites have a good potential and thus should be further characterized in detail. The assessment is based on all presently available, respectively known and accessible, geological, geophysical, geochemical, and other relevant data about these geothermal hot spring systems coming from various sources produced over time (Campos, 1988; Quinao and Zarrouk, 2018; Campos, 1988). Available information about land uses and market feasibility were also assessed as they are part of the fundamentals for an economic feasibility of the geothermal development project.

2.4.1 Positive attitude factors design

The design for the geothermal resource assessment here is using the positive attitude factors for the characterization of geothermal resources listed. The assessment was designed to find factors, which allow all resources to be evaluated on a common basis and thus to allow resource sites to be ranked (Bignall and Sanders, 2016; Muffler and Cataldi, 1978). This technique can help to collate geothermal resource data and to provide continuously updated estimates of geothermal resources potential. Each of these factors is briefly described along with the positive attitude and possible applications Figure 2.6.

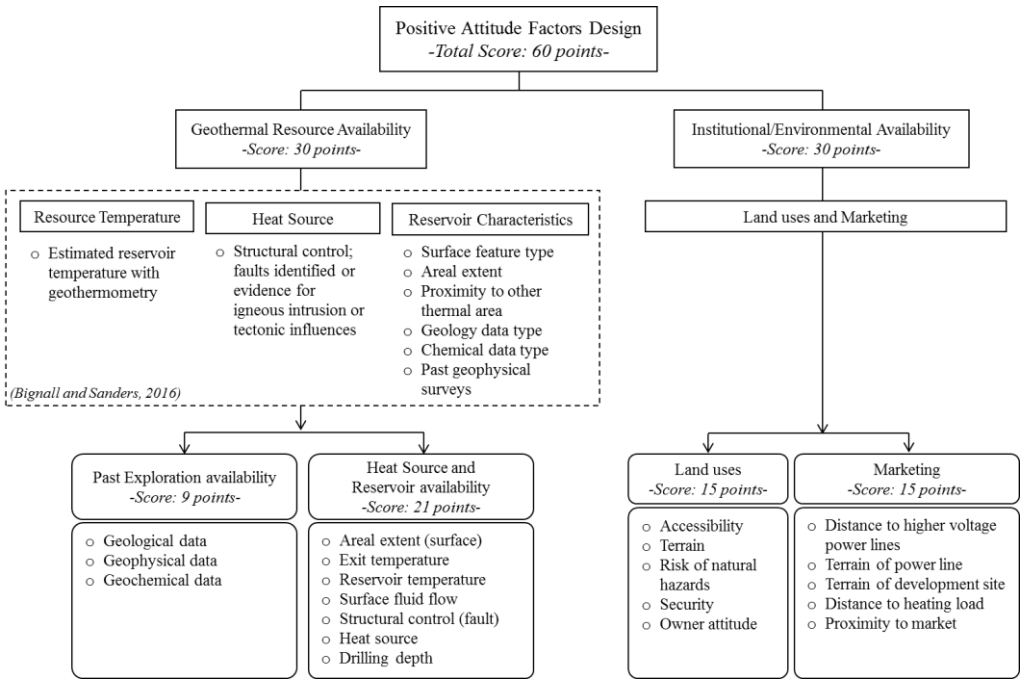

Figure 2.6 Positive attitude factors design flowchart. Final criteria in the bottom row.

The relative ranking of geothermal resources shown in Figure 2.6 is an analytical method based on a weighted variable evaluation of geothermal resource favorability (Bignall and Sanders, 2016). Factor analysis of the geothermal development potential is divided into four broad concerns (fractions): land use, exploration, reservoir, and market factors (Figure 2.6). Ranking criteria are given to each variable to indicate its relative importance in the assessment. Normalized scores of the positive attitude factors method are given from 3 (highest) to 1 (lowest), which are independent variables that relate to the characterization of each factor. Subsequently the scores of all factors will be summarized into a total score, which is an indication if a site has a good potential to be developed or not; a higher total score is better than a lower one. According to Muffler and Cataldi, (1978), these scores should not be strictly interpreted. Uncertainty may exist in an assignment of the numbers. In the following ranking criteria and weights procedure are given and explained in detail. Numbers in brackets are the normalized scores assigned to each factor.

Land use availability

1) Accessibility factors rated;

[3] main road or highway

[2] paved road

[1] rural non-paved road

2) Terrain factors rated;

[3] flat or almost flat topography

[2] hilly, forest, or mangrove

[1] mountainous

3) Risk of natural hazards factors rated;

[3] never

[2] non-frequent events

[1] more frequent events

4) Security factors rated;

[3] no security incidents

[2] security incidents from time to time

[1] security incidents occur monthly

5) Owner attitude (e.g. local people, village, etc.) factors are rated;

[3] strongly agree

[2] agree

[1] indifferent

Past exploration availability

1) Geological factors rated;

[3] complete data, surface, shallow, and deep

[2] almost complete: surface or shallow or deeper

[1] incomplete, or no data available

Supportive comments can be given: Surface information include maps and geological walking survey, for example. Shallow information comprises of rock analysis, X-ray diffraction (XRD) data, or others, whereas deeper information come from geological modeling, for example.

2) Geophysical factors are rated;

[3] complete: surface, shallow, and deeper data

[2] almost complete: surface or shallow or deeper data

[1] incomplete, or no data available

Supportive comments can be given: Surface information comprise of maps or GIS data, whereas shallow information include electrical resistivity data. Deeper information can come from gravity and magnetotelluric surveys, or others.

3) Geochemical factors (not separated into shallow to deep) are rated;

[3] complete isotope data

[2] cation/anion composition, geothermometer data

[1] no data

Reservoir availability

1) Areal extension (surface) was rated;

[3] large-surface expression ($\geq$ 1 km^2)

[2] medium-surface expression (>0.5 km^2 to <1 km^2)

[1] small-surface expression (<0.5 km^2)

2) Exit temperatures rated;

[3] high-surface discharge temperatures ($\geq$80 °C)

[2] intermediate-surface discharge (>70°C to <80°C)

[1] low-surface discharge temperatures (60°C to <70°C)

3) Shallow reservoir temperature factors rated;

[3] high-temperature systems (≥150°C)

[2] intermediate-temperature (150°C to ≥90°C)

[1] low-temperature systems (<90°C)

4) Surface fluid flow factors rated;

[3] higher flow rates (≥1 L/s)

[2] lower flow rates (>0.1 L/s to <1 L/s)

[1] no data

5) Structural control rated;

[3] main large faults or fractures

[2] subordinate faults or fractures

[1] no faults or fractures

6) Heat source rated;

[3] only granite settings

[2] granite and sedimentary/metamorphic settings

[1] only the sedimentary or metamorphic settings

7) Drilling depth rated;

[3] less than 150 meters

[2] over 150 meters, but not exceeding 500 meters

[1] exceeding 500 meters

Marketing availability

1) Distance to higher voltage power lines rated;

[3] close-less than 500 meters

[2] over 500 meters, but not exceeding 1,000 meters

[1] far-exceeding 1,000 meters

2) Terrain of power line corridor rated;

[3] flat or almost flat topography

[2] hilly, forest or mangrove

[1] mountainous terrain

3) Terrain of development site rated;

[3] flat or almost flat topography

[2] hilly, forest or mangrove

[1] mountainous terrain

4) Distance from well to plant site rated;

[3] close to less than 200 meters

[2] over 200 meters, but not exceeding 500 meters

[1] far-exceeding 500 meters

5) Proximity to market factors rated;

[3] close, less than 20 km

[2] moderate, over 20 km, but not exceeding 50 km

[1] far-exceeding 50 km

2.4.2 Site selection criteria

The proposed assessments and subsequent ranking of the hot spring sites in Southern Thailand requires a certain selection or prioritization before due to the overall number of hot springs, which is the step 1. This initial step here was done using a surface discharge temperature of less than 60 °C, and a silica geothermometer of the reservoir temperature of less than 100 °C; with higher temperatures favorable. Due to recent advances in binary generator technology hydrothermal systems with temperatures in the 90-150 °C temperature range are capable of generating electricity. For the reservoir temperature, a silica geothermometer was chosen because the ion concentrations used here depend on the temperature-dependent solubility. Thus, the silica concentration in a residual liquid increases in proportion to the amount of boiling. In the step 2, the percentage of each fractional score of the land and exploration factors was set by ≥80%, whereas for reservoir and marketing factors the value was set lower, ≥60%, as for the latter two less data were available. In the step 3 all hot spring sites are separated in sites favorable for geothermal resource based electricity generation and in sites only possible for direct use shown in Figure 2.7.

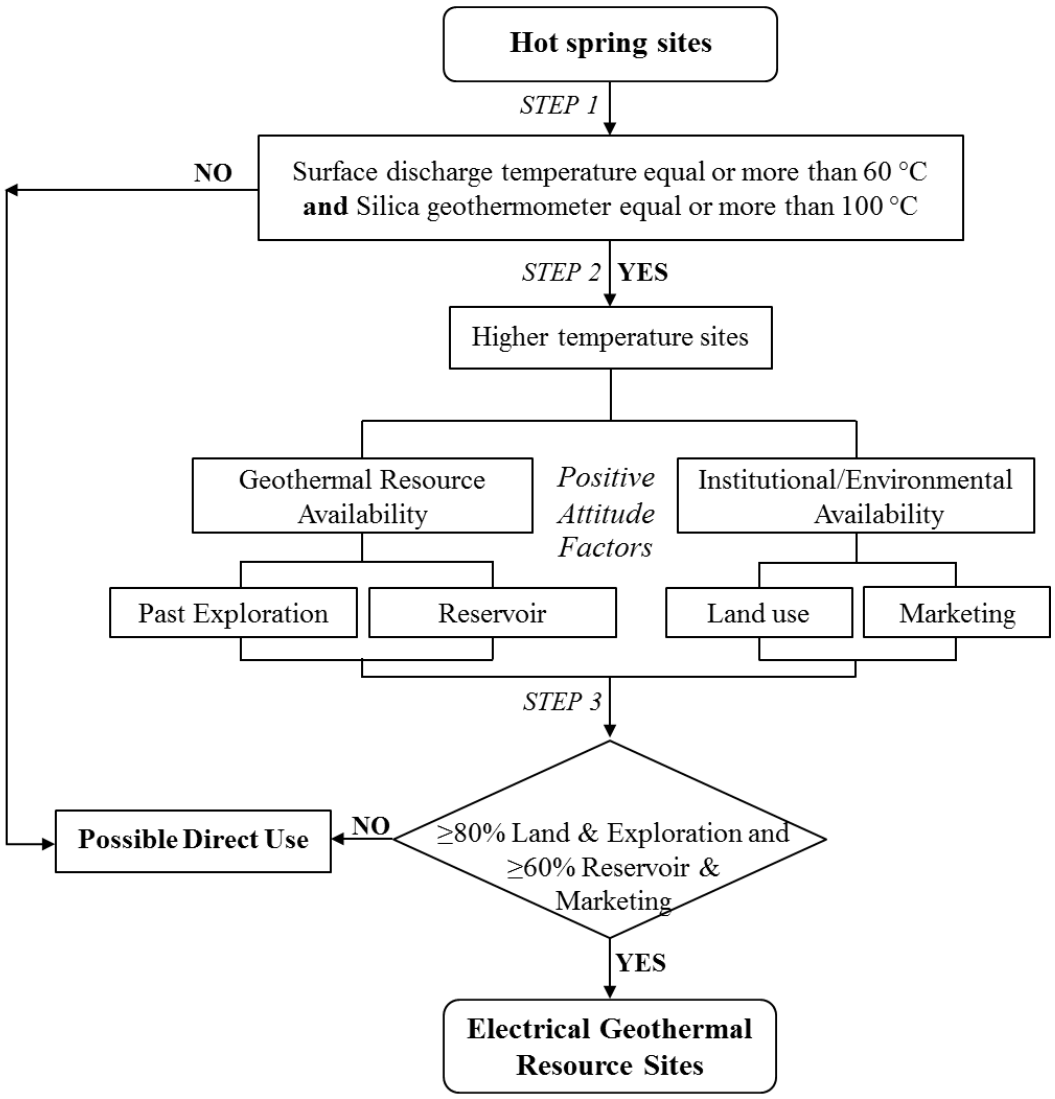

Figure 2.7 Site selection criteria flowchart.

Geothermal hot spring sites, which pass the selection criteria for the electrical generation sites, will be placed on the final list. Potential direct utilization sites which lack the geothermal resource availability of resource temperatures or reservoir characteristics are dropped to the scores as shown in Figure 2.7. The site that passes the selection criteria, and is listed as the electrical generation site, may also be considered as the direct utilization site.

2.5 Geothermal power generation

Although no well data are available for the geothermal sites, the potential of the geothermal electrical power production can be estimated by using properties of hydrothermal fluids (e.g. Yuksel et al. 2018; Zarrouk and Moon, 2014; Bertani, 2012), as the amount of electrical power output depends on them and the technology and type of power plant used (Zarrouk and Moon, 2014; Bertani, 2012).

A possible choice of a geothermal power plant technology in Southern Thailand is a binary cycle power plant; a closed system that converted heat from a thermal fluid into electricity by transferring heat to an organic working fluid, and then produces vapor to generate electricity. Calculating generated electricity was presented with net generated electric power (NEP) (Bertani, 2012; DiPippo, 2007), assuming the plants was running at full capacity. DiPippo (2007) proposed Equation 2.15 for calculating NEP. Based on that value for the feasibility of a binary power plant were calculated using inlet temperatures between 80 and 150°C and outlet temperatures of 40°C and 50°C. The relative efficiency will be roughly 58±4% of the triangular efficiency, when adequate accuracy is represented by the Equation 2.15 (DiPippo, 2007).

$$NEP = 2.47\dot{m}\left(\frac{T_{in} - T_o}{T_{in} + T_o}\right)(T_{in} - T_{out}) \text{.....} (2.15)$$

where NEP is the net generated electric power, kWe, ṁ is the total mass, kg/s, T_o is the dead-state temperature, 20°C, T_{in} is the geothermal inlet temperature of the primary fluid, °C, and T_{out} is the geothermal outlet temperature, °C.

CHAPTER 3
RESULTS AND DISCUSSIONS

3.1 Geochemistry of hot springs in Southern Thailand

3.1.1 Water properties

Altogether 30 hot spring water samples of eight geothermal hot spring systems in Southern Thailand were collected with the surface discharge temperatures on-site represented by Table 1.1. All samples were collected and transported in the heat and chemical resistant plastic bottles. Chemical analysis of major cations and anions and also pH determination, all shown in Table 3.1, were carried out not more than one or two days after water collection at the Central Equipment Division, Faculty of Science, Prince of Songkla University, Thailand, using standard procedures outlined in Table 2.1. The pH values of all samples are in a normal range between 6.7 and 8.4. For a total dissolved solid (TDS) content is in a general moderate with some quite high exceptions, SR1, SR3, KB2, KB4, and TR2; mostly related to higher Na^+ and Cl^- content and to a minor extent Ca^{2+}, K^+, and SO_4^{2-}. These five hot springs are all more or less influenced by shallower marine water ingression as their locations are relatively close to an estuary or a major river system connecting to the ocean. KB4 site of Krabi geothermal system is classified and named saline hot spring as a salinity reaches more than 2.1 ppt (21,000 mg/L) giving the water a clear salty taste.

Table 3.1 Surface temperatures, pH, concentrations of cations and anions and reservoir temperatures of hot springs in Southern Thailand

Hot spring	Surface temp. (°C)	pH	Content (mg/L)					Geothermometer (°C)		
			TDS	Na^+	K^+	Ca^{2+}	SiO_2	Silica	Na-K	Na-K-Ca
CP1	50	7.8	580	63.50	6.80	89.50	64.20	114	223	154
RN1	65	8.3	330	48.40	2.80	44.10	79.30	125	174	128
RN2	40	8.3	330	46.40	3.20	44.10	75.50	122	187	135
RN3	45	8.4	330	46.90	3	44.30	72	120	181	132
RN4	50	8.2	240	46.10	2	17.80	87	130	155	121
RN5	46	8.3	310	51.30	3.50	28.10	111	130	155	122
RN6	75	8.1	580	63.50	6.80	89.50	64.20	143	186	139
SR1	45	7.7	13690	3850	1320	933	65	114	140	147
SR2	40	7.8	7180	1855	64.20	400	39	91	140	143
SR3	60	7.9	12610	3655	115	840	58.50	109	135	143
SR4	41	8.3	270	20.5	2.40	27.80	37.40	89	231	150
SR5	42	8.4	320	55.90	6.00	20.90	80.20	125	223	164
SR6	53	8.1	740	44.80	5.20	97.10	53.60	105	230	152
SR7	70	7.9	1980	64.50	13.60	381	60.70	111	291	177
SR8	56	7.2	62	59.70	12.80	69.60	66.30	115	292	192
SR9	62	6.8	1300	12.10	4.60	265	62	112	367	182
PG1	78	7.8	280	84.00	3.30	6.90	77.70	124	148	132
PG2	55	6.8	390	108.60	3.10	2.60	62.50	123	150	142
PG3	45	6.9	5100	1250	50.30	515	77	123	150	142
KB1	45	7.2	350	24.90	2.50	86.30	26.80	75	217	137
KB2	47	7.3	16120	4450	125	975	44.40	96	128	140
KB3	45	7.2	3300	986	22.10	382	25.50	73	115	115
KB4	47	7.2	20600	12500	395.50	833	32.10	82	134	147
KB5	47	7.0	480	2.30	1.30	86.30	61	111	426	182
TR1	52	7.1	590	79.10	2.80	82.10	61	111	142	111
PL1	57	7.7	265	39.10	3.70	45.50	25.50	73	212	146
PL2	46	8.0	255	72.90	3.20	3.00	84.30	128	156	142
PL3	50	8.0	240	69.70	3.20	5.10	73.60	121	158	139
PL4	41	6.9	418	21.70	2.90	21.90	38.90	90	243	159
YL1	80	7.8	330	76.60	6.40	16.70	97.60	136	202	159

Piper and Cl^{-}-SO_4^{2-}-HCO_3^{-} diagrams were used to provide graphical displays of a major cation and anion chemistry for hot spring waters in Southern Thailand represented by Figure 3.1 and Figure 3.2. Most of the chemical compositions of hot spring water samples are illustrated that waters are the Ca–Na–bicarbonate rich waters, e.g. Ranong, Phang Nga, Surat Thani and Trang geothermal systems. Moreover, the hot spring water samples are also classified into the Ca^{2+}–Na^{+}–K^{+}–(Mg^{2+})–HCO_3^{-} water, but excepted waters from Krabi (KB) and Surat Thani (SR) systems are indicated a high chloride concentration (Figure 3.1 and Figure 3.2).

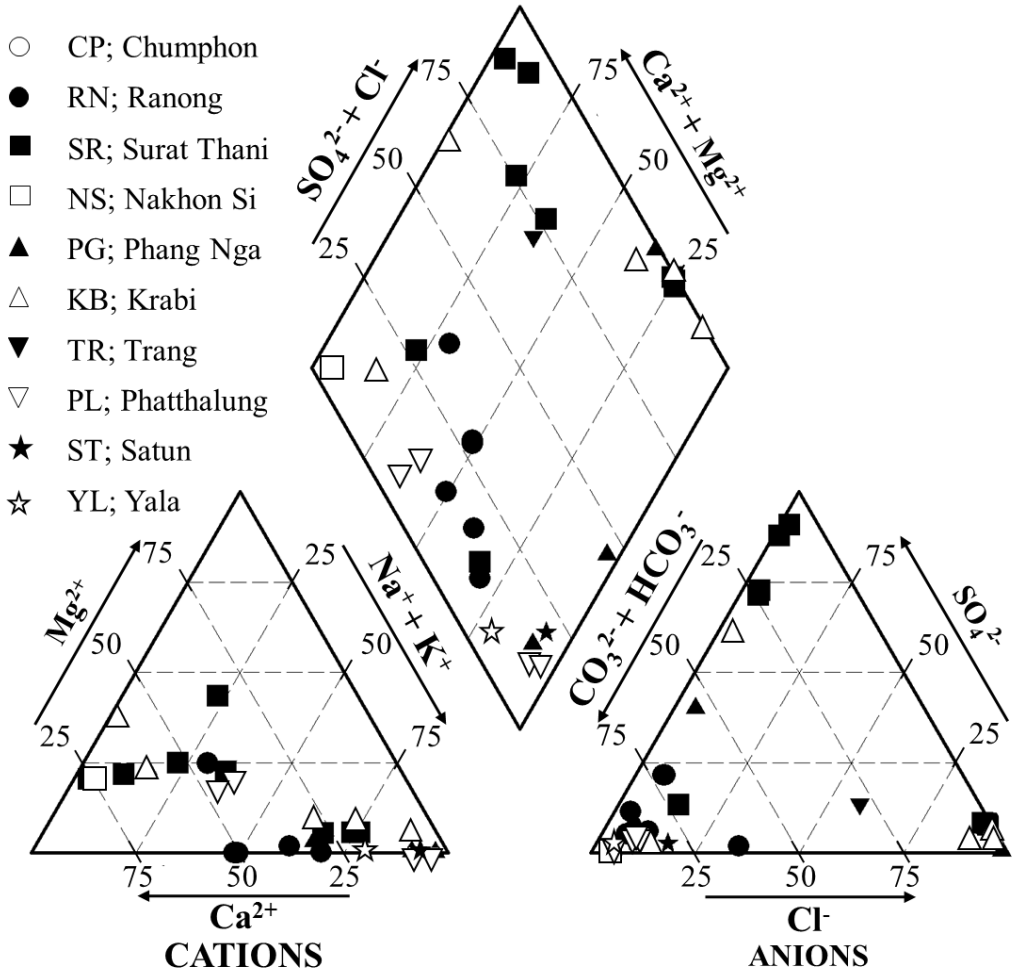

Figure 3.1 Piper diagram of hot spring water samples in Southern Thailand.

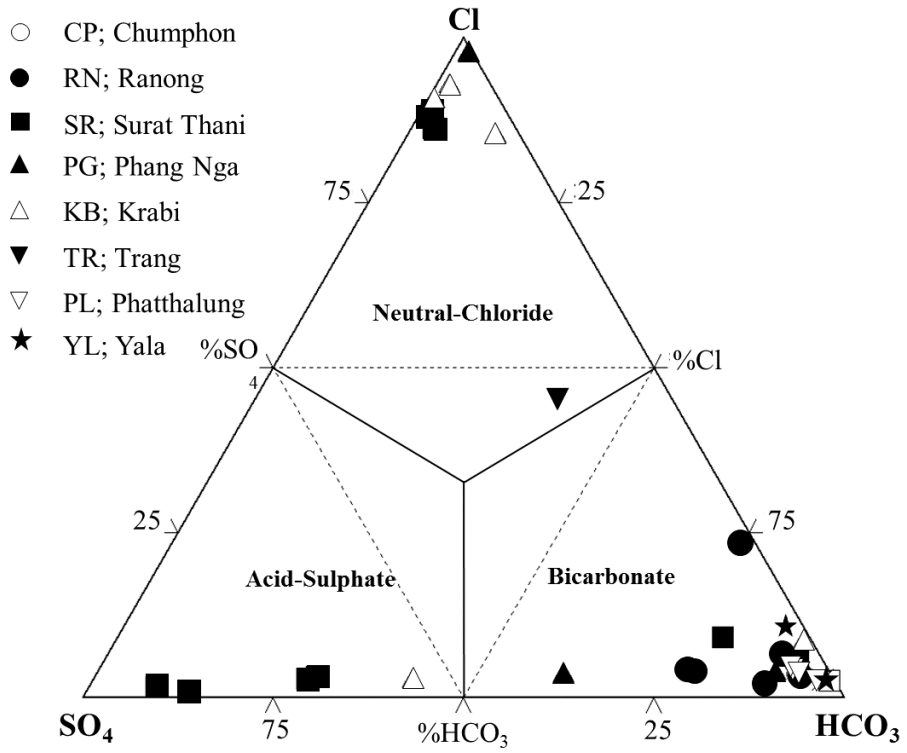

Figure 3.2 Cl-SO_4-HCO_3 diagram of water samples in Southern Thailand, most samples plot in the bicarbonate water region.

The variation of concentrations shown in Figure 3.3a to Figure 3.3f was represented positive proportion trends of Na^+, K^+, Mg^{2+}, Ca^{2+} and SO_4^{2-} against conservative component of Cl^-. Only HCO_3^- concentrations scattered relationships that are not correlated with Cl^-. Although there are wide range of concentrations in Na and Mg, the plots exhibit a progressive increasing trend. Consequently, most of the hot spring waters from southern region are taken part in the much longer and deeper flow path with low concentration of Cl^- than groundwater with high value.

Hence the geochemical data (Table 3.1 and Figure 3.1-3.3) are indicated that all geothermal systems in Southern Thailand experiences mixing before exiting to the surface between the original hot water and the meteoric waters of the shallow subsurface, but of different degree. Bicarbonate-rich chemistry represents the main part of shallow groundwater aquifer characteristics, thus, evidence points to rather extensive mixing in most cases.

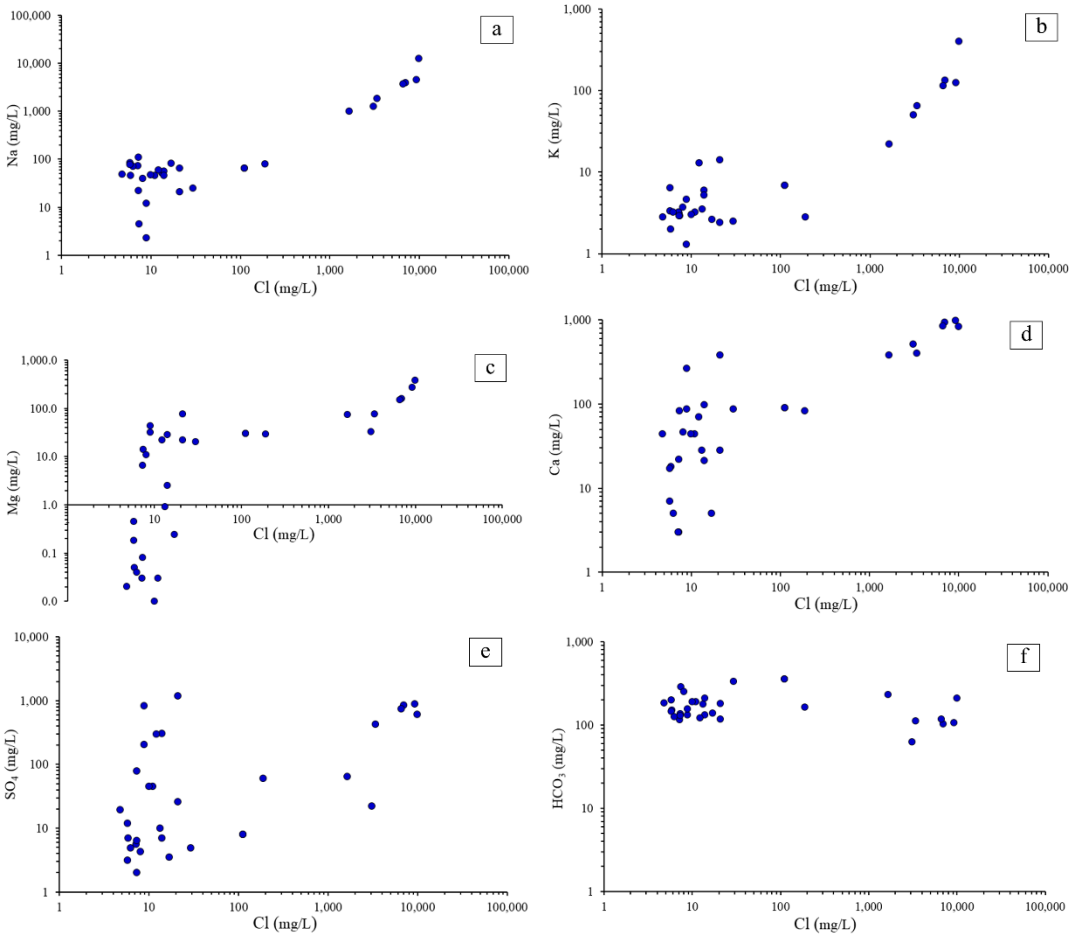

Figure 3.3 Variations of concentrations of major inorganic ions against conservative component of Cl.

3.1.2 Subsurface temperatures

Subsurface temperatures were estimated by utilizing the chemical water composition with silica and cation geothermometers as shown in Table 2.2, Table 2.3 and Table 3.1. The Na–K geothermometer provides subsurface temperatures for Ranong, Surat Thani and Krabi's KB4 geothermal system of about 220 to 420 °C, which represent also the hottest sites (Figure 3.4). For the Na-K-Ca geothermometer for subsurface temperatures are lower than from the Na-K geothermometer, with values range from 150 to 180 °C. While the silica geothermometer estimated temperatures varied between 70 and 120 °C, which are lower than from the cation geothermometers for all geothermal systems (Figure 3.4). Main difference in the determined subsurface temperatures using different geothermometers can be explained by the mixing of hot water with shallow groundwater, which at some

locations contains seawater related cations (Carotenuto et al., 2016). The silica geothermometer, therefore, seemingly provides more realistic values, although relatively low in comparison.

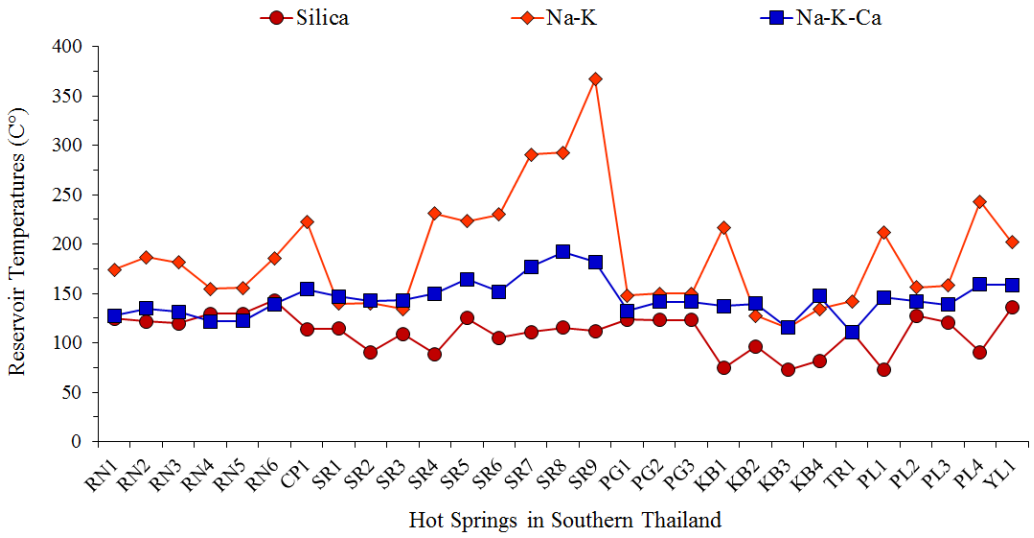

Figure 3.4 Subsurface temperatures of the hot spring systems inferred from Silica, Na–K, and Na–K–Ca of the Cation geothermometers.

3.2 Geothermal resources assessment and ranking

3.2.1 Stage One: Prioritization

All the surface discharge temperatures and the subsurface temperatures of hot spring systems in Southern Thailand are presented in Table 3.1 and Figure 3.4. From the section 2.4.2, the Step 1 was done using a surface discharge temperature of less than 60 °C, and a silica geothermometer of the reservoir temperature of less than 100 °C; with higher temperatures favorable (Figure 2.7). Hence, the subsequent list after Step 1 shows seven geothermal hot springs, RN1, RN6, SR3, SR7, SR9, PG1 and YL1, which were used for the assessment in the second step (Figure 3.5). All the sites selected were assessed in terms of land uses, exploration feasibility, reservoir characteristics, and marketing potential as followed the section 2.4.1. Details of each geothermal hot spring site are as followed.

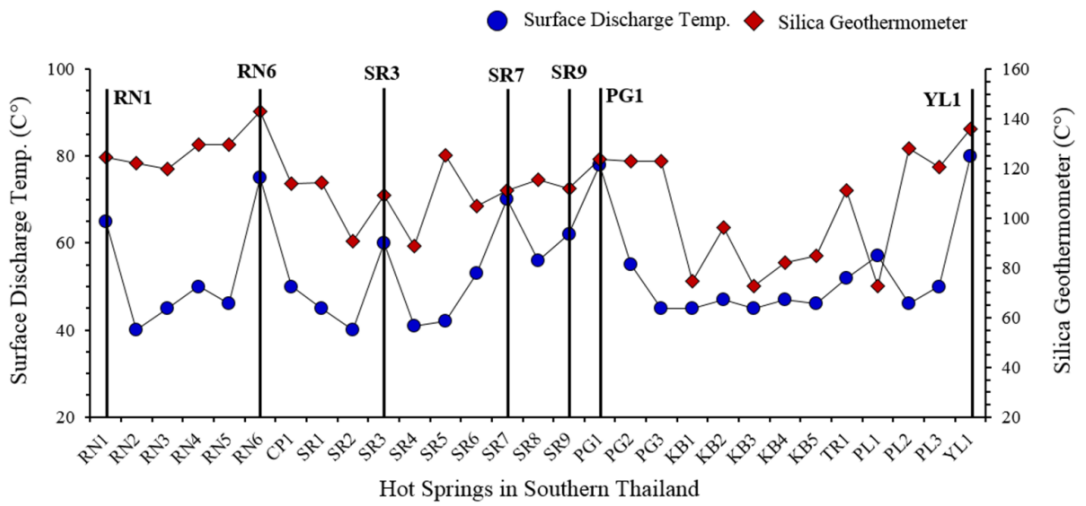

Figure 3.5 Surface discharge temperatures and subsurface temperatures inferred from silica geothermometers; Ranong, RN1 and RN6, Surat Thani, SR3, SR7, and SR9, Phang Nga geothermal system, PG1, and Yala geothermal system, YL1.

RN1 and RN6 of Ranong Geothermal System

The RN1 and RN6 hot spring sites have the highest temperature of the Ranong system. Relatively detailed geological and geophysical investigations have been carried out for all hot spring sites of the system, which is located close to the Ranong Fault Zone (RFZ), a major strike-slip fault. Land gravity and airborne magnetic survey data were used for investigations of possible heat sources and hot water pathways. Results show a greater negative Bouguer gravity anomaly at depth likely to be caused by a batholith, an igneous body in the subsurface, with lower densities than the surrounding rocks due to higher rock temperatures. Gravity modeling put this batholith at a depth of about 4 to 6 km when a density contrast of this batholith to the surrounding rocks is -100 kg/m^3 (Sanmuang et al., 2007). Observed magnetic anomalies show no correlation with the surface geology; therefore it is possible that these magnetic anomalies are caused by rocks enriched in magnetic minerals at depth, around 2 to 5 km, thus supporting igneous bodies at depth. Magnetic susceptibility values used in the modeling were 0.000015 SI for surrounding rocks and 0.01 of the igneous bodies (Khoonphunnarai et al., 2007). In summary, the gravity and magnetic anomalies might resemble the heat source of the Ranong geothermal system.

Chemical compositions of all hot spring water samples show low contents of TDS, Na^+, and Cl^-, thus confirming that the Ranong geothermal system is not influenced by seawater intrusion, although several hot springs are located relatively close to the Andaman Sea. Shallow reservoirs temperatures estimated by silica and cation geothermometers show for 1 km depth 100 to 120 °C.

SR3, SR7 and SR9 of Surat Thani Geothermal System

The SR3, SR7, and SR9 sites show the highest exit temperatures of the Surat Thani system. For the SR3 is located on Mesozoic sedimentary rocks consisting of the small extensional faults in the NNE–SSW to N–S direction (Tan, 1992). Directions of brittle fracture, which cut through major structures, can be interpreted to be associated with the KMFZ, a major strike-slip fault zone. The overall extensional trend indicates a stress pattern where open factures provide open pathways for the geothermal fluids to move upwards (Chinoroje, 1993). Several geophysical surveys were conducted in the Surat Thani geothermal area, utilizing gravity and the resistivity method vertical electrical sounding (VES), see Khawdee et al. (2007) and Khawtawan et al. (2007). Gravity surveys covering the three hot spring areas, SR3, SR7, and SR9, reveal in general a more or less north-south trending complex extensional horst and graben system (also Carnarvon Petroleum Ltd., 2013). Positive gravity anomalies can be correlated to mountains or shallow massive bodies of Permian limestone, which was also confirmed through VES and well data (Khawdee et al., 2007; Khawtawan et al., 2007).

As outlined above, faults and fractures of the horst and graben system can be considered the pathways of the hot water from a deep heat source to the hot spring sites. Geochemical analysis of hot water samples showed that the hot water from deep aquifers mix with shallow groundwater while emerging along faults. The shallow reservoir temperature was estimated by silica and cation geothermometers with 90 to 100 °C at 1.5 km depth, thus indicating a shallow geothermal reservoir due to mixing with fresh meteoric water.

PG1 of Phang Nga Geothermal System

The PG1 can be found close to and at the banks of the Pai Phu River, an area of about 1,000 x 200 m in size. Rocks in and around the PG1 are dominantly granites, which are distributed in the southeastern part and a sedimentary/metamorphic rock unit, which covers other parts (Duerrast et al., 2016). For surface electrical methods, VES and magnetic telluric (MT), were chosen to image hot water pathways and reservoirs at depth. VES surveys for shallow parts gave very similar results when compared to MT data at 50-100 m depth. A low resistivity layer extending to a depth of down to 50-100 m can be considered as topsoil and freshwater aquifers. Deeper than 1 km depth and down to 2 km low resistivity values indicate areas of hotter water-rock systems. Data suggest that the deeper resistivity values are connected along N-S trending larger vertical faults planes; one of it might be the boundary between two granitic bodies at depth (Ngansom et al., 2016). Residual magnetic intensities derived from aeromagnetic measurements show different values suggesting such magnetic bodies at depth, likely to be granites.

Cation and anion concentrations of the hot spring waters are shown in Table 3.1. Isotope signature of hydrogen and oxygen confirms that these waters are of meteoric origin, which then cycle deep along the faults and fractures into the granites (Ngansom et al., 2016). A negative Eu anomaly in the hot spring waters has been induced by the water-rock interaction between these meteoric waters and the igneous rocks with a negative Eu anomaly at depth (Ngansom et al., 2016). Silica geothermometers give an average value of 120 °C for the reservoir temperature representing lower values than most of the cation geothermometers and is probably due to the precipitation of the silica. It is possible that the reservoir depth is deeper than 1 km with possible higher reservoir temperatures (Ngansom et al., 2016).

YL1 of Yala geothermal system

The YL1 site occurs along the N-S trending fault located at the contact between the Betong Formation and the Pa Ret Tu granite. Due to its low content in dissolved minerals and high temperature, the hot water of the YL1 site is believed to have some therapeutic value. Reservoir temperatures are estimated with cation and silica geothermometers give 110 to 120 °C at 1 km depth.

3.2.2 Stage Two: Numerical scoring assessment

For each of factors dependent variable is selected that allows the correlation to determine the relative score for each resource sites (Figure 2.6). Resource scores for seven hot springs in Southern Thailand are shown in Table 3.2 and Figure 3.6 based on the information and data presented at Figure 2.6 and section 2.4.1. Results of the four fractional scores are as follows: 1) Land use: higher scores for RN1, SR7, and PG1 sites, but not maximal values, and lower score for RN6, SR9 and YL1. 2) Exploration: maximal sore for PG1, and also high scores for RN1, RN6, SR3, and SR7. Lowest score is for YL1 site, as exploration efforts are hampered by security issues. 3) Reservoir: Highest score for PG1, but not maximal value, and higher scores for RN1 and RN6. Lower score are for SR3, SR7, SR9 and YL1 sites. 4) Market: Almost maximal score value is for SR7, and higher scores are also for RN1, SR3, and PG1. Relatively low scores are for RN6, SR9, and YL1 sites. The final score of each geothermal hot spring sites was then derived from the summation of the four fractional scores of all factors. Resource sites with the highest total scores are ranked as those with the greatest development potential, which for Southern Thailand are PG1 (47 out of 60), SR7 (46), and RN1 (45).

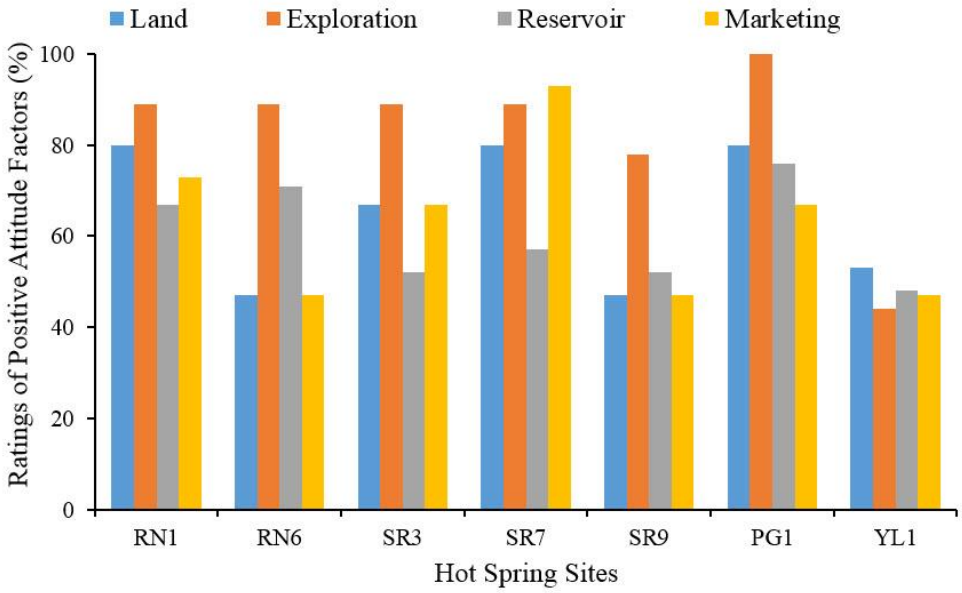

Figure 3.6 Rating of geothermal hot springs in Southern Thailand with the positive attitude factors; RN1, RN6, SR3, SR7, SR9, PG1, and YL1.

Table 3.2 Positive attitude factors of geothermal hot springs in Southern Thailand

Positive attitude factors list	Hot Spring Sites						
	RN1	RN6	SR3	SR7	SR9	PG1	YL1
1) Land uses availability:							
1.1) Accessibility	3	1	2	3	1	2	2
1.2) Terrain	3	1	2	3	1	2	2
1.3) Risk of natural hazards – to be specified (e.g. earthquakes, tsunami)	2	2	2	2	2	2	2
1.4) Security	2	2	2	2	2	3	1
1.5) Owner attitude	2	1	2	2	1	3	1
Fractional Score: 15 points	**12**	**7**	**10**	**12**	**7**	**12**	**8**
2) Past Exploration availability:							
2.1) Geological data	3	3	3	3	2	3	1
2.2) Geophysical data	3	3	3	3	3	3	1
2.3) Geochemical data	2	2	2	2	2	3	2
Fractional Score: 9 points	**8**	**8**	**8**	**8**	**7**	**9**	**4**
3) Reservoir availability:							
3.1) Areal extent (surface)	2	2	2	2	2	2	1
3.2) Exit temperature	1	2	1	1	1	2	2
3.3) Reservoir temperature	2	2	2	2	2	2	2
3.4) Surface fluid flow	2	2	2	2	2	2	1
3.5) Structural control (fault)	3	2	2	2	2	3	1
3.6) Heat source	2	3	1	1	1	3	2
3.7) Drilling depth	2	2	1	2	1	2	1
Fractional Score: 21 points	**14**	**15**	**11**	**12**	**11**	**16**	**10**
4) Marketing availability:							
4.1) Distance to higher voltage power lines	2	1	2	3	1	2	2
4.2) Terrain of power line corridor	2	1	2	3	1	2	1
4.3) Terrain of development site	2	1	2	3	1	2	1
4.4) Distance from well to plant site	3	2	2	3	2	3	2
4.5) Proximity to market	2	2	2	2	2	1	1
Fractional Score: 15 points	**11**	**7**	**10**	**14**	**7**	**10**	**7**
Total Score: 60 points	**45**	**37**	**39**	**46**	**32**	**47**	**29**

For each fractional score a minimum value in percentage was assigned (Figure 3.6). The values were above the threshold the site was given a positive mark and all marks were added. Results, shown in Table 3.3, can be classified into three groups; hereinafter, RN1 and PG1 with a good potential, RN6, SR3, and SR7 arbitrarily considered having average potential, and SR9 and YL1 show poor potential. Hot spring sites with a good potential got relatively higher scores in all four fractions, although they might not get top scores in each fraction. In comparison to the summation of positive attitude factors shown in Table 3.2 the final ranking in Table 3.3 lost SR7 as a site with a good potential. This is due to a lower score in the

reservoir fraction, specifically, structural control (3.5) and heat source (3.6). This highlights the emphasis on and the importance of all four fractions rather than a summation of all positive attitude factors.

Table 3.3 Final ranking of the geothermal hot springs in Southern Thailand

Positive attitude factors (available)		**Hot Spring Sites**						
		RN1	**RN6**	**SR3**	**SR7**	**SR9**	**PG1**	**YL1**
Land	≥80%	x			x		x	
Exploration	≥80%	x	x	x	x		x	
Reservoir	≥60%	x	x				x	
Marketing	≥60%	x		x	x		x	
Sites ranking		**Good**	**Average**	**Average**	**Average**	**Poor**	**Good**	**Poor**

3.2.3 Final sites ranking

All positive factors of all fractional scores are important a simple summation might not fully represent the potential of a site (Table 3.2, Table 3.3 and Figure 3.6). Therefore, for each fractional score a minimum value in percentage was assigned. For land and exploration factors the value was set by ≥80%, whereas for reservoir and marketing factors the value was set lower, ≥60%, as for the latter two less data were available. If values were above the threshold the site was given a positive mark and all marks were added. Results, shown in Table 3.3, can be classified into three groups; hereinafter, RN1 and PG1 with a good potential, RN6, SR3, and SR7 arbitrarily considered having average potential, and SR9 and YL1 show poor potential (Table 3.3 and Figure 3.6). Hot spring sites with a good potential got relatively higher scores in all four fractions, although they might not get top scores in each fraction. In comparison to the summation of positive attitude factors shown in Table 3.2 the final ranking in Table 3.3 lost SR7 as a site with a good potential. This is due to a lower score in the reservoir fraction, specifically, structural control (3.5) and heat source (3.6), see Table 3.2. This highlights the emphasis on and the importance of all four fractions rather than a summation of all positive attitude factors.

3.3 Possibility of electrical resources: Case study of PG1 hot spring

3.3.1 Local Geology of PG1 hot spring system

Local geological settings in and around the PG1 hot spring system are dominated by granites, sedimentary and metamorphic rocks (Figure 3.7 and Figure 3.8) (Garson et al., 1970; Ngansom et al., 2016). An overlay of the geological map with the residual magnetic intensity from aeromagnetic surveys has revealed differences between mid-lows magnetic and mid-high magnetic areas in in areas of sedimentary and metamorphic rocks as shown in Figure 3.7b (Ngansom et al., 2016; Duerrast et al., 2016; DMR, 2011; DMR, 2014). This distribution of the residual magnetic intensity indicates igneous rocks below sedimentary and metamorphic units. Boundaries and intersections of various igneous bodies at depth might provide pathways for the upwards migrating hot fluids through an enhanced permeability of in general low-permeable igneous rocks. The distribution of granitic intrusions is controlled by the transcurrent KMF and its postulated continuation south-west through the study area according to Watkinson et al. (2008) (Figure 3.7). Features regarded as essential characteristics of igneous intrusions in general are present, including local folding, sharp contacts and the conversion of wall rocks (Garson and Mitchell, 1970; Metcalfe, 2013). Moreover, pegmatite and minor intrusions infill dominant fracture patterns which postdate the main period of igneous intrusion but which are in part synchronous with the movement along the KMF (Garson et al., 1970; Kanjanapayony et al., 2009; Kanjanapayont et al., 2012).

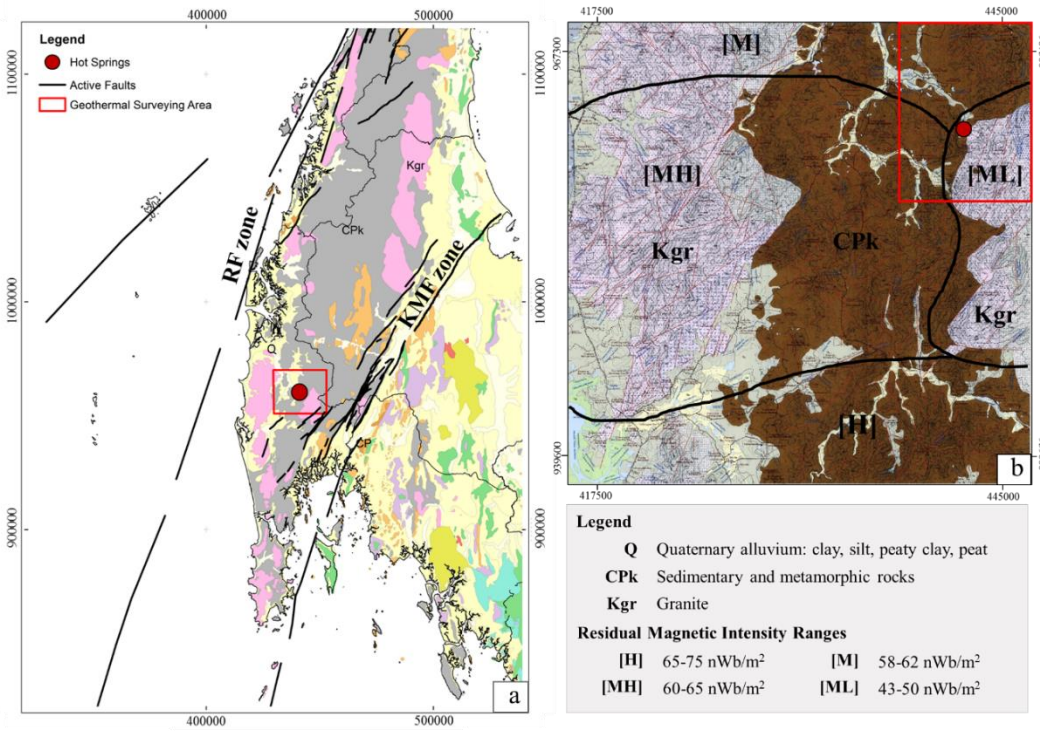

Figure 3.7 (a) Location of Kapong hot spring site showing the geological setting with the main faults zone both of the Khlong Marui Fault (KMF) and Ranong Fault (RF) Zones and (b) relationship between the geological map and the residual magnetic intensity from aeromagnetic data in the Kapong hot spring area.

Figure 3.8 (a) Pai Phu Channel is located at PG1hot spring as tributaries of the Kapong River, (b) the main natural hot spring at PG1-1 pool, (c) and (d) sandstone and granite outcrops around and inside the study area.

3.3.2 Chemical characteristics of PG1 hot spring system

3.3.2.1 Water properties and chemistry of PG1 site

Results of the chemical analysis of the PG1 hot spring waters are shown in Table 3.4. The location that has received the most attention is the PG1-1 natural pool, which shows the highest surface discharge temperature of the PG geothermal system with 78 °C. Variations of surface temperatures, from 65 to 75 °C, can be attributed to near surface mixing processes along the banks of the Pai Phu River nearby (Dimick, 2007). The total discharge at the natural hot spring pools is between 1 L/s and 1.5 L/s. Data of cation and anion concentration measurements are shown in Table 3.4. Slightly higher than neutral pH values, around 8.0, indicate likely the dissolution of a significant part of the dissolve silica (Hem, 1970; Baioumy et al., 2015). A composition of these waters appears to be water of fairly low TDS with about 247 mg/L. Concentrations of Ca^{2+}, Mg^{2+}, Na^{+} and K^{+} are approximately 11.35 mg/L,

0.1 mg/L, 68.63 mg/L, and 3.54 mg/L, respectively. Na^+ and K^+ concentrations are likely the results of ion exchanges of Ca^{2+} and to a lesser extent of Mg^{2+} from sandstone sources, which are rich in feldspar and which are likely to be found in the recharge areas and/or along the flow paths of PG1 geothermal system (e.g. CPk unit in Figure 3.7). For the SiO_2 concentration silica is a major constituent of igneous rocks and sandstones, and quartz is one of the most weathering resistant minerals (Hem 1970; Guo and Wang, 2012). For this system the SiO_2 values range between 80 and 90 mg/L, which are comparable higher than other geothermal springs located in Southern Thailand region (approximately 25 to 75 mg/L).

Table 3.4 pH, surface temperatures, and concentrations of major cations and anions (mg/L) of hot spring water samples in PG1 (1-6) hot spring sites and local groundwater well (GW)

Content	**Water sample**						
	PG1-1	**PG1-2**	**PG1-3**	**PG1-4**	**PG1-5**	**PG1-6**	**GW**
pH	8.12	8.18	8.03	8.03	8.08	7.33	6.98
Surface temp.; °C	78	75	68	75	73	65	28
TDS; mg/L	241.50	246.40	229.95	259.00	256.20	208.60	43.00
SiO_2; mg/L	90.24	91.93	80.28	87.06	84.09	61.64	1.2
Ca^{2+}; mg/L	12.14	12.14	11.00	12.43	12.29	11.29	2.52
Mg^{2+}; mg/L	0.12	0.11	0.11	0.12	0.12	0.84	0.45
K^+; mg/L	3.38	3.38	3.74	3.42	3.42	3.13	0.37
Na^+; mg/L	69.64	68.21	61.43	69.64	68.57	47.86	7.40
Fe; mg/L	<0.005	<0.005	<0.005	<0.005	<0.005	<0.005	<0.005
HCO_3^-; mg/L	183.00	180.50	155.00	165.50	155.50	115.50	19.22
SO_4^{2-}; mg/L	11.20	11.20	8.70	9.40	9.40	25.10	10
Cl^-; mg/L	15.20	16.20	15.80	14.20	16.90	15.20	15.52
F^-; mg/L	0.80	1.20	2.50	7.50	7.60	0.50	0.02

PG1 hot spring water samples described in terms of relative concentrations of their major cations and anions and presented in the Piper diagram shown in Figure 3.9 indicate that they are of Ca–Na–bicarbonate rich type. These bicarbonate-rich waters are likely from the basement and alluvial aquifers (Hem 1970; Guo and Wang, 2012).

Plots of the ion concentrations versus the concentration of the conservative component chloride for all six hot spring water samples are shown in Figure 3.10a-f. The absolute values for all components a rather close (Table 3.4) and no positive or negative trends against the conservative Cl^- are clearly identifiable. In general,

concentrations show scattered relationships that are not correlated with Cl^-, while only Mg^{2+} and Ca^{2+} show almost no change over the different sample site, probably because all sites are close together. The scattering however is likely due to some mixing with shallow aquifer and river water.

Subsurface temperatures of the PG1 hot spring system were estimated with the silica geothermometer as others are not likely applicable (Table 3.4); an initial restriction being the lack of boiling hot springs (Fournier, 1977). For the reservoir temperatures determination it has been assumed that quartz is in equilibrium, so that the silica content can be used to obtain minimum temperature values for the system (Mutlu, 1998; Baioumy et al., 2015; Fournier and Truesdell, 1973). Hydrothermal rock alteration at depth can reveal which of the silica minerals controls the amount of silica in solution (Guo and Wang, 2012). However, if it is assumed that the PG1 hot spring system has not a deep circulation then no equilibrium has been reached and the silica content does not give reliable information about the water temperatures at depth (Fournier, 1977; Fournier and Truesdell, 1973). The reservoir temperatures of last equilibrium reached with quartz gives a range from 100 °C to 130 °C for reservoir temperatures of the PG1 geothermal system (Table 3.4).

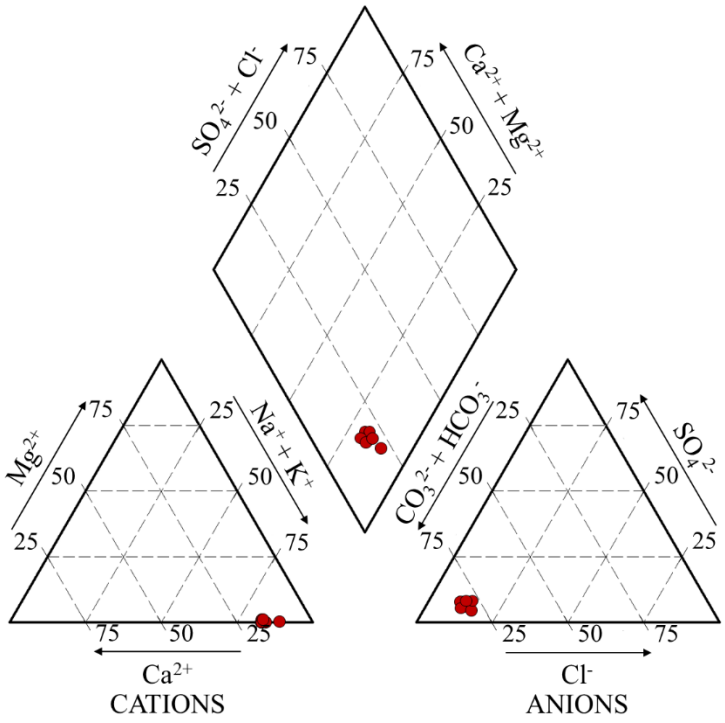

Figure 3.9 Piper diagram of PG1 hot spring system.

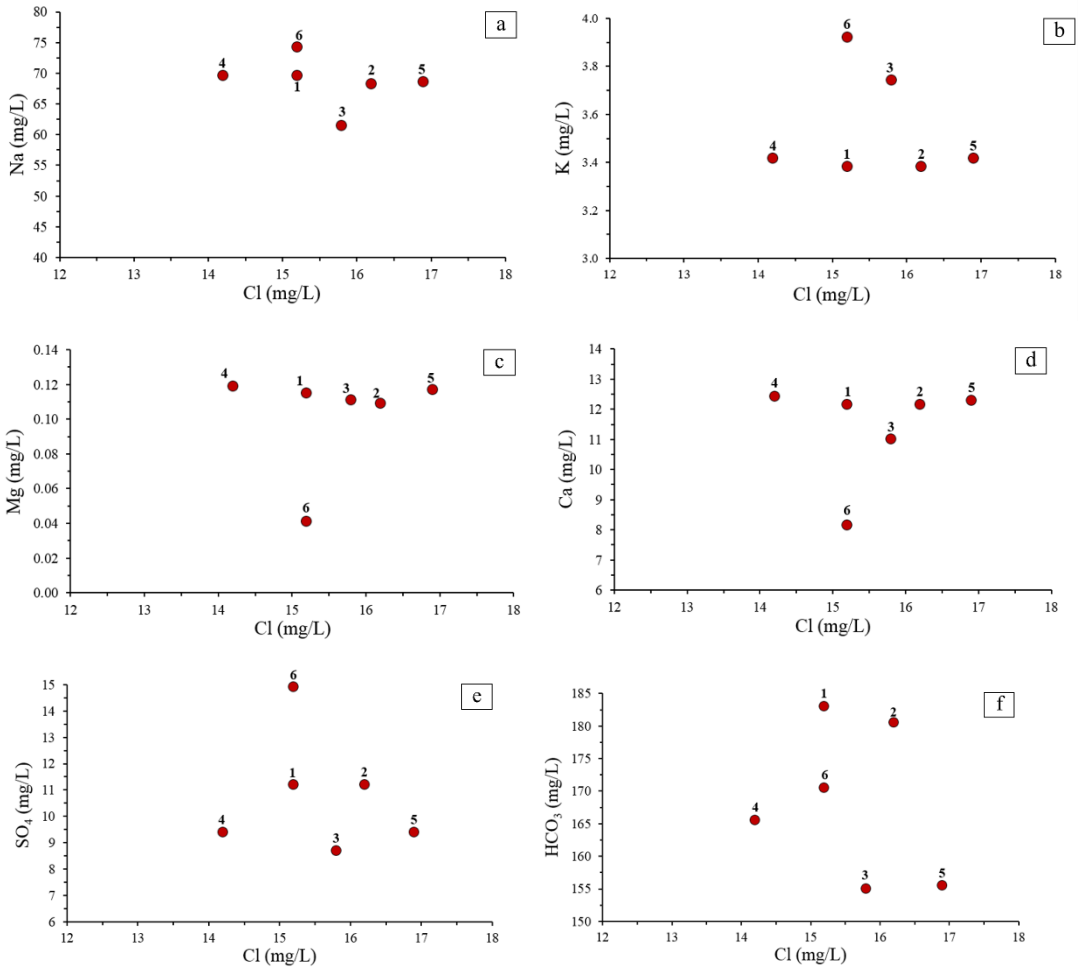

Figure 3.10 Variations of concentrations of major inorganic ions against conservative component of Cl^-.

3.3.2.2 Isotopes of PG1 site

The relationship between δD and $\delta^{18}O$ of the PG1 hot spring waters are plotted with the local meteoric water in Figure 3.11. The isotopic compositions of the PG1-1 water and groundwater are close to the global meteoric water line (GMWL) (Craig 1961), with δD and $\delta^{18}O$ values of -29.61 and -5.29% for KP1 and -24.88 and -3.01% for groundwater, respectively. From the isotopic compositions the origin of the PG1-1 geothermal waters can be concluded to be of local meteoric water origin (Craig, 1961; Hirukawa et al., 1987). However, the isotope data did not exclude a possible small contribution from fresh groundwater.

The water samples at the PG1 hot spring can be clearly differentiated from the other hot spring systems in southern region such as Krabi and Trang geothermal systems by their Sr concentration and $^{87}Sr/^{86}Sr$ ratios shown in Table 3.5. The $^{87}Sr/^{86}Sr$ ratios of the PG1 water sample has very low Sr content compared to KB and TR geothermal systems about 0.0455 μg/g and $^{87}Sr/^{86}Sr$ ratios about 0.754465 (Table 3.5). Thus, the water samples in this study case can be classified by low Sr content and higher $^{87}Sr/^{86}Sr$ ratio.

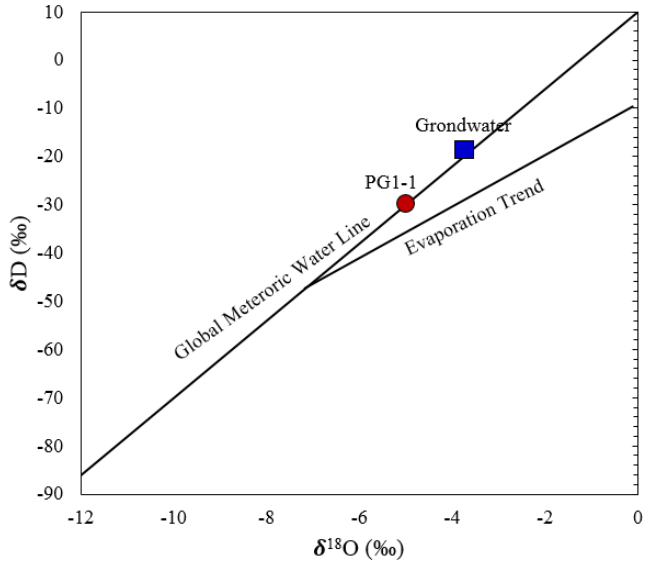

Figure 3.11 Stable isotope of $\delta^{18}O$ and δD composition.

3.3.2.3 Rare earth elements of PG1 site

Chondrite-normalized rare earth element (REE) concentrations from a water sample of the PG1-1 hot spring system are presented in Table 3.6 and Figure 3.12; chondrite data are from Taylor and McLennan (1981). The heavier REEs (HREE) are less fractionated then the light REEs (LREE) in comparison to chondrite, with the LREEs almost forming a plateau at around 0.03. A negative Eu anomaly might be explained through water-rock interaction at depth. Originally, granites are produced by a fractionation between a residual melt and a coexisting aqueous high-temperature fluid, which has taken the Eu from the granite during the circulation at depth (Xiao et al., 2010). The negative Eu values are consequently induced by water-rock interaction between the deep-cycling meteoric water and the Eu depleted igneous rocks.

Table 3.5 Concentrations and isotope ratios of nitrogen and strontium of PG1-1 site, Krabi geothermal system (KB1, KB3 and KB5), Trang geothermal system and local groundwater well

Water sample	**UTM (WGS-84)**		**Isotope**			
	East (m)	North (m)	δD	$\delta^{18}O$	Sr (µg/g)	$^{87}Sr/^{86}Sr$
Kapong hot spring; KP1	441455	960807	-29.61	-5.29	0.0455	8.243386
Krabi geothermal system; KB1	499622	900439	-	-	0.1500	8.294542
Krabi geothermal system; KB3	510462	888220	-	-	0.9510	8.294207
Krabi geothermal system; KB5	523171	876867	-	-	0.9850	8.322538
Trang; TR1	551391	818787	-	-	0.4700	8.330919
Local groundwater well	654053	760972	-24.88	-3.01	-	-

Table 3.6 Concentrations of REEs in hot spring water (PG1-1 site), groundwater sample and continental crust from sedimentary rocks (Taylor and McLennan, 1981)

Water sample	**Concentration of REEs (water; µg/L and continental crust; µg/g)**												
	La	Ce	Pr	Nd	Sm	Eu	Gd	Tb	Dy	Er	Tm	Yb	Lu
Kapong hot spring; KP1	0.159	0.220	0.114	0.088	0.055	0.018	0.039	0.018	0.026	0.021	0.054	0.017	0.016
Continental crust (Taylor and McLennan, 1981)	19.00	38.00	4.30	16.00	3.70	1.10	3.60	0.64	3.70	2.30	0.32	2.20	0.30

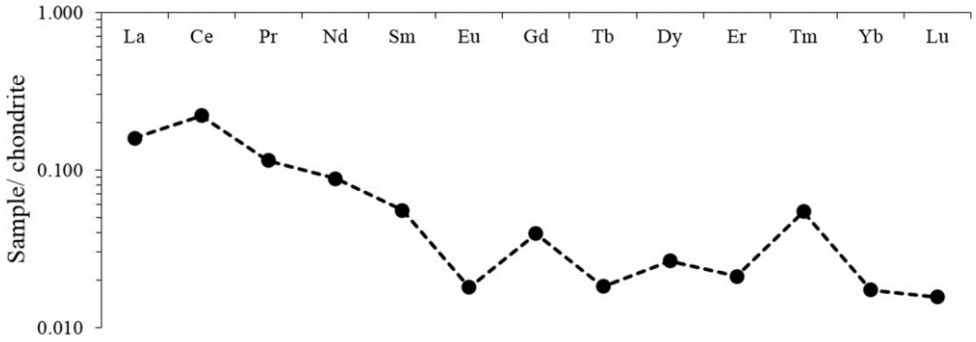

Figure 3.12 Chondrite-normalized plot of the REE concentrations of the PG1-1 hot spring system.

3.3.3 Geophysical investigation of PG1 hot spring system

3.3.3.1 VES profiles of PG1 site

Three profiles, each combining 6 to 7 1D VES survey data, located in the proximity of the hot spring PG1 as well as north and northeast of it are presented in Figure 3.14– Figure 3.16 (see map in Figure 3.13). From the inversion in general three layers of different resistivity could be delineated, with the first one a layer of top soil. The depth of investigation is not deeper than 100 m.

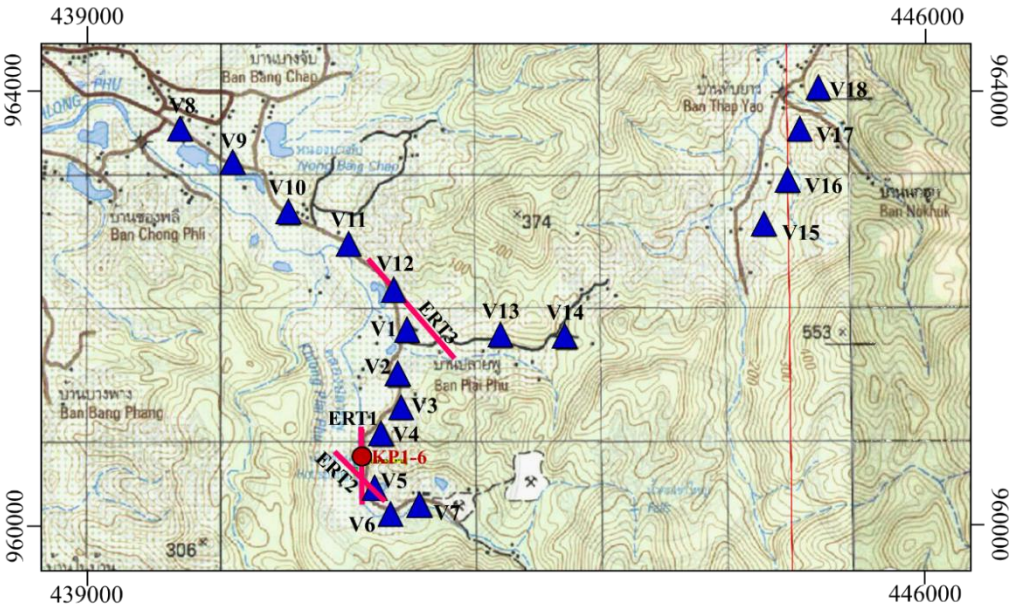

Figure 3.13 Locations of geophysical surveys of VES survey points and ERT profiles.

The profile VES1 comprises altogether seven VES points including V1 to V7 from N to S direction thus crossing the PG1-1 hot spring site at V5 location as shown in Figure 3.14 and Figure 3.13. Below the 5 to 10 thin top soil layer with a resistivity of 1,000 to 6,400 ohm-m the sequence shows a several 10th of meter-thick layer of sand and coarse gravel deposited from the river system (147-505 ohm-m). The resistivity values indicate a partly to less water saturation of this layer. The third layer is sandstone at a depth range of between 30 and 100 m. Here, resistivity values of more 600 ohm-m and up to 2,100 ohm-m reveal almost no water saturation in this layer. Significant depth differences of up to a few tenths of meters between comparable layers at different VES locations have been resolved by adding almost vertical (normal) faults.

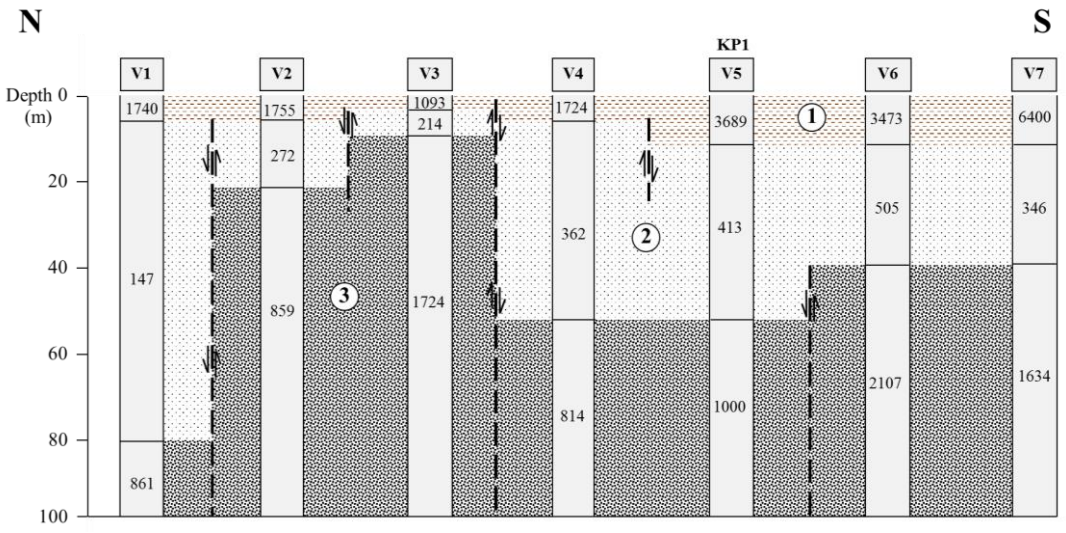

Figure 3.14 VES1 profile using Schlumberger array, with (1) topsoil, (2) sand and coarse gravel layer and (3) sandstone, which sharp resistivity contrasts are indicated as possible faults (black dashed lines).

VES2 profile consists of six VES points including V1 and V8 to V12 from NW to SE direction. This profile continues to the south as VES1 as explained above (see Figure 3.13 and Figure 3.15). Comparable to VES1 three different layers have been delineated by the inversion process due to different resistivity values. The first layer is the up to 10 m thick top soil with resistivity values of 680 to more than 3,300 ohm-m. Below, the second layer represents sand and coarse gravel, partly to less

water saturated, with resistivity values between 129 and 404 ohm-m. The third layer represents sandstone and other possible hard rock formations with less to no water saturation, represented by resistivity values of 861 to 2,471 ohm-m. At the V8 location in the NW of the study area no high-resistivity formation has been detected above maximal survey depth. Also here, comparable to VES1, significant depth differences of up to a few tenths of meters between comparable layers at different VES locations have been resolved by adding almost vertical (normal) faults.

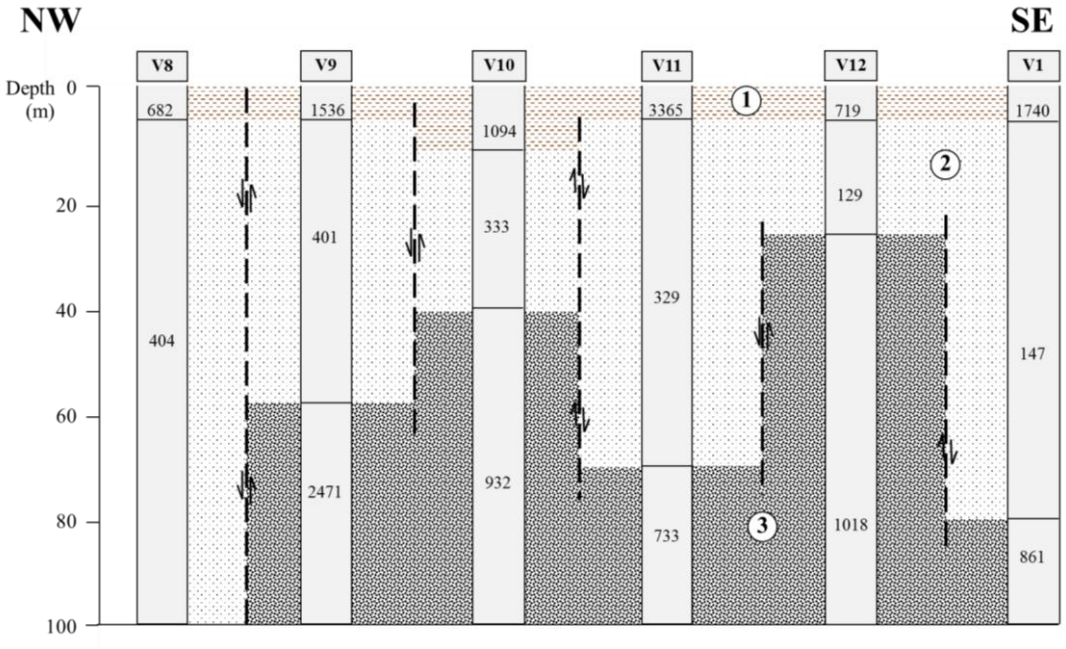

Figure 3.15 VES2 profile using Schlumberger array, with (1) topsoil, (2) sand and coarse gravel layer and (3) sandstone, which sharp resistivity contrasts are indicated as possible faults (black dashed lines).

The VES3 profile was obtained for seven VES points including V1 and V13 to V18 from SW to NE direction; it crossed the mountain between V14 and V15 of about 1.7 km distance as shown in Figure 3.13 and Figure 3.16. Here distribution of the layers and resistivity ranges is similar and comparable to VES1 and VES2. Also here vertical (normal) faults have been introduced to explain the depth differences of comparable layers. From V15 to V18 the third layer, likely sandstone, is much shallower than between the locations of V1 to V14.

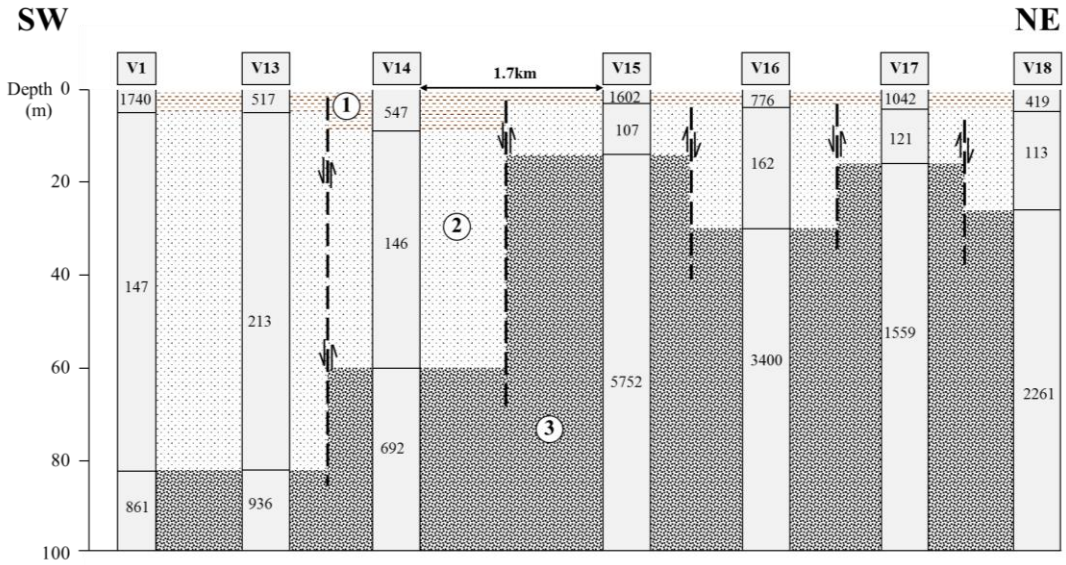

Figure 3.16 VES3 profile using Schlumberger array, with (1) topsoil, (2) sand and coarse gravel layer and (3) sandstone, which sharp resistivity contrasts are indicated as possible faults (black dashed lines).

3.3.3.2 ERT surveys of PG1 site

From three, two ERT surveys were carried out over and in the vicinity of the hot spring PG1-1, ERT1 and ERT2, while ERT3 is located further north of it (Figure 3.13, Figure 3.17-3.19). ERT1 crosses ERT2 at 300 m, while ERT2 crosses ERT1 at 350 m (Figure 3.12a, Figure 3.12b).

ERT1 profile revealed the subsurface resistivity distribution from N to S direction, which crossed over the PG1-1 hot spring site at 230 m as shown in Figure 3.17. The first layer, topsoil, from the surface down to about 10 m is not well delineated when compared to the VES data (VES4 and VES5 in Figure 3.11a). However, the resistivity values are higher (50 to 300 ohm-m), than for the second layer with around 100 ohm-m and below, representing water saturated sand and gravel. At around 60 to 100 m depth the resistivity increases significantly to 800-1,000 ohm and higher, indicating sandstone with less to no water saturation. This resistivity distribution reflecting different layers is comparable to the VES data shown in Figure 3.14–3.16. However, the ERT section shows differences in the lateral continuation of the different resistivity layers, which could be resolved by introducing vertical (normal) faults. In layer 2 very low resistivity patches of less than 25 ohm-m

indicate hot water with higher TDS values (240 mg/L) than the groundwater (43 mg/L; see Table 3.4). The hot water is distributed in the porous and permeable sand and gravel layer before exiting to the surface.

ERT2 section was carried out in the NW to SE direction crossing over the ERT1 profile at a lateral distance of 300 m as shown in Figure 3.18. The general distribution of the resistivity is similar to ERT1, also with very low resistivity patches in the shallow subsurface, 10 to 60 m depth at a lateral distance of 180 to 300 m. Semi-vertical and inclining faults also have been introduced to explain the lateral variations in the third layer, the higher resistivity sandstone (800-1,000 ohm-m). However, in this section the faults can be traced are deeper than the survey depths (approx. 130 m) and they are seemingly of reverse character.

ERT3 section is similar and comparable to section ERT2, however the second sand and gravel layer is quite thin and very low resistivity patches are almost not found (Figure 3.19). However, faults with reverse character also have been introduced here to explain the horizontal resistivity changes. Seemingly, the river sediments here are thinner while the hard rock sandstone is much shallower. At this location further north of PG1-1 hot water seemingly does not occur.

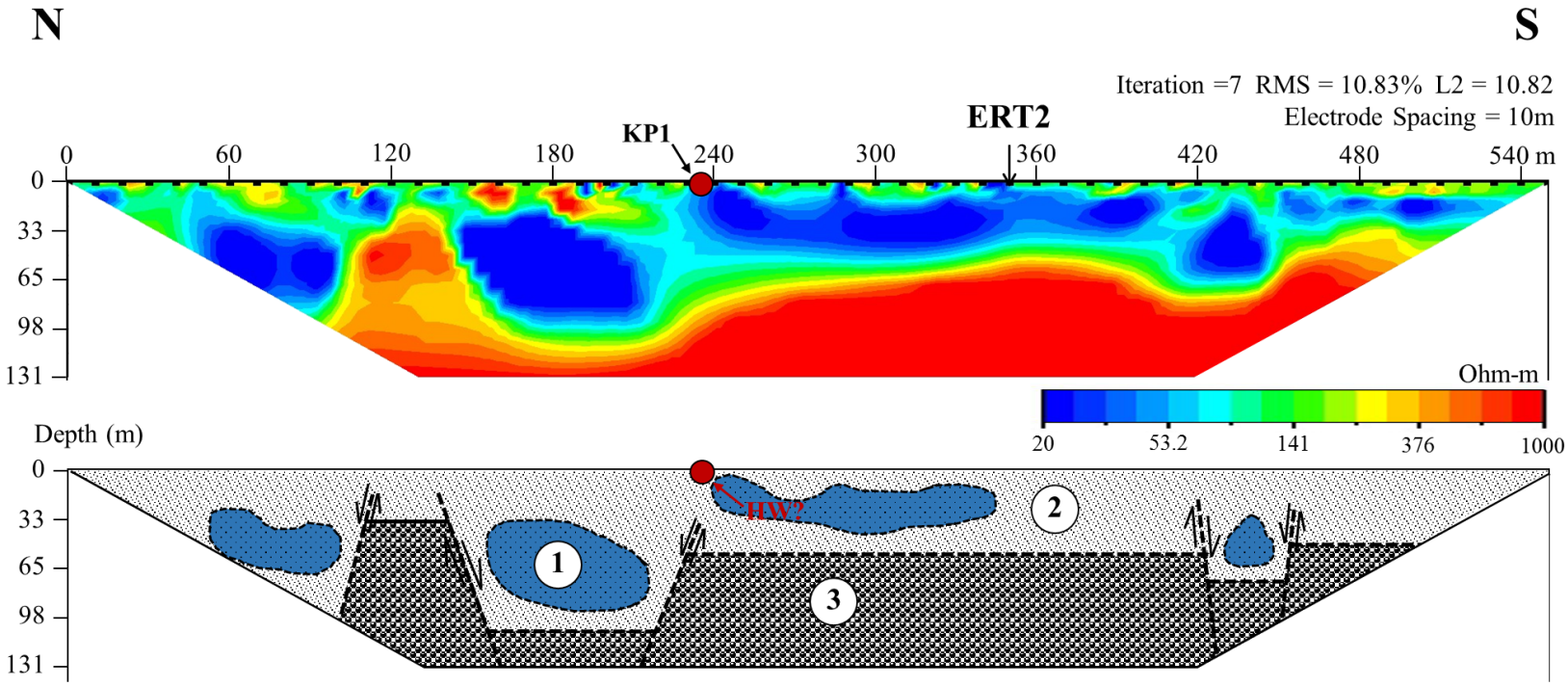

Figure 3.17 2D sections of ERT1 profile using dipole–dipole configuration, with (1) a zone indicated as very low resistivity (below 25 ohm-m) (2) a thin layer of topsoil and unconsolidated sediments of sand and coarse gravel layers, and (3) sandstone.

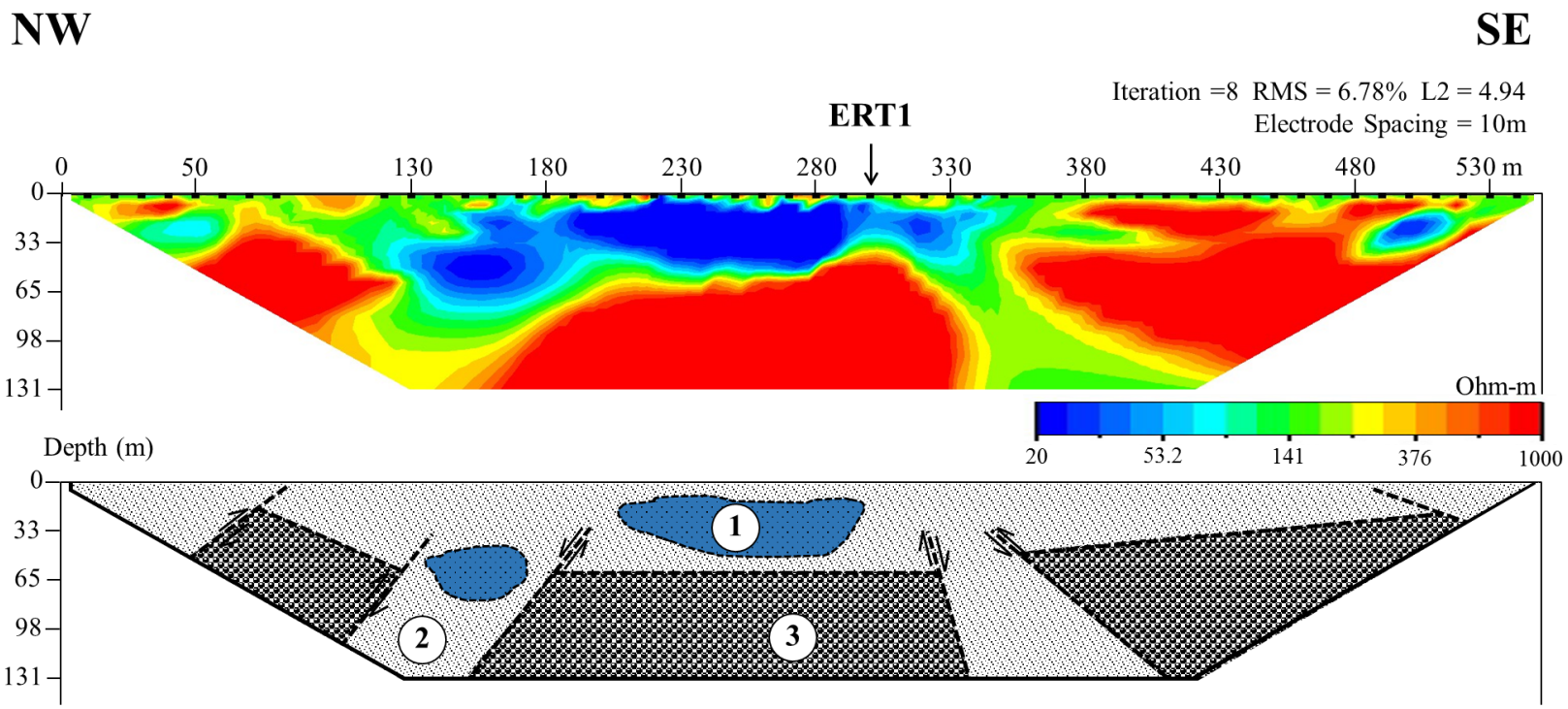

Figure 3.18 2D sections of ERT2 profile using dipole–dipole configuration, with (1) a zone indicated as very low resistivity (below 25 ohm-m) (2) a thin layer of topsoil and unconsolidated sediments of sand and coarse gravel layers, and (3) sandstone.

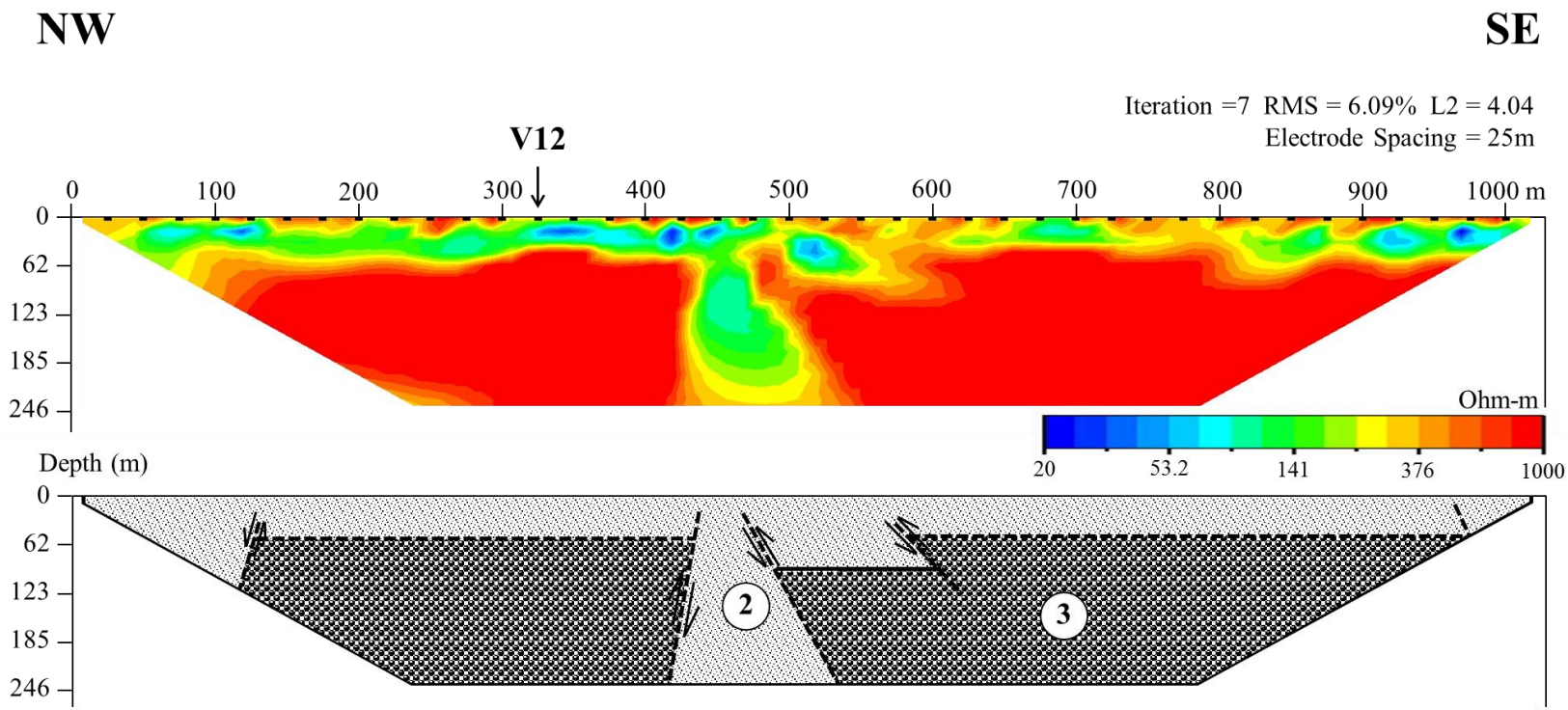

Figure 3.19 2D sections of ERT2 profile using dipole–dipole configuration, with (1) a zone indicated as very low resistivity (below 25 ohm-m) (2) a thin layer of topsoil and unconsolidated sediments of sand and coarse gravel layers, and (3) sandstone.

3.3.3.3 MT survey of PG1 site

Horizontal slices of the 3D electrical resistivity model with increasing depth based on MT measurements are shown Figure 3.20 and Figures 3.21 to illustrate the spatial resistivity distribution at the PG1 site.

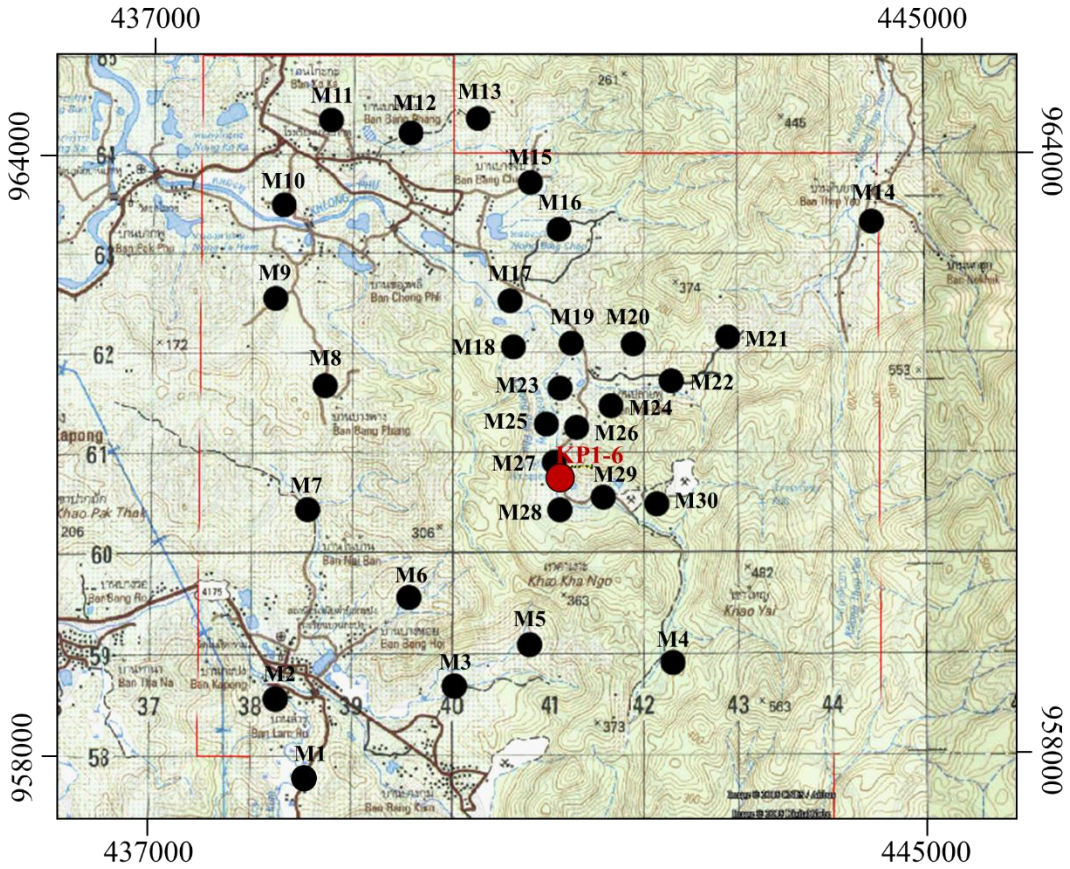

Figure 3.20 Locations of geophysical surveys of MT surveys.

Near surface resistivity values range from 100-300 ohm-m in the northwestern area and increased to about 1,000–2,000 ohm-m in the southeastern area in the 0-50 m depth slices (Figure 3.21a – Figure 3.21c). The resistivity contrast resembles the local geological setting (see Figure 3.7b). Higher surface resistivity is seen in the northeastern part of the PG1 site agreeing with granite rocks (Kg) and lower surface resistivity values are corresponding to sedimentary/ metamorphic rocks (CP). Down to 300 m depth (Figure 3.21d – Figure 3.21f) the resistivity in general increases with a background value of around 3,000 ohm-m indicating very low porous

hard rock with almost no water saturation, here likely metamorphic or granitic rocks. Lower resistivity areas with about 100 ohm-m indicate possible water saturated sediments and/or weathered granitic rocks. This corresponds well with the VES and ERT data, where in some areas (VES8) or ERT2, for example, lower resistivity areas along faults and fractures extend beyond the survey depth of about 130 m (Figure 3.18).

Below 300 m down to 2,000 m (maximal survey depth) the resistivity in most areas increase up to 3,000 ohm-m; however some patches (C1, C2 in Figure 3.21g – Figure 3.21) of lower resistivity, around 300-500 ohm-m, remain and continue downwards (see Amatyakul et al., 2016; Amatyakul et al., 2015). These patches at different depth slices resemble an almost vertical structure, like a conduit, and they even might be traced below 2,000 m depth. The resistivity values of C1 and C2 indicate a possible fractured area filled with water. The horizontal area of these conduits is about 1 km^2; C1 is increasing in size from 1,500 m to 2,000 m depth and also the resistivity decreases (Figure 3.21k and Figure 3.21l) indicting a possible larger fluid reservoir at a depth below 2,000 m. The conduits might be located at the boundary between different igneous bodies when comparing the results here with the residual magnetic intensity data and the geological map shown in Figure 3.7b.

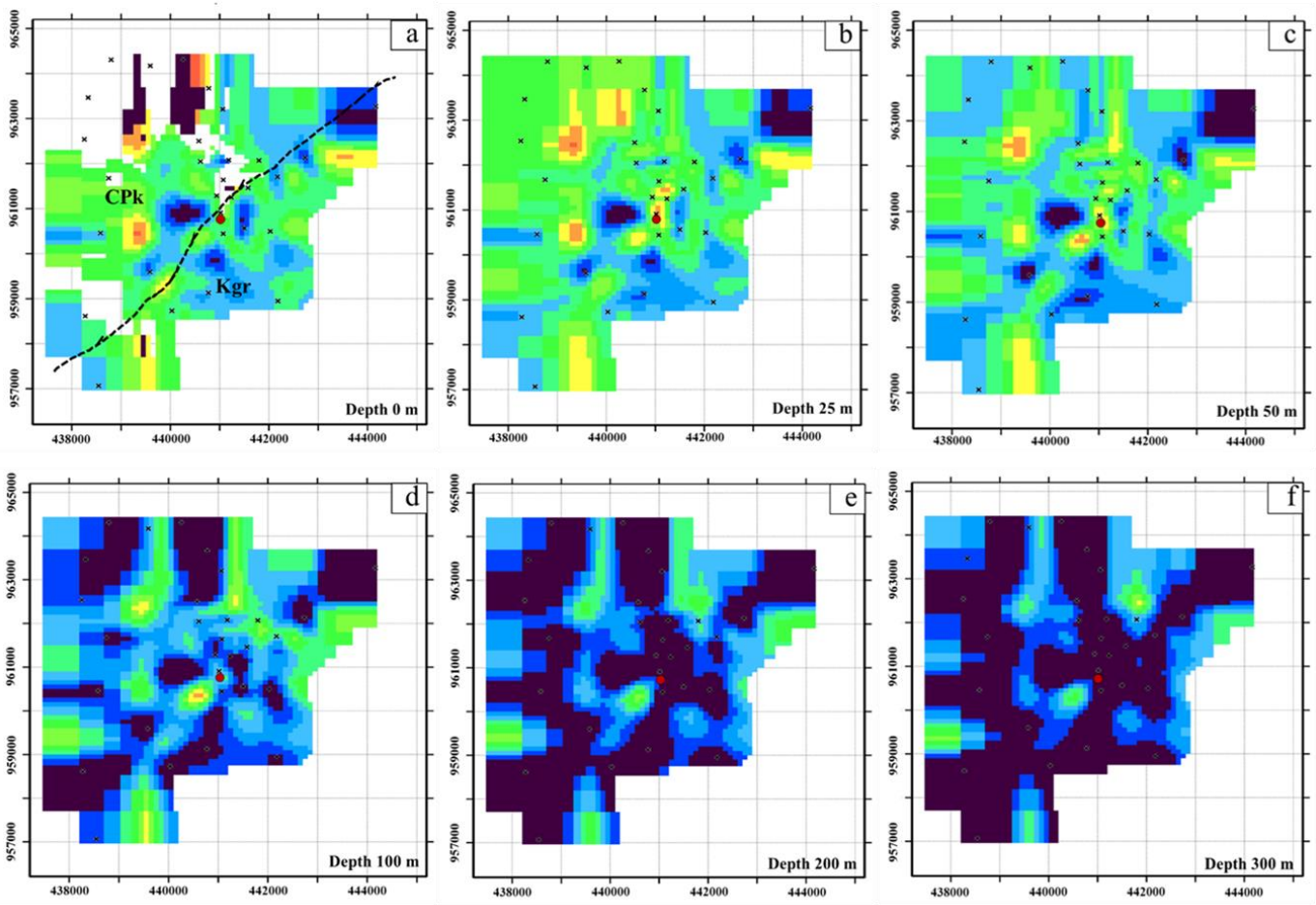

Figure 3.21 Plane-view of the final inverted resistivity model based on the MT measurements; (a) surface, (b) 25 m, (c) 50 m, (d) 100 m, (e) 200 m, (f) 300 m. CPk and Kgr are sedimentary/metamorphic rocks and granite rocks, respectively.

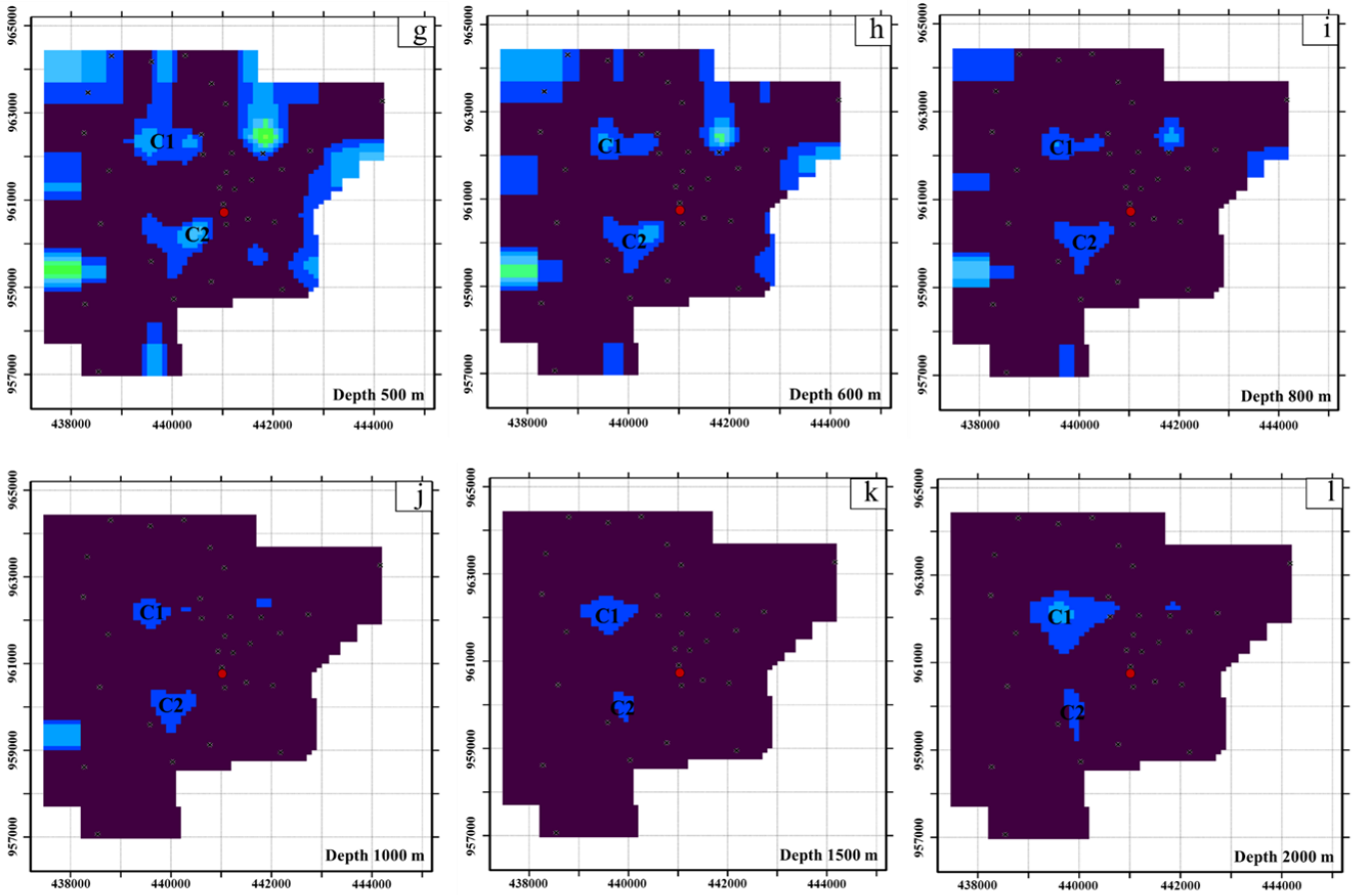

Figure 3.21 Continued; (g) 500m, (h) 600m, (i) 800m, (j) 1,000m, (k) 1,500m, and (l) 2000m depths. CPk and Kgr are sedimentary/metamorphic rocks and granite rocks, respectively. C1 and C2 are zones of low resistivity value at depth (indicated from 500 to 2,000m).

3.3.4 Hydrogeothermal system of PG1 hot spring system

From combination of the 3D MT data with surface geology and geochemical results a schematic hydrogeothermal model of the PG1 hot spring system has been drawn as shown in Figure 3.22.

The main geological units in the area are igneous bodies (Kgr) partly overlain by sedimentary and metamorphic units (CPk) as shown in Figure 3.7b. However, differences in residual magnetic intensities suggest different igneous bodies, likely four as indicated in Figure 3.7b. The emplacement of the igneous bodies might be correlated with occurrence of the Khlong Marui fault zone further south and the Ranong Fault Zone further north of the PG1 site (Figure 3.7a). Late Eocene sinistral transpression along the Khlong Mauri fault zone formed positive flower structures, which resulted in igneous bodies uplifted closer to the surface (Watkinson et al. 2008). This might also explain the existence of reverse faults identified in the ERT sections (Figure 3.18, 3.19). Earlier deformation stages were extensional resulting in normal faults shown also in the ERT and VES sections (Figure 3.14-3.16 and Figure 3.17; Watkinson et al. 2008). The igneous bodies are likely also the heat source for the PG1 geothermal system due to their radiogenic heat production from U, Th, and K contents (see Charusiri, 1989). Silica geothermometer provide a reservoir temperature of around 125 to 130 °C (Table 3.4). With possible temperature gradients in the range of 25 to 35 °C the reservoir depth can be estimated to be 3.6 to 5.2 km.

The lower resistivity conduits at depths below 300 m in the MT data (Figure 3.21) might resemble boundaries of different igneous bodies, which have experienced some contractions related to final cooling during exhumation and by this open some pathways. Another possibility is that these conduits are faults or fault intersections related to the movement of the nearby Khlong Marui fault zone (Figure 3.7a). Along these higher permeable conduits with their almost vertical orientation meteoric water could flow downwards into the regions of the igneous bodies and by this progressively heated up as the isotope data show (Table 3.5 and Table 3.6). The lower density hot water, which has taken the geochemical signature of the granitic rocks (Table 3.6) then moved up along the same conduits into the shallower subsurface, where fluivatile sand and gravel layers from the nearby river (Figure 3.8a and Figure 3.8b) provided a near-surface reservoir, before exiting to the surface as the

PG1 hot spring (78 °C for PG1-1), illustrated by the VES profiles and ERT sections (Figure 3.11 and 3.12).

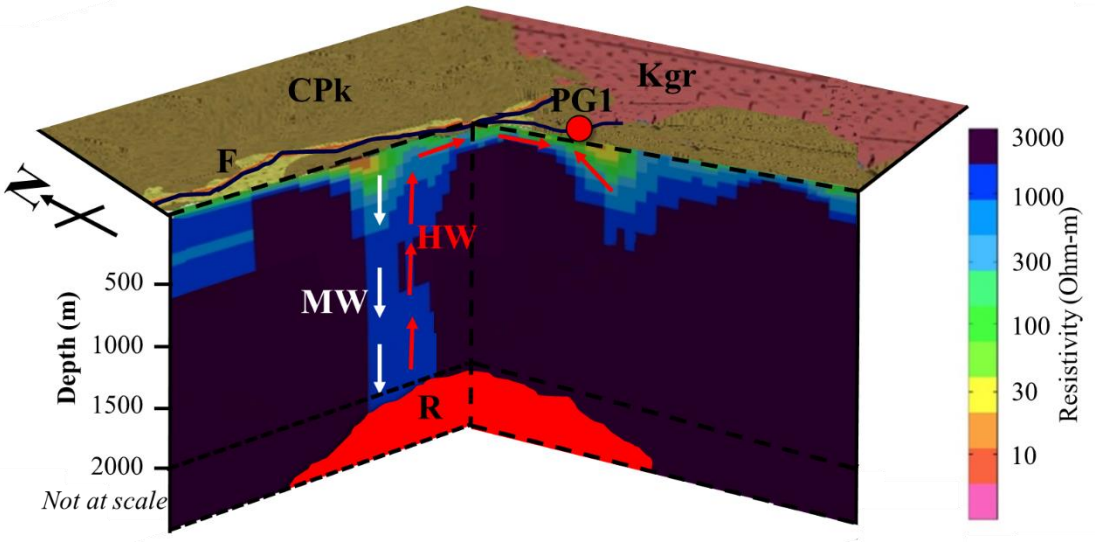

Figure 3.22 Schematic geological model of the PG1 hot spring system along a north-south profile with resistivity data from the MT survey. Surface resembles the geological map with brown color being sedimentary/metamorphic units (CPk) and red color granites (Kgr); KP is the PG1 hot spring site, MW – cooler meteoric water; HW – hot water; R – geothermal reservoir, and F – fault.

3.4 Possibility of power generation at PG1 hot spring system

PG1 site was represented a reservoir temperature of about 120 to 150 °C and estimated total mass flow rates of around 20 to 30 kg/s. Therefore, PG1 site has been classified as a low-enthalpy resource, however, binary power plants can be operated (Bertani, 2012; DiPippo, 2007). A major feature of the PG1 site is that the technology adopted for the power plant needs to be tailored to the geothermal fluid available at the surface. Calculating generated electricity was presented with net generated electric power (NEP) (Bertani, 2012; DiPippo, 2007), assuming the plants was running at full capacity. Based on that values for the feasibility of a binary power plant for PG1 site were calculated using inlet temperatures between 80 and 150 °C and outlet temperatures of 40 °C and 50 °C (Figure 3.23).

At possible NEP for the PG1 site is about 4±0.5 MW, depending on a total mass flow rate of 25±5 kg/s and a geothermal inlet temperature of about 130±5°C. Thus the calculation of generated power for the PG1 with a total mass flow of 25 kg/s lies within the expected range. The net power output of the PG1 power plant was represented about 4±0.5 MW, which would be considered electricity for local scale development (Rubio-Maya et al. 2015). However, this estimate is based on theoretical and pilot plant results and is still has to be proven commercially.

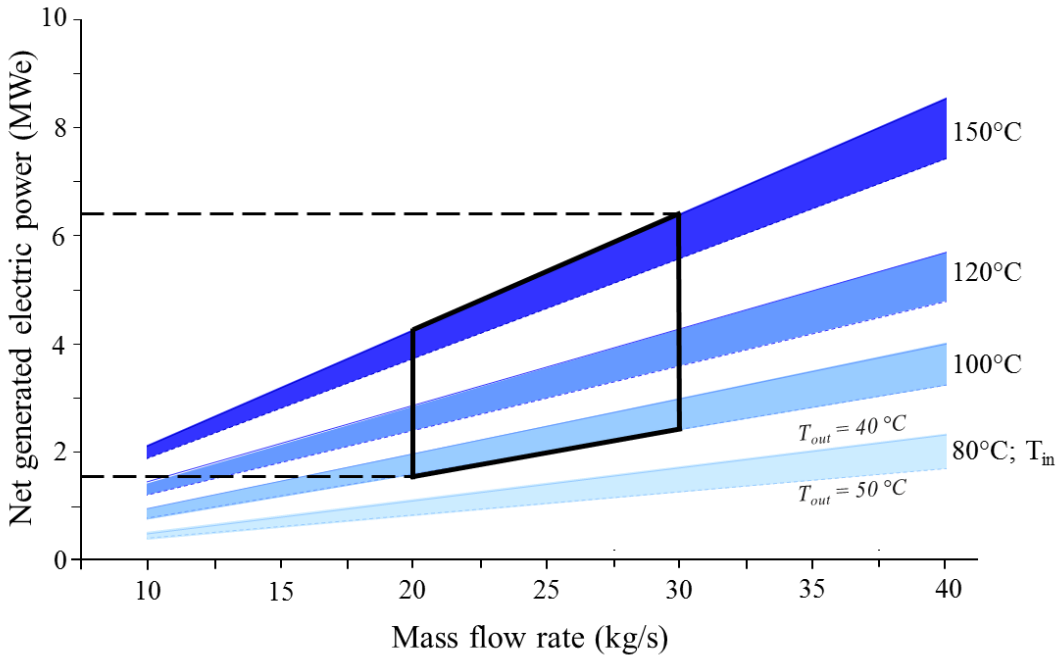

Figure 3.23 Net generated electrical power output for the PG1 geothermal fluids for different total mass flow rate estimates, inlet (T_{in}) and outlet temperatures (T_{out}).

3.5 Case study of Saline Hot Spring Khlong Thom (KB4)

3.5.1 Local Geology of KB4 hot spring system

Several natural saline hot spring pools were found in the study area, both inside and outside the mangrove area (Figure 3.23), which is covering larger parts of the study area. Rock outcrops of Triassic sandstone can also be found as shown in Figure 3.23; some of them form small hills of up to 15 m height, whereas about 1 to 2 km further north and south of the KB4 area Triassic sandstone mountains of 78 m and 100-160 m height, respectively, can be found. The sandstone in the outcrops appears to be highly fractured and chemically altered, often bleached, by the hot spring water (Figure 3.24a and Figure 3.24b). Sand as a weathering product of the sandstone is found in the shallow subsurface overlain by black marine clay, which indicates seasonal flooding events. Natural carbonate crusts with their natural layering structure of up to several decimeters thickness can be found around natural hot springs (Figure 3.24c and Figure 3.24d) and they also develop at geothermal wells recently drilled (not shown). Results of X-ray diffraction analysis of samples taken from sandstone outcrops and the natural carbonate crust at a few meters from the KB4/1 site show mainly quartz and kaolinite as a weathering product for the sandstone, and mainly calcite and quartz for the carbonate crust.

In the southern part of the study area is a salt marsh, a low lying area with an elevation of only a few decimeters above mean sea level; an area between high tide and near-shore sublittoral zone in close proximity to smaller estuary fingers (Figure 3.23). Shallow geological investigations reveal black clay of more than one-meter thickness at the surface above clayey sand layers with sandstone fragments; whereas cutting data from nearby Well 4 show several clay and sand layers down to 42 m depth (Figure 3.25), with the clay likely to be marine deposits (e.g. Spencer and Harvey 2012). Cuttings from Well04 provide a further insight into the subsurface geology down to 150 m depths (Figure 3.23 and Figure 3.25). Below 42 m and down to 112 m sandstone can be found, mainly fine- to medium-grained. For deeper parts, below 112 m, cuttings show larger-grained sandstone.

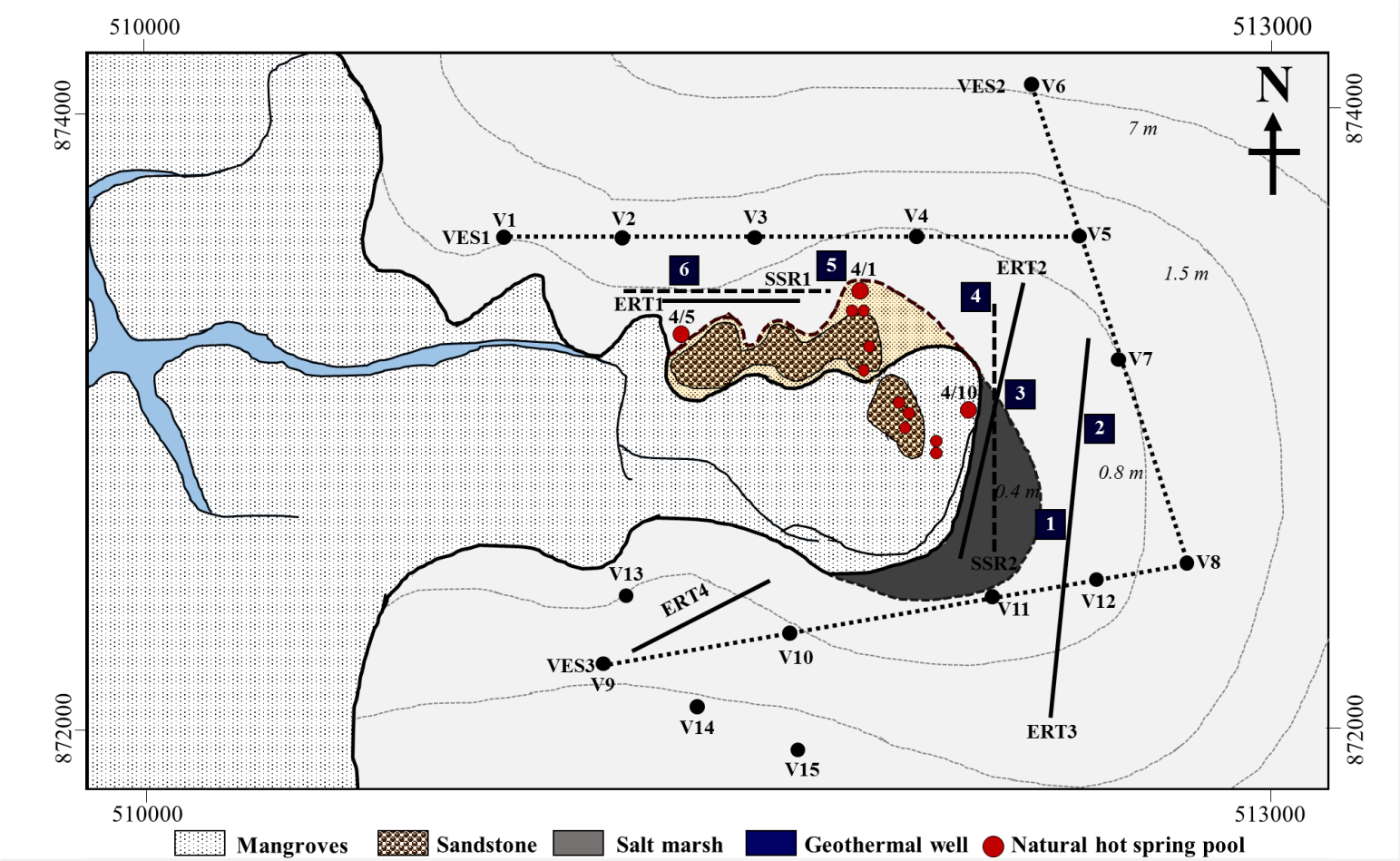

Figure 3.24 Map of KB system, elevation data (dotted lines), location of salt marsh, boundary of shoreline, hot spring locations (selected with numbers), well locations and numbers (black squares), as well as VES cross sections, and ERT and SSR survey line locations.

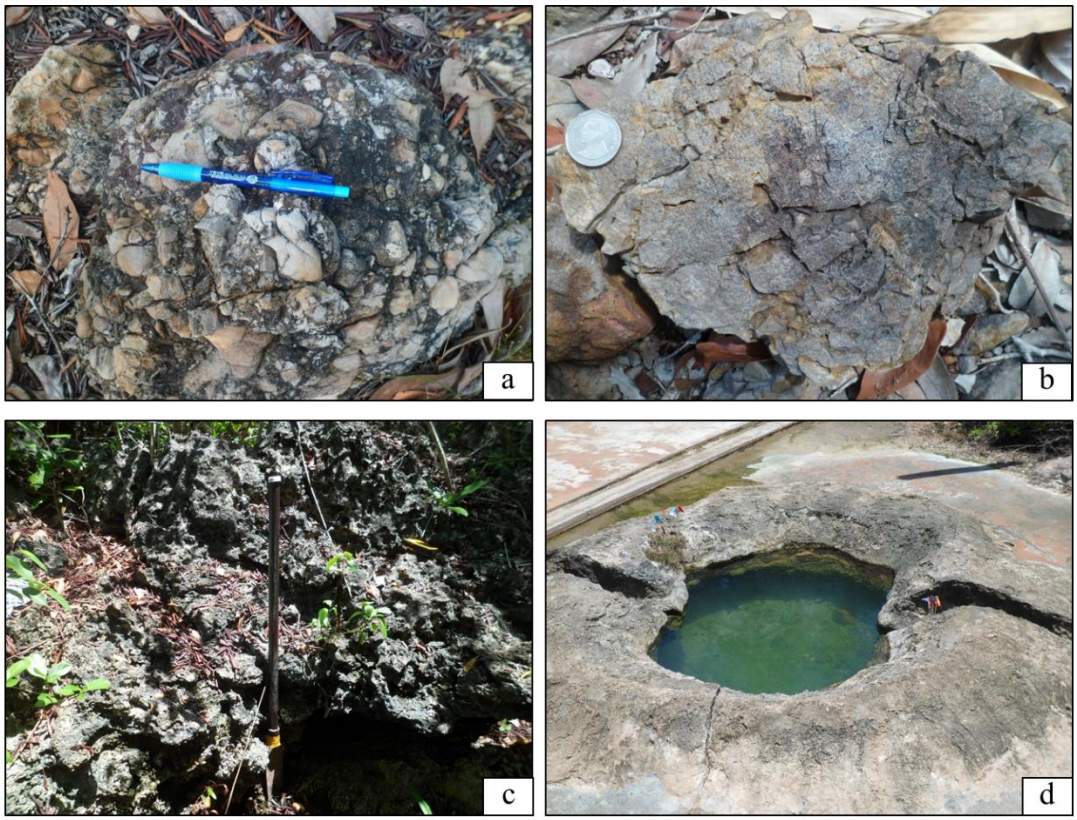

Figure 3.25 (a) and (b) Triassic sandstones bleached by hot spring water and heavily fractured, (c) and (d) Carbonate crusts found around natural hot spring pools both inside and outside the mangrove area.

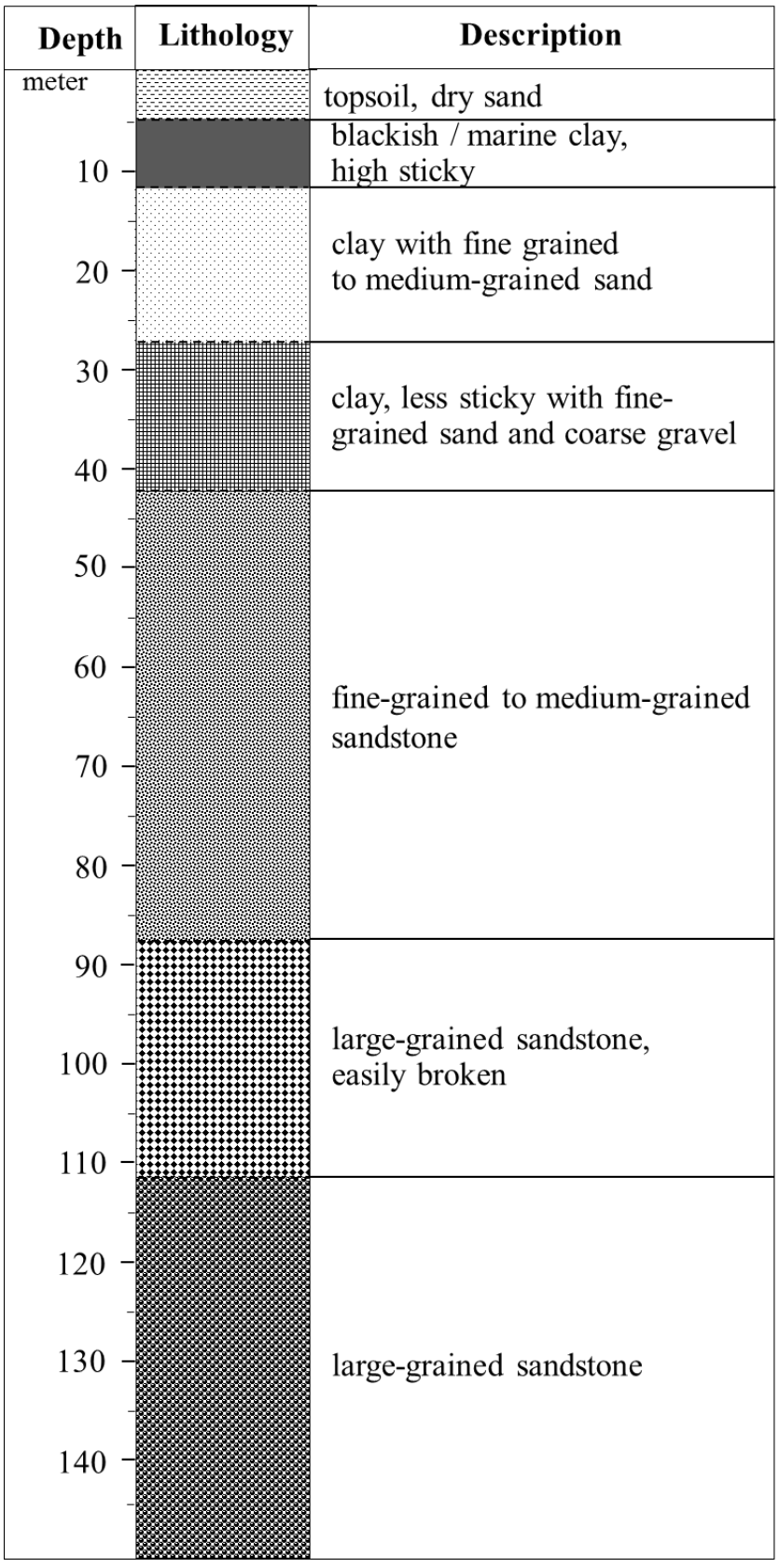

Figure 3.26 Litho-stratigraphy of the Well 04 from cuttings.

3.5.2 Geochemistry of KB4 hot spring system

3.5.2.1 Water properties and chemistry of KB4 site

Results from on-site measurements and chemical laboratory analysis of samples taken from the natural hot spring KB4/5, wells, non-saline groundwater well, and water from the estuary are presented in Table 3.7. KB4/5 has with 46 °C the highest surface discharge temperature of all hot springs and wells within the study area; all wells have lower values, 43 to 40 °C. Due to their non-geothermal character natural groundwater and estuary water have much lower temperatures. The pH is 6.81 for KB4/5 and 6.79 to 6.85 for the wells. Total dissolved solid (TDS) for all geothermal samples is around 12,600 mg/L, which can be considered already saline; whereas the estuary water sample has an almost three times higher value, thus it can be considered seawater (saline) already. In general, TDS can be used as an expression of salinity, where a value of up to 1,000 mg/L is considered fresh water, 1,000-3,000 mg/L fresh to brackish, 3,000-5,000 mg/L brackish, 5,000-35,000 mg/L saline, and 35,000 mg/L and above hyper-saline (e.g. EPA-SA, 2018). The sodium (Na^+) content is with 5,176 mg/L slightly higher in KB4/5 than in the wells, whereas the Cl^- content is almost comparable with around 10,000 mg/L. Other chemical parameters show similar values for all geothermal samples, although with few differences, e.g. Ca^{2+} is slightly higher in Well 3 than in other samples. As expected non-saline groundwater have much lower values for the ion concentrations, whereas the estuary water has much higher values than the hot spring water of the KB4 system. From the chemical composition the estuary water can be considered normal seawater (e.g Millero et al., 2008).

Table 3.7 Surface discharge temperature, pH, salinity, electrical conductivity (EC) and concentrations of some cations and anions (mg/L) of all water samples

Water sample	Surface Temp. (°C)	pH	Salinity (mg/L)	EC (µS/cm)	mg/L (milligrams per liter)								
					TDS	HCO_3^-	Na^+	K^+	Ca^{2+}	Mg^{2+}	SiO_2	Cl^-	SO_4^{2-}
Hot spring pool (KB 4/5)	46	6.76	21,000	27,027	13,451	290	5,198	183	948	339	32	10,361	420
Geothermal wells													
Well01	43	6.80	21,000	25,641	12,669	211	5,128	158	656	260	35	10,011	687
Well02	42	6.85	21,000	26,316	12,673	222	5,148	165	672	265	34	10,336	608
Well03	41	6.79	21,000	25,641	12,671	214	5,126	168	703	269	34	10,336	608
Well04	40	6.92	21,000	25,641	12,550	209	5,132	172	689	259	33	9,998	617
Well05	43	6.75	21,000	25,641	12,669	210	5,128	158	651	259	34	10,111	787
Well06	41	6.81	21,000	25,641	12,739	213	5,208	165	710	264	34	10,386	724
Estuary water	27	7.8	36,000	47, 619	34,483	145	10,752	390	416	1,295	28	19,345	2,701
Non saline groundwater	28	6.98	250	237	43.00	19.22	7.40	0.37	2.52	0.45	1.2	15.52	10

For the further water quality classification of the samples percentages of cations and anions are used (Carvalho et al. 2006; Baioumy et al. 2015). With the Piper diagram major cations and anions are plotted on $(Na^{+}+K^{+})$-Ca^{2+}-Mg^{2+}, Cl^{-}-SO_4^{-}-(CO_3^{2-}-HCO_3^{-}) and (SO_4^{2-}-Cl^{-}) -(Ca^{2+}-Mg^{2+}) (Figure 3.27 and Figure 3.28; Güler et al. 2002). Hot spring KB 4/5 sample, geothermal well waters, and estuary water can be clearly classified as sodium chloride type water (Figure 3.27) and all values plot rather close but clearly far from the non-saline groundwater sample region. In the tertiary plot Cl^{-}-$SO4^{2-}$-HCO_3^{-} (Figure 3.28) the non-saline groundwater sample plots clearly in the bicarbonate region, significantly away from the other water values.

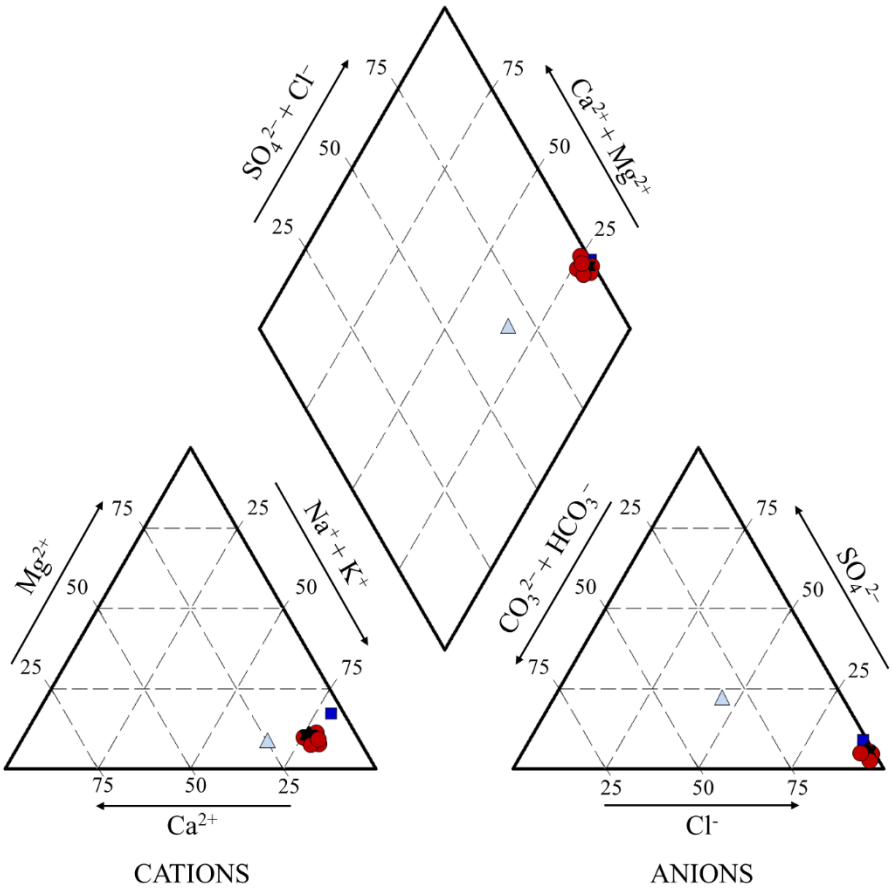

Figure 3.27 Geochemical water analysis of major cations and anions of piper diagram of KB4 hot spring system.

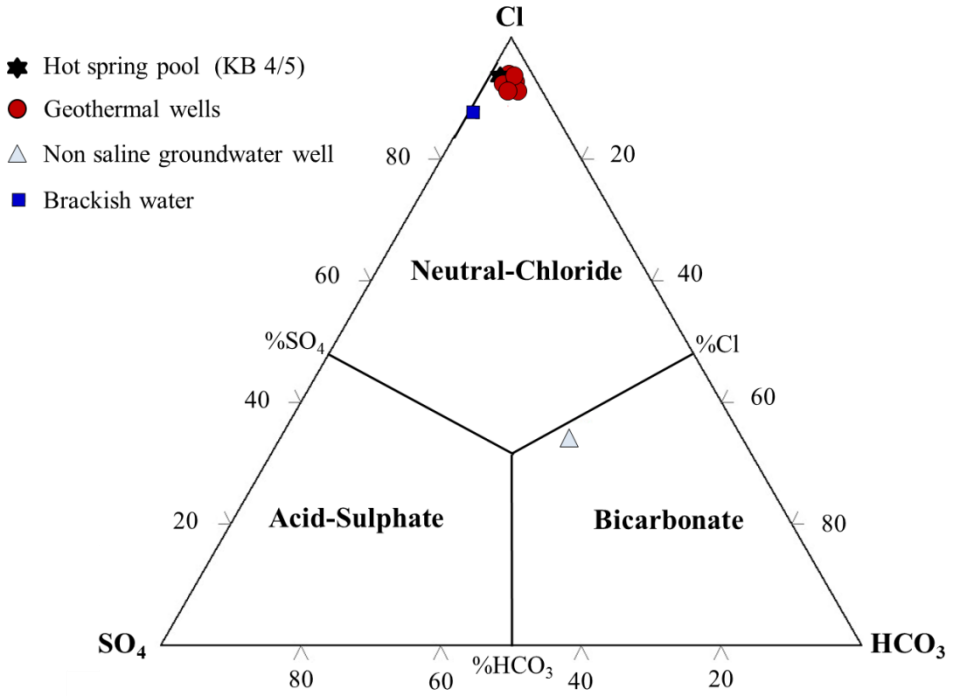

Figure 3.28 Geochemical water analysis of major cations and anions of Cl^{-}-SO_4^{2-}-HCO_3^{-} diagram of KB4 hot spring system.

Plots of ion concentrations versus the concentration of the conservative component chloride for all water samples are shown in Figure 3.29a – Figure 3.29f (see Khaska et al., 2013; Wang et al., 2017). Although the absolute values a rather close (Table 3.7) Na^{+}, Mg^{+}, and HCO_3^{-} exhibit positive trends against the conservative Cl^{-} (Figure 3.29a, 3.29c and 3.29f), while K^{+}, Ca^{+}, and SO_4^{2-} concentrations show scattered relationships that are not correlated with Cl (Figure 3.28, 3.29d and 3.29e). For Ca^{+} the value for the hot spring sample is much higher than the well data; if excluding this value, the well data also shows a positive trend. Together with a positive HCO_3^{-} trend this indicates that much calcite (and dolomite) dissolution occurs along the flow path of the thermal water, with Permian carbonates are assumed at depth below the sandstone formation making the outcrops. Positive trends in Na^{+} and Mg^{+} might indicate progressive mixing of the thermal waters with seawater along preferential pathways in the subsurface. As Well01, 04, and 05 show lower icon concentrations, Well 02, 03, and 06 shows higher values.

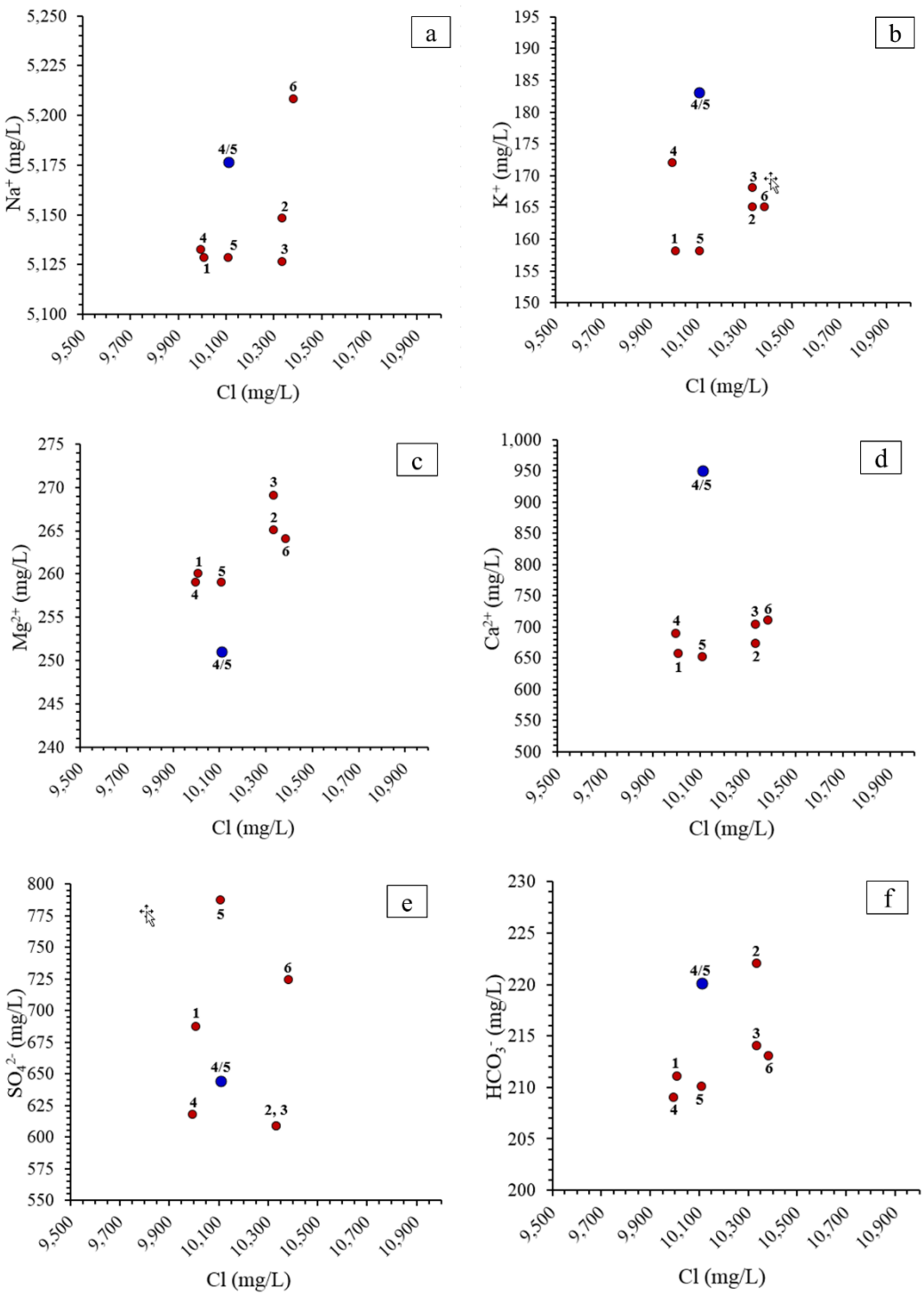

Figure 3.29 Variations of concentrations of major inorganic ions against conservative component of Cl^-.

The subsurface temperature in the KB4 hot spring system was estimated with the silica geothermometer as others cannot be applied here due to the high saline water influx (Mohammadi et al. 2010). Representing temperatures of the geothermal reservoir are in the range from 80 to 90 °C. Dissolved silica concentrations of around 34 mg/L indicate rapid, low-temperature dissolution by the fresh recharge of silica from the water-rock interaction with the Triassic sandstone. Therefore, little re-precipitation occurs in this system because of slow equilibration rates for the more stable silica phases. Silica was found in the carbonate crust precipitated at the hot spring KB4/5.

3.5.2.2 Sr isotope of KB4 site

The value of the Sr and the $^{87}Sr/^{86}Sr$ isotope composition ratios for water samples from the KB4/5 hot spring and the estuary are shown in Table 3.8. The ratios are quite close with 0.7082 and 0.7078, respectively and only slightly lower than the general value for seawater with 0.7092 (Krabbenhöft et al., 2010). The Sr ratio and absolute Sr content of the estuary water (4.88 µM) indicate possible influx from the river (estuary) itself as seawater has much higher absolute Sr concentrations (around 90 µM; Krabbenhöft et al., 2010). Despite that the similarity in the Sr ration is supporting the notion that the main part of the hot spring water at KB4/5 is of seawater origin.

Table 3.8 Strontium isotope concentrations and ratios of hot spring pool (KB 4/5) and estuary water

isotope	**Water samples**	
	Hot spring pool (KB 4/5)	Brackish water
Sr (µM)	4.8800	7.9000
$^{87}Sr/^{86}Sr$ ratio	0.7082	0.7078

3.5.2.3 Rare-earth elements of KB4 site

Rare-earth elements (REEs) were determined to differentiate main sources of water (Goldstein and Jacobsen 1988; Johannesson and Lyons 1994). In general, the chondrite-normalized REE values of the hot spring water are higher than those of the estuary seawater, and those are higher than the groundwater values (Table 3.9,

Figure 3.30), however the patterns of the saline hot spring water and estuary water are similar. As the main sources of REEs to seawater are the river water influx and aeolian flux it seems that the REE distribution of the hot spring water relates to the seawater. Elderfield et al. (1990) suggested that light REEs are preferential removed from river water entering the ocean occurs at low salinity values by salt induced coagulation of river-borne colloids. The increase of TDS content in water samples is associated with an increase in REE concentrations, whereas an increase in the pH value is going parallel with a decrease in REE concentrations (McLing et al. 2014). These REEs might be stored and enriched in the shallow brackish (highly saline) sediments in the estuary and the later mobilized by the upcoming hot water in the shallow geothermal reservoir (Alibo and Nozaki 1999; Hannigan et al. 2010). On other hand, the anomalous behavior of Ce and Eu as well as the degree of fractionation in REE patterns between KB4/5 and estuary waters indicate that the KB4 system composition results from mixing processes with local saline groundwater. However, the positive Eu anomaly of the hot spring water reflects isotopic enrichment of the hot water itself during up flow indicating a relatively reduced environment of reaction in subsurface rock formations (Sholkovitz, 1993).

Table 3.9 Concentrations of REEs in hot spring pool (KB 4/5), brackish water and normal groundwater well samples

Content (ng/L)	**Water sample**		
	KB 4/5	**estuary**	**non-saline**
Lanthanum, La	40.95	3.4	0.08
Cerium, Ce	55.12	1.2	0.07
Praseodymium, Pr	9.04	0.64	0.03
Neodymium, Nd	35.63	2.80	0.01
Samarium, Sm	9.68	0.45	0.02
Europium, Eu	7.53	0.13	0.01
Gadolinium, Gd	16.51	0.70	0.02
Terbium, Tb	2.63	0.14	0.00
Dysprosium, Dy	11.82	0.91	0.01
Erbium, Er	5.59	0.87	0.01
Thulium, Tm	1.93	0.17	0.00
Ytterbium, Yb	3.79	0.82	0.01
Lutetium, Lu	0.77	0.15	0.00

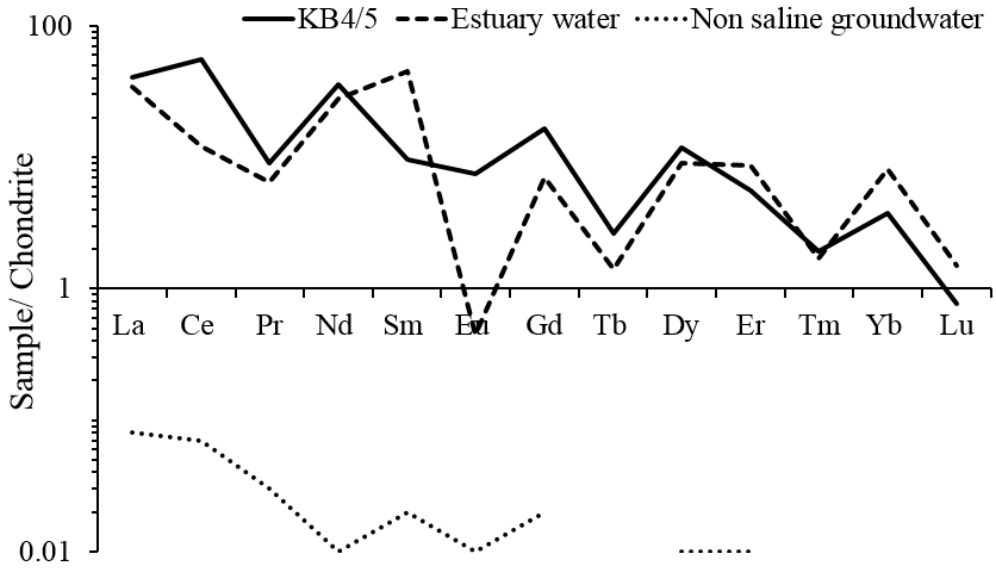

Figure 3.30 Chondrite-normalized plot of REE concentrations of KB4 system.

3.5.3 Geophysical investigation of KB4 hot spring system

3.5.3.1 VES data of KB4 site

Vertical electrical soundings (VES) profiles displayed as lithological sections comprise mainly of 3-4 structural layers with a maximum depth of around 50 m (Figure 3.31-3.33). Geoelectrical soundings of the shallow subsurface consists of a very low resistivity layer with 1-5 ohm-m consisting to sandy, clayey sediments saturated with saline (hot) waters. The temperature effect on the resistivity is here relatively small as the temperature differences themselves are small and the resistivity values are very low (Schön, 1996). Therefore, it is not possible in this area to separate hot saline water from saline water. Further, a layer with low to medium resistivity of 5-40 ohm-m represents sediments rich in sand and gravel deposits, with or without clay, saturated with saline waters. A medium resistivity layer with 40-100 ohm-m indicates sand and gravel sediments with minor clay layers and saturated with freshwater. A higher resistivity value of much more than 100 ohm-m indicates sandstone.

The VES 1 profile from W to E (Figure 3.24 and Figure 3.31) shows on top a thin layer of topsoil, followed by a layer comprised of clay and sand with saline water, and below then saturated sediments, sand and coarse gravel.

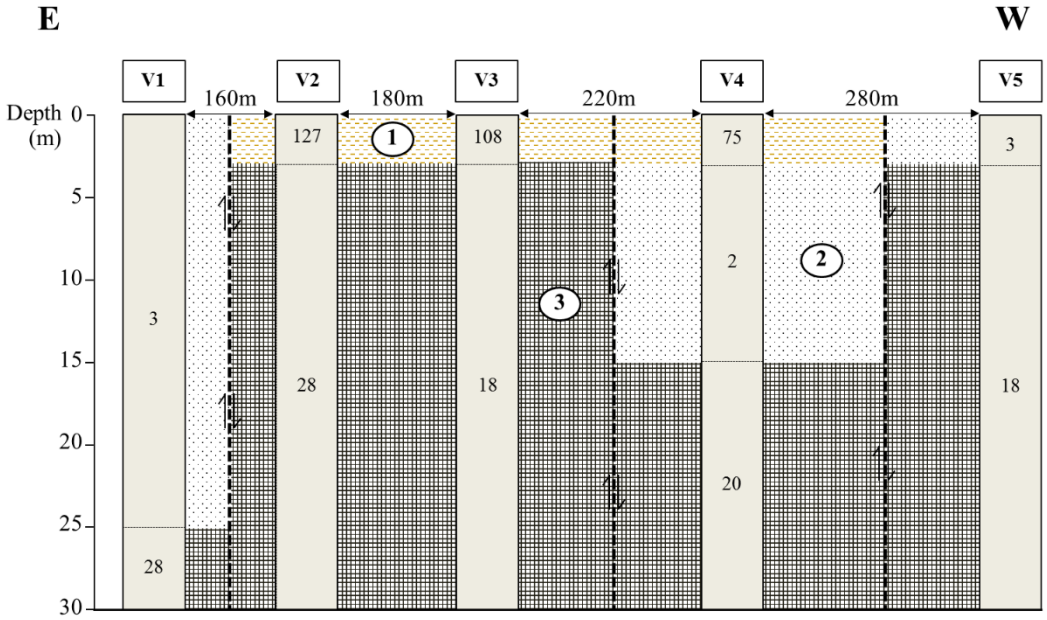

Figure 3.31 VES1 profile, the east-west direction, using the Schlumberger array, where (1) topsoil, (2) clay/sand layers with saline water, (3) coarse gravel layer with saline water and (4) fine grained sandstone. A sharp resistivity contrast indicates a possible vertical fault (black dashed line).

The VES 2 profile from NW to SE (Figure 3.24 and Figure 3.32) exhibits a layer of clay and sand on the top and below layers of sand and gravel with clay and with saline water.

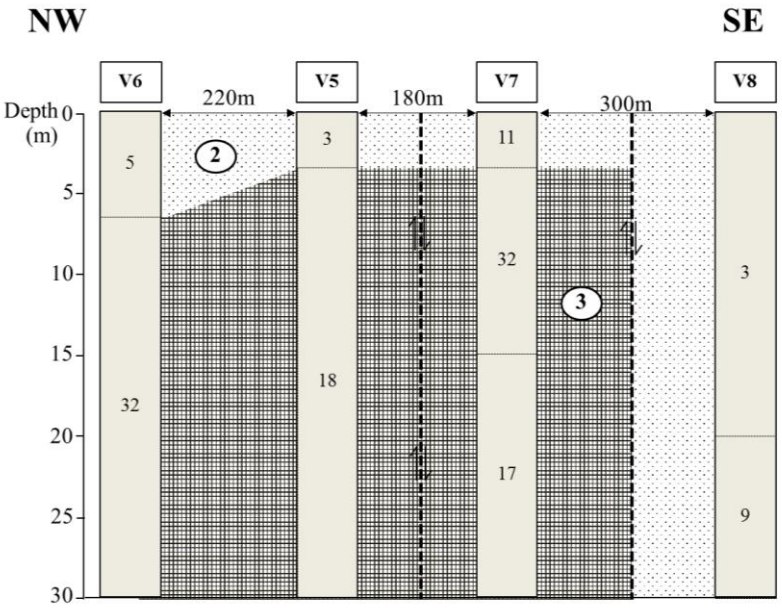

Figure 3.32 VES2 profile, the northeast- southeast direction, using the Schlumberger array, where (1) topsoil, (2) clay/sand layers with saline water, (3) coarse gravel layer with saline water and (4) fine grained sandstone. A sharp resistivity contrast indicates a possible vertical fault (black dashed line).

The VES 3 profile from W to E (Figure 3.24 and Figure 3.33) parallel to VES1 south of the mangrove area consists of topsoil, as well as sand and clay layers, followed by coarse gravel layers and a sand/gravel layer with saline water and/or with clay. Below is high resistivity sandstone, partly saturated with saline water, resulting in lower resistivity values.

Resistivity values of water-bearing sand and gravel layers depend mainly on the salinity of the local groundwater and degree of saturation in the shallow aquifers. Relatively high resistivity values (more 100 ohm-m) indicate sandstone which agrees with cutting information of the geothermal well (Figure 3.24 and Figure 3.26). Abrupt changes in depths and characteristic of layers at short horizontal distances indicate vertical faults in the area.

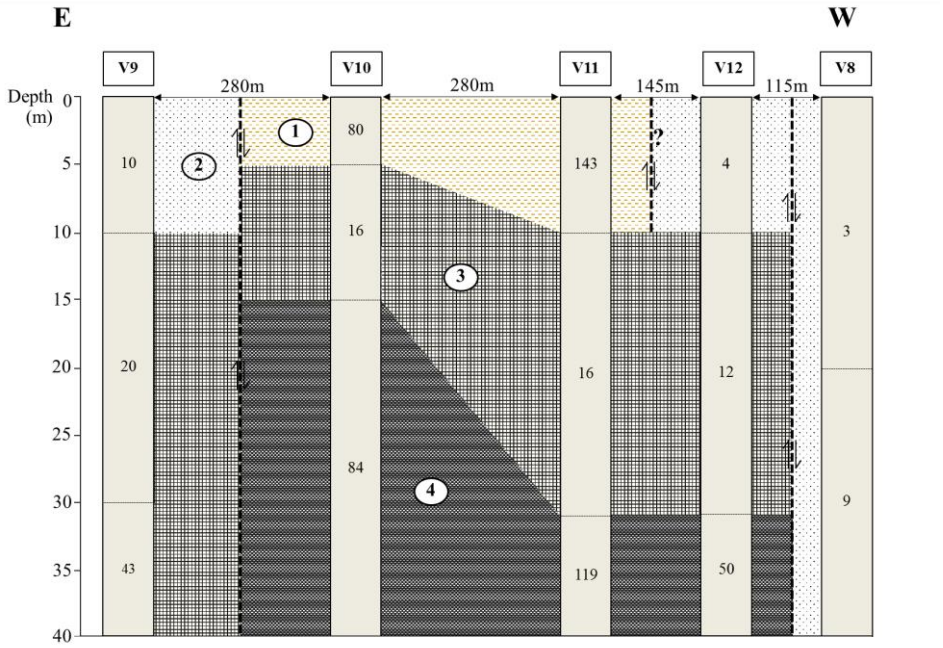

Figure 3 . 33 VES3 profile, the east-west direction (the south of VES1), using the Schlumberger array, where (1) topsoil, (2) clay/sand layers with saline water, (3) coarse gravel layer with saline water and (4) fine grained sandstone. A sharp resistivity contrast indicates a possible vertical fault (black dashed line).

3.5.3.2 ERT data of KB4 site

The cross section of ERT1 profile extends from Well 06 in the west almost parallel and south of the VES1 profile towards the east, with a total length of 200 m (Figure 3.24 and Figure 3.34). This line is as close as possible to hot spring KB4/5 considering pools, walkways, and other man-made structures. A very low resistivity layer with around 1 ohm-m is dipping from around 110 m towards the west into the mangrove and estuary area representing sand and clay layers filled with saline water. At around 20 m depth higher resistivity values of 20 ohm at the center of the line indicates saline water saturated sandstone. Sharp resistivity contrasts present almost vertical faults close to the main hot spring KB4/5 at 75 m and another pool at 85 m.

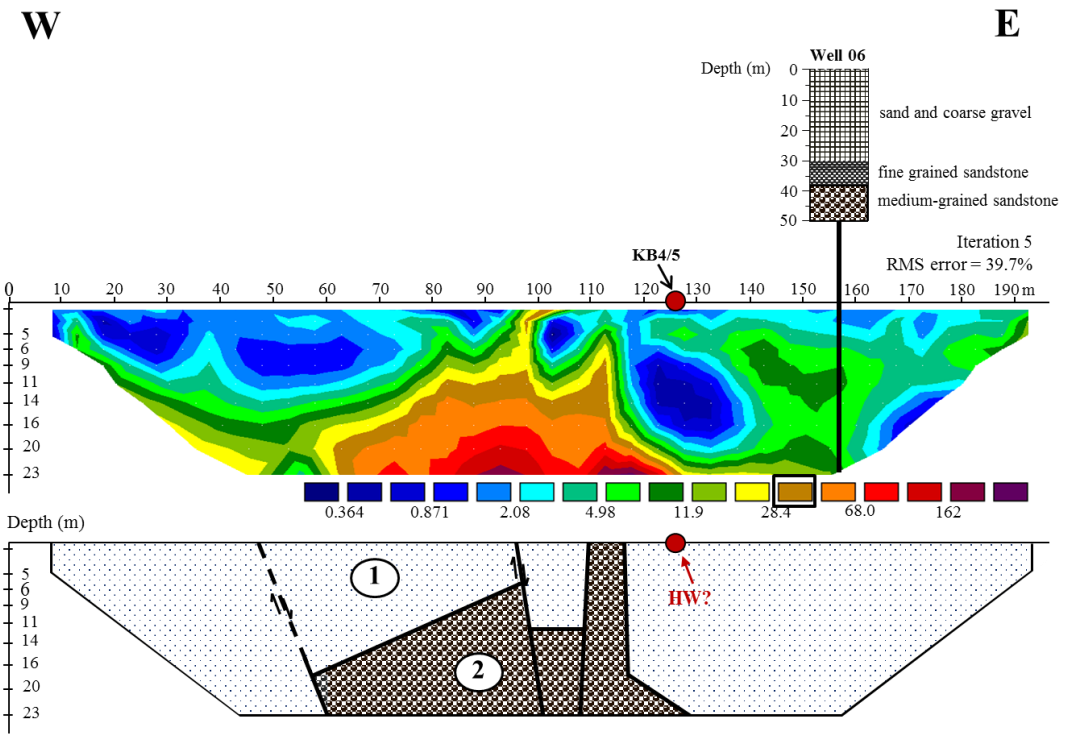

Figure 3.34 2D sections of ERT1 profile, the east-west direction with the Well 06, using dipole–dipole configuration, where (1) clay/sand layers with saline water (2) medium-grained sandstone.

The cross section of ERT2 profile was carried out in the western part of the study area close to a natural hot spring KB4/10 and close to the beginning of the salt marsh further west (Figure 3.24 and Figure 3.35). Anomalously low resistivity values (below 5 ohm-m) at slightly less than 30 m thicknesses in the southwest of the KB4/10 can be interpreted as saline waterlogged zones comprising clay, sandy clay and sand layers, which can be correlated to the cutting data of Well 03 (Figure 3.26; see Table 3.7) and also to the cross section profile of VES2 (Figure 3.24 and Figure 3.35). Here the resistivity values are slightly higher as VES cannot resolve vertical structures and integrates horizontally (see Keary et al., 2002). For depths ranges from 40 m and deeper higher resistivity value of 75 ohm-m can be observed; representing saline water saturated sediments and fractured sandstones (Figure 3.35). Layers of low resistivity values in between 80 m and 130 m distance and below 40 m depths are likely related to vertical movement along fractures in the sandstone. In the central part of the cross section between 180 m and 250 m at approximately 25 m depth a higher

resistivity value of more than 250 ohm-m can be seen (Figure 3.35), apparently shallow sandstones, partly or likely less saturated with saline water. Clearly vertical boundaries between the structures point to shallow faults or fractures.

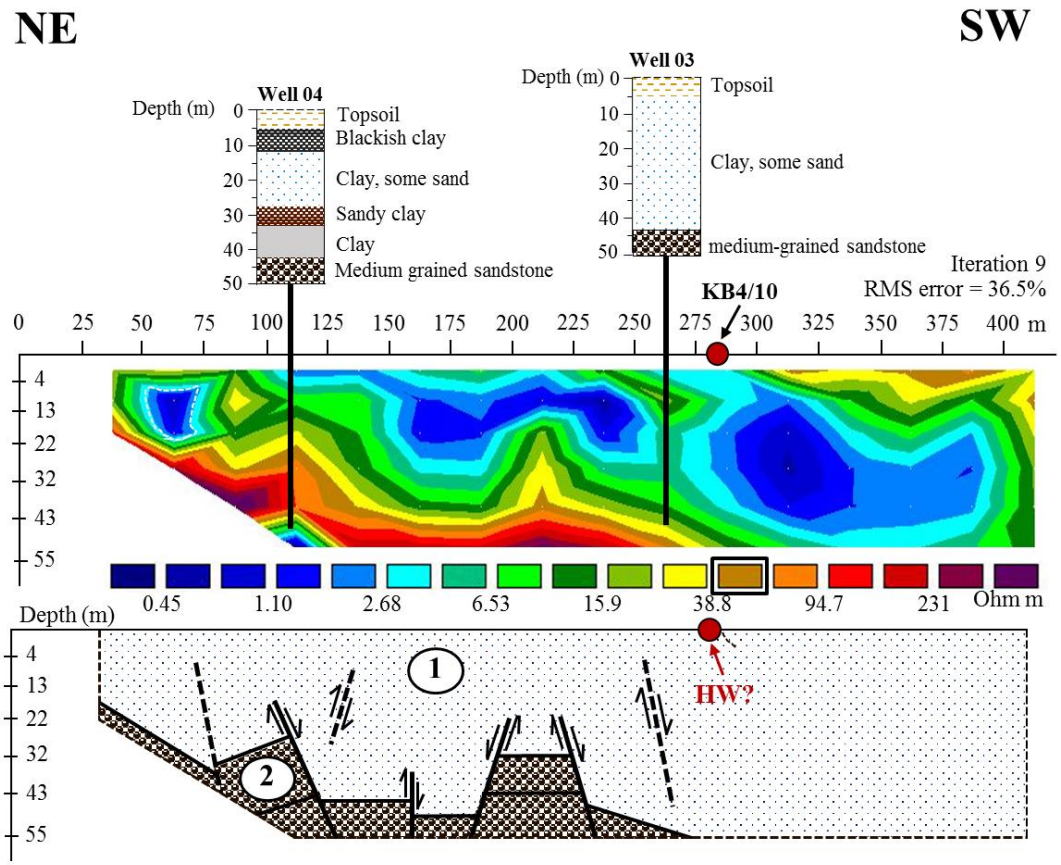

Figure 3.35 2D sections of ERT2 with location of natural hot spring (KB 4/10) and the Well 03 and Well 04, using dipole–dipole configuration, where (1) clay/sand layers with saline water (2) medium-grained sandstone.

The cross section of ERT3 profile (Figure 3.24 and Figure 3.36) is almost parallel to line ERT2, but further west crossing the salt marsh area. Although in the area no natural hot spring can be found, the cutting data of the Well 01 and Well 02 can be correlated. Geoelectrical layers with resistivity values below 5 ohm-m at approximately 5 to 40 m depth are considered to be saline water-saturated zones of sand and clay layers. The layer below 40 m depth is sandstone, which is extending upwards towards the NE and is assumed to be found in the SW below a thick cover of

saline water saturates sand and clay layers (Figure 3.36). This profile clearly reveals almost vertical faults at slightly more than 40 m depth, which are of extensional character.

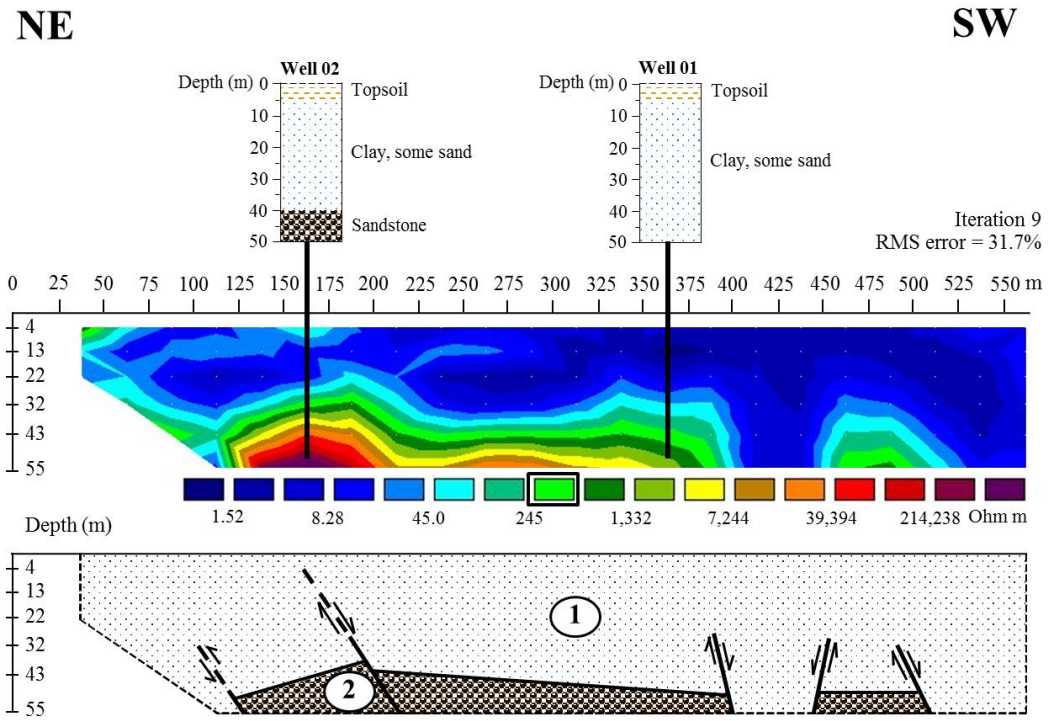

Figure 3.36 2D sections of ERT3 profile with location of the Well 01 and Well 02, using dipole–dipole configuration, where (1) clay/sand layers with saline water (2) medium-grained sandstone.

The cross section of ERT4 profile (Figure 3.24 and Figure 3.37) was shows saline water saturated layers at the top down to depths of about 15 m over the whole profile with some deeper section at 280-300 m line distance (Figure 3.33). Higher resistivity layer of much more than 300 ohm-m below indicate non-saturated dry sandstone. At around 180-210 m and 280-300 m discontinuities in the resistivity distribution indicate major vertical faults of extensional character as seen in ERT 3.

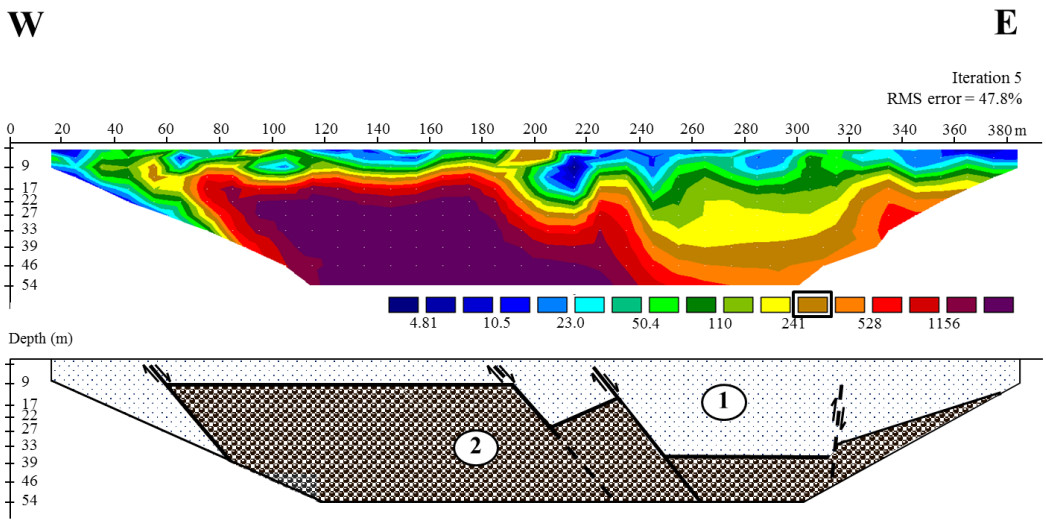

Figure 3.37 2D sections of ERT4 profile, the east-west direction, using dipole–dipole configuration, where (1) clay/sand layers with saline water (2) medium-grained sandstone.

3.5.3.3 SSR data of KB4 site

Geological interpretations of two shallow seismic-refraction (SSR) profiles in E-W and N-S direction in the northern and western part of the area are shown in Figure 3.38-3.39 (Figure 3.24). Subsurface layers and structures have been identified by reflections and their discontinuities (Liberty, 1998). Cross sections illustrate layers in the shallow parts filled with sediments, clay, sand, and coarse gravels, corresponding to cutting data of the Well 03 to 06. Results from the VES and ERT profiles show that main parts of these layers are saturated with saline (hot) water. Below these layers fractured sandstones has been interpreted with mainly more or less vertical faults. The fracture spacing is often only 20 m and they can be interpreted as normal or reverse movement, indication compressional as well as extensional tectonics. The first type relates to the larger geotectonic setting, whereas the latter ones were also found in the ERT sections. Any lateral movement is not resolved in the cross sections. Some faults can be drawn as deep as 250 m (Figure 3.38-3.39). The hot water flow is likely controlled by these shallow faults from depth into the shallow sediment. The cutting data from Well 04 (Figure 3.26) suggest that only the approx. upper 100 m of the sandstone are densely fractured as indicated also in the seismic

refraction sections. Faults or fractures where the hot spring water flows up from depth are not resolved here.

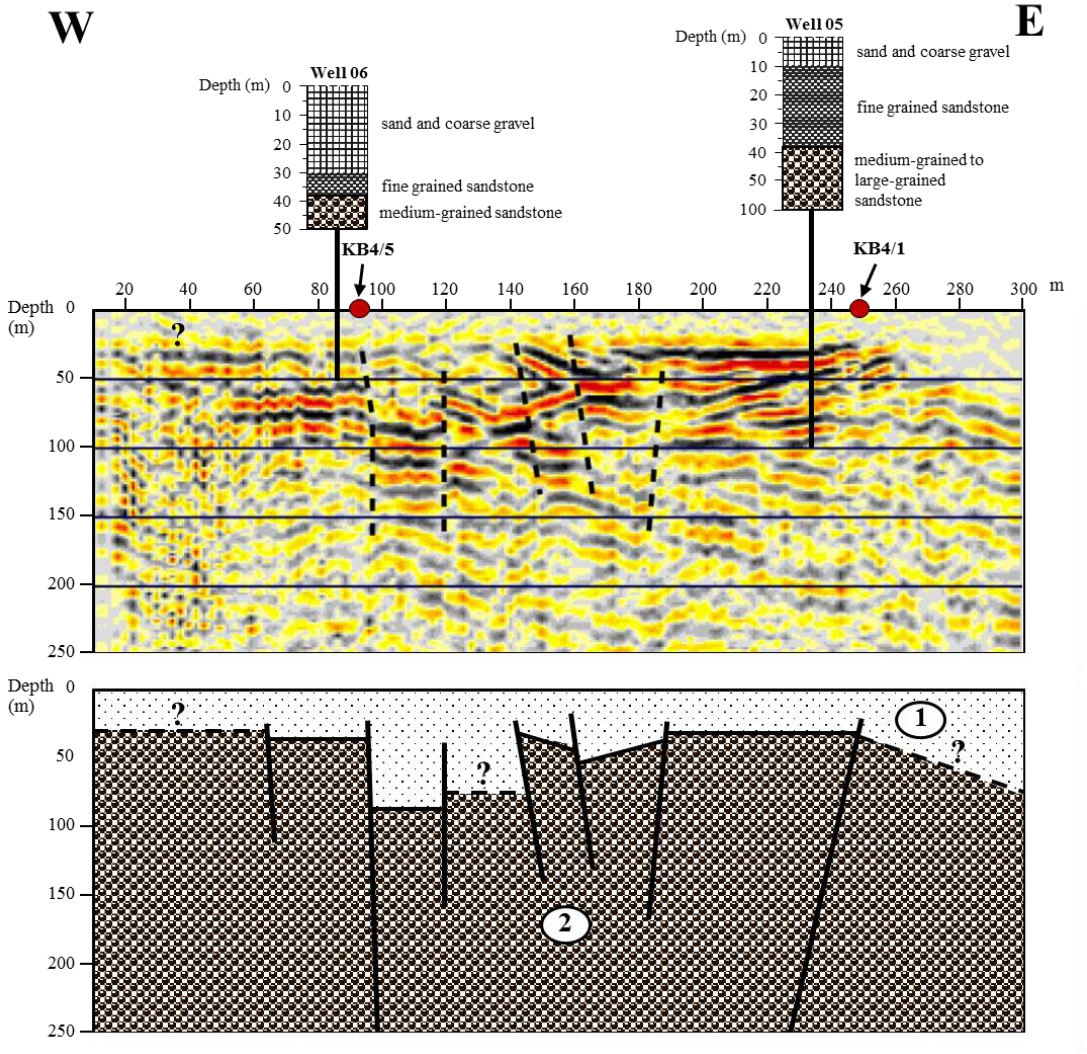

Figure 3.38 Geological section based on well data along seismic reflection profiles of interpreted West–East seismic line with location of natural hot spring (KB 4/1 and KB 4/5), where (1) clay/sand layers with saline water (2) medium-grained sandstone. A sharp seismic contrast indicates a possible vertical fault (black dashed line).

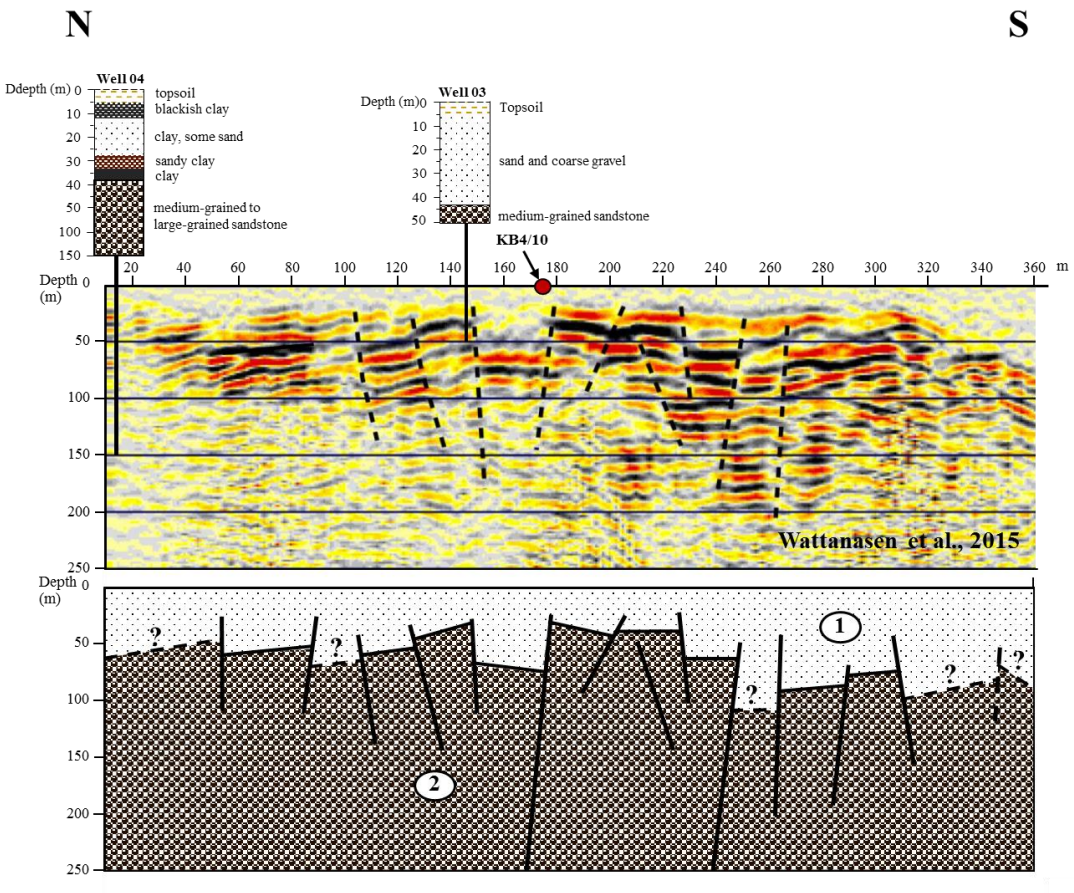

Figure 3.39 Geological section based on well data along seismic reflection profiles of interpreted North–South seismic line with location of natural hot spring (KB 4/10), where (1) clay/sand layers with saline water (2) medium-grained sandstone. A sharp seismic contrast indicates a possible vertical fault (black dashed line).

3.5.4 Hydrogeological model of KB4 hot spring system

The integration of all result from geological, geochemical, and geophysical investigations allows drafting a schematic picture of the saline hot spring system in Krabi (Figure 3.40). The heat source of this and of other hot springs in the area is not known yet (Bunopas and Vella 1992; Raksaskulwong and Thienprasert 1995). North of the study site is Krabi basin of Tertiary age assumed to be separated by the larger fault system to the south as indicated in Figure 1.2. This extensional tectonics seemingly also has affected the study area as indicated by small scale horst and graben structures in the Triassic sandstone with almost vertical clearly identified in the seismic and ERT sections. In such stress regime these faults are providing open

pathways for hot water coming up from the depth. Seismic sections reveal that some of these faults can be traced down to 250 m depth. However, an earlier tectonic phase has to be of compressional character as shown in Figure 1.2 with a roughly NE-SW maximum horizontal stress direction, which would correlate to Sunda Subduction Zone further west in the Andaman Sea. This tectonic phase resulted in NW-SE elongated outcrops of Permian-Carboniferous to Cretaceous-Jurassic formations, including Permian limestone, which is considered to be found below the Triassic sandstones of the study area, deeper than 150 m as Well 04 has not encountered it (Figure 3.40). Outcrops of this formation can be found on small islands further west of the hot spring area (Figure 1.2). The compressional tectonic phase probably has already created the almost vertical faults in the Triassic sandstones, but would not have provided open pathways upwards.

The proximity of the KB4 location to a major estuary system that is connected to the Andaman Sea in the west resulted in saline water intrusion into the local aquifer system, which is a common situation of near coastline aquifers (e.g. Paster, 2010). The morphology shows an almost circular shaped low lying area, which includes the salt marsh, with increasing elevation towards north, east, and south (Figure 3.24), thus defining the shallow aquifer with a maximal thickness of around 50 m, which comprises sand, gravel and clay layers (e.g. Well 04, Figure 3.26). The dipping of this shallow aquifer towards the center of the low lying area and towards west is well documented in ERT 1, 2, and 3 (Figure 3.34 – Figure 3.36) and thereby defining it boundaries. The saline waters likely infiltrated also the groundwater at larger depth, at about 100 to 150 m, through the fractured sandstone along (open) faults presented in the seismic sections in Figure 3.20. Such saline infiltrations in deeper parts are harder to identify and evaluate (Barlow and Reichard 2009; McCarthy et al. 2005).

Silica geothermometer provides a possible geothermal reservoir of 80-90 °C, which translates into a depth of about 1.5 km considering the surface discharge temperature of 46 °C and a possible geothermal gradient of about 30 °C/km (Turcotte and Schubert, 2002), although no heat flow data from this area are available. The geothermal reservoir can be still in the Triassic sandstone formation or in deeper Permian carbonates as both rock types can provide pore space and permeability (e.g.

Schön, 1996). Further, seismic sections in Figure 3.20 reveal faults at least down to 250 m, probably deeper, thus offering open pathways for the hot water upwards to the shallow subsurface (Figure 3.40).

The strontium isotope ratio (Table 3.7) and rare-earth element distribution (Figure 3.30) show that the water from hot spring KB4/5 and the estuary seawater have a quite similar geochemical signature indicating a mixing of both waters in the fractured sandstone formation of upper 150 m. The cation and anion concentrations between KB4/5 water and the geothermal wells in the area are also quite similar, however with some differences. Positive trends for Na, Mg, and Ca in the binary plots in Figure 3.27, Figure 3.29e, and Figure 3.29d, respectively, indicate differential mixing from Well 01, 04, and 05 towards Well 02, 03, and 06. Shallow fractures delineated by geophysical results, VES, ERT, and seismic reflection data (Figure 3.31– Figure 3.39), can act as fluid conduits but also can act as barriers, thus separating the geothermal reservoir in small blocks, which results in a highly localized groundwater and geothermal water flow regime, which consequently leads to differential mixing patterns. On the other side the geothermal samples, KB4/5 hot spring and wells, exhibit significant higher concentrations of Ca, HCO_3, SiO_2 in comparison to the seawater from the estuary, thus indicating another source rather than the saline groundwater. It is likely that those elements where dissolved through water-rock interaction during the flow of the geothermal water upwards, through Permian limestone and Triassic sandstone (Figure 1.2). This and other results presented here would indirectly indicate a recharge of the geothermal system KB4 by meteoric water (Figure 3.40); however, no further data are available here.

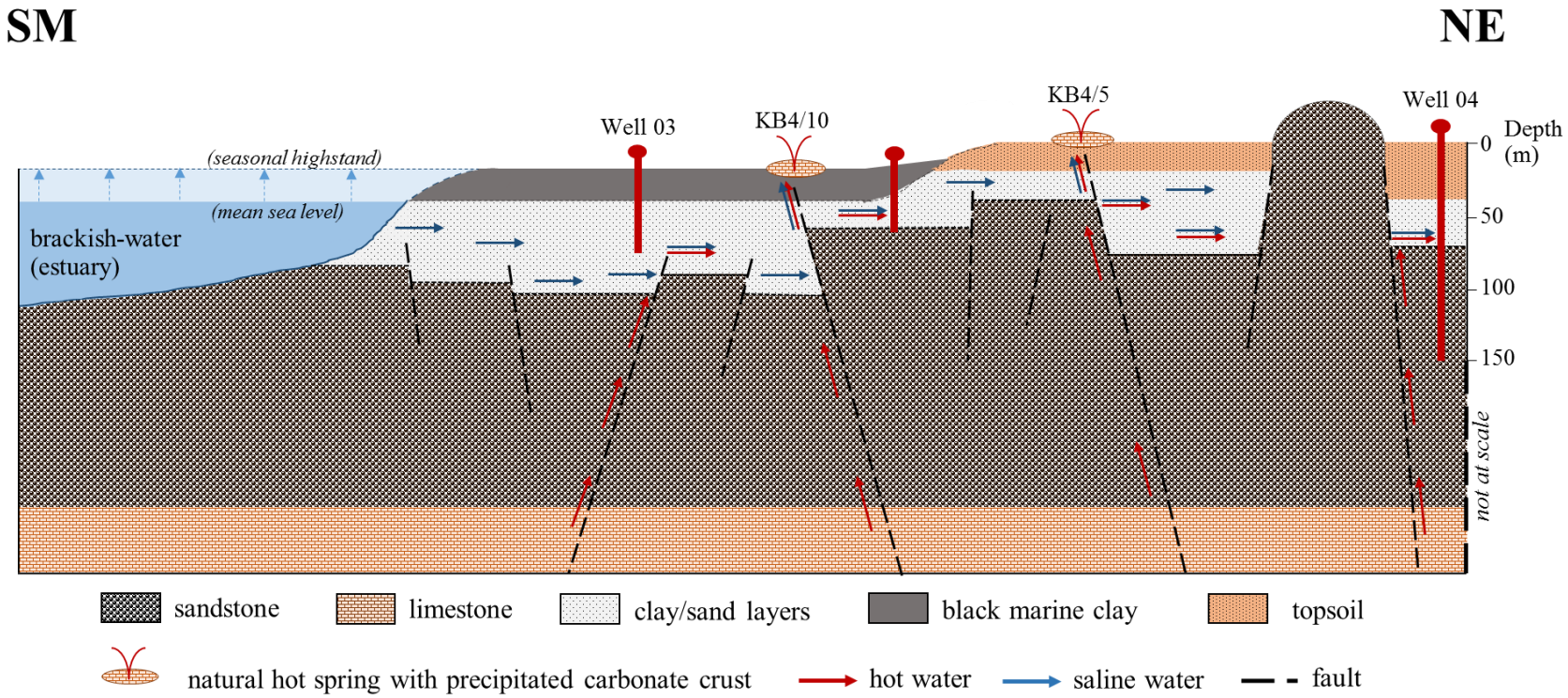

Figure 3.40 Schematic cross section of geological and hydrogeological system of the geothermal system of KB4.

CHAPTER 4
CONCLUSIONS AND OUTLOOKS

Geothermal hot springs in Southern Thailand are characterized by the medium to high surface discharge temperatures, the wide concentration range of dissolved chemical compositions, and also similar to meteoric waters. Most of the hot spring waters are similar characterized as the sodium bicarbonate types. Moreover, the observation from Krabi, Phang Nga and Surat Thani geothermal systems shows a seasonal fluctuation on the chemical contents of Na, K, Ca and HCO_3 suggesting that geothermal systems represent secondary reservoirs. For all hot springs in Southern Thailand the real heat sources are not known. It can be either an igneous body where radioactive decay produces heat or a higher heat flow during basin development onshore. One exception is the Phang Nga and Ranong hot springs as geophysical investigations hint a possible igneous (magmatic) body at larger depth as the possible heat source.

For the geothermal assessment of geothermal hot spring systems in Southern Thailand, analysis has focused on the reservoir potential evaluation and the economic potential of the hot spring sites, which are directly linked to financial investments and subsequent risks. Reasons for this are twofold. First, the ranking of the reservoir available is most important for the development success as it indicates the geothermal potential of a region, whereas exploration efforts can be improved. Second, land and market availability factors are quantitatively accessible to a company management. However, as all positive factors of all fractional scores are important a simple summation might not fully represent the potential of a site. From altogether 30 hot spring sites in Southern Thailand used in this assessment finally two have been chosen which likely have a good potential for electricity production. Although the positional ranking of geothermal sites might not be very robust (sensitive) to uncertainties and to the quality of data used for such an assessment, but it is robust enough to provide some kind of quantitative assessment, which can be easier translated into economic values and financial risks. It should be noted that the ranking presented here is somewhat subjective since it uses researchers for qualitative

evaluations. To a certain extent this opinion may be incorrect or biased, or does not reflect the actual conditions. As many assumptions are used for individual site assessments, such as depth of reservoir, flow rates, it would be preferable if more precise data were known. Generally, methods employed are likely to create a bias in favor of sites with more complete information (e.g. Campos, 1988; Muffler and Cataldi, 1978; Quinao and Zarrouk, 2018). Since the certainty of all information available of the inputs is more favorable. There are certain sites of geothermal hot springs in Southern Thailand instead of RN6 of Ranong system, SR3 and SR7 of Surat Thani system and YL1 of Yala system, where additional new data could alter some of the results of the study. Even though authors were aware of that the results can be used as a guide for a future definition of sites that should receive further scientific investigations and financial investments. The final ranking shows that two hot springs sites, RN1 in Ranong and PG1 in PhangNga Province, have a good potential for further development.

The PG1 hot spring of Phang Nga geothermal system was the possibility of the electrical resource site in Southern Thailand. The heat source for this system is likely the igneous bodies, which are partly exposed at the surface, but also extend further downwards. MT measurements suggest that meteoric water is flowing down at least 2,000 m and heating up. Geothermometer calculation suggest a geothermal reservoir as deep as 3.6 to 5.2 km. Facture and/or faults, respectively their intersections, related to the nearby Khlong Marui fault zone, are providing the main pathways for the meteoric water to descent downwards and the hot water to flow up. PG1 hot spring is currently used mainly by locals for bathing, but the system provides a potential for further uses, especially for electricity generation via low enthalpy technology. A possible demand side for the electrical power is only 20 to 50 km west of the hot spring site with the international tourist destinations along the Andaman Sea beaches.

On the other hand, the Khlong Thom Saline Hot Spring Krabi, KB4, is hydrogeological of unique occurrence as it is in real sense a saline hot spring. Through the integration of result from geological, geochemical, and geophysical investigations schematic image of a complex saline hot spring system could be drafted, although still some questions remain, especially about the heat source.

Saltwater intrusion into highly fractured sandstone formations and overlain sand and clay bearing sediments in a low lying area near a saltwater estuary combined with hot water flowing towards the surface via tectonically opened fractures resulting in saline hot springs exhibit a unique hydrogeological setting. Through integrated geoscientific investigations a better understanding of this system has been achieved as it is of importance, because the site is currently under intense development as a tourist place.

Outlook

Geothermal systems in Southern Thailand can be characterized as low enthalpy geothermal resources with temperatures as low as 80 °C, suitable for electricity production in the first level of the cascade. Shallow reservoir temperatures of geothermal fluids for cascade systems in Southern Thailand range between 80 and 120 °C. Regarding low enthalpy geothermal fields, Kenya is among the world's most active regions for geothermal development with about 381.6 MW of geothermal power generated (Shortall et al., 2015). It has to be noted that Kenya is one of the African countries with the largest geothermal exploration efforts and the first country to harness geothermal energy for power generation on the continent. The low-enthalpy systems occur along the flanks of the African rift systems, with hot spring exit temperatures of 52 to 95 °C (Shortall et al., 2015).

Thailand also has formulated ambitious plans to develop a further 5 to 10 MW (or more) of geothermal power generation. This requires significant new investment capital, which might be raised largely by PTT, the Department of Alternative Energy Development and Efficiency (DEDE), and the Department of Groundwater Resources (DGR) under a Memorandum of Understanding (MOU) on exploration and development of geothermal resources for electricity generation in Thailand. Although in the recent *Renewable Energy Outlook* (IRENA, 2017) it was stated that "*the development of geothermal has since [1989] then been stagnant due to very little resource availability*" this paper has shown that at least for Southern Thailand there are geothermal resources, which, with further exploration and development, might be part of the renewable energy mix in near future.

REFERENCES

Alibo, D.S., Nozaki, Y., 1999. Rare earth elements in seawater: Particle association, shale-normalization, and Ce oxidation. Geochimica et Cosmochimica Acta 63(3/4), 363–372.

Apollaro, C., Vespasiano, G., Rosa, R.D., Marini, L., 2015. Use of mean residence time and flow rate of thermal waters to evaluate the volume of reservoir water contributing to the natural discharge and the related geothermal reservoir volume. Application to Northern Thailand hot springs. Geothermics 58, 62–74.

Ármannsson, H., Ólafsson, M., 2007. Geothermal sampling and analysis. Presented at Short Course II on Surface Exploration for Geothermal Resources, organized by UNU-GTP and KenGen, at Lake Naivasha, Kenya, 2-17 November.

Arnórsson, J.O., Bjarnason, N., Giroud, N., Gunnarsson, I., Steffánsson, A. 2006. Sampling and analysis of geothermal fluids. Geofluids 6, 203–216.

Arnorsson, S., 1983, Chemical equilibrium in Icelandic geothermal systems-Implications for chemical geothermometer investigations. Geothermics12, 119-128.

Awaleh, M.O., Hoch, F.B., Kadieh, I.H., Soubaneh, Y.D., Egueh, N. M., Jalludin, M., Boschetti, T., 2015. The geothermal resources of the Republic of Djibouti — I: Hydrogeochemistry of the Obock coastal hot springs. Journal of Geochemical Exploration 152, 54–66.

Barkaoui, A.E., Boldyryev, S., Duic, N., Krajacic, G., Guzović, Z., 2016. Appropriate integration of geothermal energy sources by Pinch approach: Case study of Croatia. Applied Energy 184, 1343–1349.

Barlow, P.M., Reichard, E.G., 2009. Saltwater intrusion in coastal regions of North America. Hydrogeology Journal 18, 247–260.

Barnett, A., Cerin, E., Zhang, C. J. P., Sit, C. H. P. Johnston, J. M., Cheung, M. M. C., Lee, R. S. Y., 2016. Associations between the neighborhood environment characteristics and physical activity in older adults with specific types of chronic conditions: the ALECS cross sectional study. Barnett et al. International Journal of Behavioral Nutrition and Physical Activity 13 (53), 1–13.

Bhongsuwan, T., Auisui, S., 2015. A high natural radiation area in Khao-Than hot spring, Southern Thailand. Radiation Protection Dosimetry 167, 284–288.

Bignall, G., Sanders, F., 2016. Proposed methodology for assessment and ranking of geothermal Systems. The 11th Asian Geothermal Symposium, Chiang Mai, Thailand, 18–20 November.

Bunopas, S., 1982. Paleogeographic history of Western Thailand and adjacent parts of Southeast Asia - A plate-tectonics interpretation. Ph.D. Thesis, Victoria. University of Wellington, New Zealand, p. 810; reprinted 1982 as Geological Survey paper, No.5, Department of Mineral Resources, Thailand.

Bunopas S, Vella P (1992) Geotectonics and geologic evolution of Thailand. Proceedings of the National Conference on Geologic Resources of Thailand: 209–228.

Cagniard, L., 1953. Basic theory of the magnetotelluric method of geophysical prospecting, Geophysics 18, 605–635.

Campos, T., 1988. Geothermal Resources of El Salvador. Preliminary Assessment. Geothermics 17(2/3), 319–332.

Carnarvon Petroleum Ltd., 2013. http://www.carnarvon.com.au/wp-content/uploads/2013/04/Quarterly-Activities-Report-March-2013-FINAL.pdf

Carotenuto, A., Ciccolella, M., Massarotti, N., Mauro, A., 2016. Models for thermo-fluid dynamic phenomena in low enthalpy geothermal energy systems: A review. Renewable and Sustainable Energy Reviews 60, 330–355.

Carvalho, M.R., Forjaz, V.H., Almeida, C., 2006. Chemical composition of deep hydrothermal fluids in the Ribeira Grande geothermal field (São Miguel, Azores). Journal of Volcanology and Geothermal Research 156, 116–134.

Charusiri, C., Chaturongkawanich, S., Takashima, I., Kosiwan, S., Won-in, K., Cat, N., 2000. Application of geothermal resources of Thailand, Vietnam, and Myanmar to tectonic settings. The World Geothermal Congress, Tohoku, Japan, May 28-June 10, 1043–1047.

Chaturongkawanich, S., Leevongchareon, S., 2000. The geothermal resources of Changwat Ranong Southern Thailand. The World Geothermal Congress 2000, Kyushu-Tohoku, Japan, May 28-June 10, 1049-1052.

Chave, D.A. and Jones, A.G., 2012. The magnetotelluric method. Cambridge University Press, 602 pp.

Chena, W., Chiang, H., 2016. Subsurface temperature trends in response to thermal water exploitation in the Jiashi Hot Spring, northeastern Taiwan. Geothermics 60, 126–133.

Chinoroje, O., 1993. Petrographic studies of Permian carbonates in southern Thailand. Journal of Southeast Asian Earth Sciences 8(1-4), 161–171.

Chong, L. H. H., Mohd, N. D., 2000. Tawau Hill Park springs, Sabah, Malaysia, GHC Quarterly Bull 21(4), 3– 4.

Chuaviroj, S., 1988. Geothermal development in Thailand. Geothermics, 17, 2/3, 421-428.

Cid-Andres, A.P., 2015. A review on useful concepts for stable isotope of oxygen in phosphate ($\delta^{18}O_p$) extraction, purification and analysis of freshwater samples and other potential phosphate sources, Microchemical Journal 123, 105–110.

Coothongkul, V., Chinapongsanond, P., 1985. Resistivity Survey Fang Geothermal Prospect, Ban Pong Nam Ron. Electricity Generating Authority of Thailand, Amphoe Fang, Chiangmai, Thailand, 61.

Craig, H., 1961. Isotopic variations in meteoric waters. Science 133(3465), 1702-1703.

Craig, J., Absar, A., Bhat, G., Cadel, G., Hafiz, M., Hakhoo, N., Kashkari, R., Moore, J., Ricchiuto, T.E., Thurow, J., Thusu, B., 2013. Hot springs and the geothermal energy potential of Jammu & Kashmir State, N.W. Himalaya, India. Earth-Science Reviews 126, 156–177.

Dimick, N.J., 2007. The ability to predict ground water flow in a structurally faulted river valley with naturally occurring hot springs using multivariate geochemical analyses, MS Thesis, Colorado School of Mines, 93.

DiPippo, R., 2007. Ideal thermal efficiency for geothermal binary plants, Geothermics 36, 276–285.

DMR, 2011. Geological map of Amphoe Kapong, Phang Nga, 4626 II, 1:50,000, 2n edition, Department of Mineral Resources, Bangkok, Thailand.

DMR, 2014. Aeromagnetic map of Amphoe Kapong, Phang Nga, 4626 II, 1:50,000, Residual Magnetic Intensity, Department of Mineral Resources, Bureau of Geotechnology, Bangkok, Thailand.

Duerrast, H., Ngansom, W., Pirarai, K., 2016. Geothermal Exploration in Phang Nga, Southern Thailand. The 11th Asian Geothermal Symposium, Chiang Mai, Thailand, 18–20 November.

Eaton, A. D., Clesceri, L. S., Rice, E. W., Greenberg, A. E., Franson, M. A. H., 2005. Standard methods for the examination of water and wastewater: Centennial edition. American Public Health Association, Washington DC, 1368.

Elderfield, H., Upstillgoddard, R., Sholkovitz, E.R., 1990. The rare-earth elements in rivers,estuaries, and coastal seas and their significance to the composition of ocean waters. Geochim. Cosmochim. Acta 54, 971–991.

Everett, J.E., Hyndman, R.D., 1967. Geomagnetic variations and electrical conductivity structure in southwestern Australia, Phys Earth Planet Inter 1, 24–34.

Faulds, J.E., Coolbaugh, M.F., Vice, G.S. and Edwards, M.L., 2006. Characterizing structural controls of geothermal fields in the northwestern Great Basin: A Progress Report. Geothermal Resources Council Transactions 30, 69–76.

Fee, E.J., Shearer, J.A., Debrum, E.R., Schindler, E.U., 1992. Effects of lake size on phytoplankton photosynthesis. Can. J. Fish. Aquat. Sci.49, 2445-2459.

Fouillac, C., Michard, G., 1981. Sodium/lithium ratio in water applied to geothermometry of geothermal reservoirs. Geothcrmics 10, 55- 10.

Fournier, R.O., Rowe, J.J., 1966. Estimation of underground temperatures from the silica content of water from hot springs and wet- steam wells. Am. J. Sci. 264, 685- 697.

Fournier, R.O., Truesdell, A.H., 1913. An empirical Na-K-Ca geothermometer for natural waters. Geochim. Cosmochim. Acta 31, 515- 525.

Fournier, R.O., 1977. Chemical geothermometers and mixing models for geothermal systems. Geothermics 5, 41–50.

Fournier, R.O., 1983. A method of calculating quartz solubilities in aqueous sodium chloride solutions. Geochim. Cosmochim. Acfa 47, 579-586.

Garson, M.S., Young, B., Mitchell, A.H.G., Tait, B.A.R., 1975. The Geology of the Tin Belt in Peninsular Thailand around Phuket, Phangnga and Takua Pa. Institute of Geological Sciences Overseas Memoir No. 1, HMSO, London, 112.

Garson, M. S., Mitchell, A. H. G., 1970. Transform faulting in the Thai Peninsula. Nature 22, 45–47.

Giggenbach, W.F., 1988. Geothermal solute equilibria. Derivation of Na-K-Mg-Ca geoindicators. Geochim. Cosmochim. Acta 52, 2149- 2165.

Goldstein, S.J., Jacobsen, S.B., 1988. Rare earth elements in river waters. Earth and Planetary Science Letters 89, 35–47.

Guo, Q., Wang, Y., 2012. Geochemistry of hot springs in the Tengchong hydrothermal areas, southwestern China. Journal of Volcanology and Geothermal Research 215–216, 61–73.

Hannigan, R., Dorval, E., Jones, C., 2010. The rare earth element chemistry of estuarine surface sediments in the Chesapeake Bay. Chemical Geology 272, 20–30.

Hem, J. D., 1970. Study and interpretation of the chemical characteristics of natural water. U.S. Geological Survey, Water Supply Paper, 2254.

Hirukawa, T., Jarach, W., Tangool, W., Takashima, I., 1987. Preliminary study on the geochemical characters of major geothermal fields in northern Thailand. Bull Geol Soc Jpn. 38(1), 21–32.

Huang, W.J., Wang, Y., Cai, W.J., 2012. Limnol. Oceanogr. Methods 10, 2012, 711–717.

IRENA, 2017. Renewable Energy Outlook: Thailand. International Renewable Energy Agency. https://www.irena.org/publications/2017/Nov/Renewable-Energy-Outlook-Thailand.

Johannesson, K.H., Lyons, W.B., 1994. The rare earth element geochemistry of Mono Lake water and the importance of carbonate complexing. Limnol. Oceanogr 39(5), 1141–1154.

Jonjana, S., Lohawijarn, W., Dürrast, H., 2012. Geological structure and origin of the Kaochaison hot spring in Phattalung, Southern Thailand. Songklanakarin J. Sci. Technol. 34(2), 231–239.

Kanjanapayont, P., Grasemann, B., Edwards, M.A., Fritz, H., 2012. Quantitative kinematic analysis within the Khlong Marui shear zone, southern Thailand. Journal of Structural Geology 35, 17–27.

Kanjanapayont, P., 2014. Deformation style of the Mesozoic sedimentary rocks in southern Thailand. Journal of Asian Earth Sciences 92, 1–9.

Kanjanapayony, P., Edwards, M. A., Grasemann, B., 2009. The dextral strike-slip Khlong Marui Fault, southern Thailand. Trabajos de Geología, Universidad de Oviedo 29, 393-398.

Kearey, P., Brooks, M., Hill, I., 2002. An introduction to geophysics exploration 3rd ed., Blackwell science Ltd., Oxford, England, pp 183-185.

Kharaka, Y.K., Mariner, R.H., 1988. Chemical geothermometers and their application to formation waters from sedimentary basins, in Naeser, N.D. and McCollon, T.H. (eds.), Thermal History of Sedimentary Basins, Springer-Verlag, New York, 99- 111.

Khawdee, P., Lohawijarn, W., Duerrast, H., 2007. Geophysical model of Ban Na Doem Hot-spring in Surat Thani Province, Thailand. The 7th National Graduate Research Conference, Surat Thani, Thailand, 4–5 April, 86–91.

Khawtawan, A., Lohawijarn, W., Tonnayopas, D., 2004. Gravity Anomaly of Chaiya Geothermal Area. The International Conference on Applied Geophysics, Chiang Mai, Thailand, 26–27 November, 15–21.

Khawdee, W. Lohawijarn, H. Duerrast, Geophysical model of Ban Na Doem Hot-spring in Surat Thani Province, Thailand, In: The 7th National Graduate Research Conference, Surat Thani, Thailand, April 2007, 2007, p. 86–91.

Khoonphunnarai, P., Lohawijarn, W., Duerrast, H., 2007. Airborne Geophysical Anomaly of Ranong Geothermal Area, Thailand. The 7th National Graduate Research Conference, Surat Thani, Thailand, 4–5 April, 92–97.

Klaus, J.S., Hansen, B.T., Buapeng, S., 2007. $^{87}Sr/^{86}Sr$-Ratios: A Natural Tracer to characterize the Groundwater of Bangkok Area, Thailand, with respect to Public Water Supply and Freshwater Reinjection. Hydrogeology Journal 15, 745–758.

Krabbenhöft, A., Eisenhauer, A., Böhma, F., Vollstaedt, H., Fietzke, J., Liebetrau, V., Augustin, N., Peucker-Ehrenbrink, B., Müller, M.N, Horn, C., Hansen, B.T., Nolte, N., Wallmann, K., 2010. Constraining the marine strontium budget with

natural strontium isotope fractionations ($^{87}Sr/^{86}Sr^*$, $Sr^{88}/^{86}Sr$) of carbonates, hydrothermal solutions and river waters. Geochimica et Cosmochimica Acta 74, 4097–4109.

Liberty, L., 1998. Seismic reflection imaging of a geothermal aquifer in an urban setting. Geophysics 63(4), 1285–1294.

Loke, M.H., Barker, R.D., 1996. Rapid Least-Squares Inversion of Apparent Resistivity Pseudosections Using a Quasi-Newton Method. Geophysical Prospecting 44(1), 131–152.

Loke, M.H., Dahlin, T., 2002. A comparison of the Gauss-Newton and quasi-Newton methods in resistivity imaging inversion. Journal of Applied Geophysics 49, 149–162.

Lund, J.W., Boyd, T.L., 2016. Direct utilization of geothermal energy 2015 worldwide review. Geothermics 60, 66–93.

McCarthy, K.T., Pichler, T., Price, R.E., 2005. Geochemistry of Champagne Hot Springs shallow hydrothermal vent field and associated sediments, Dominica, Lesser Antilles. Chemical Geology 224, 55– 68.

McLing, T., Smith, W., Smith, R., 2014. Utilizing Rare Earth Elements as Tracers in High TDS Reservoir Brines in CCS Applications. Energy Procedia 63, 3963–3974

Millero, F.J., Feistel, R., Wright, D.G., McDougall, T.J., 2008. The composition of Standard Seawater and the definition of the Reference-Composition Salinity Scale. Deep-Sea Research I 55, 50–72.

Mohammadi, Z., Bagheri, R., Jahanshahi, R., 2010. Hydrogeochemistry and geothermometry of Changal thermal springs, Zagros region, Iran. Geothermics 39, 242–249.

Morley, C. K., Racey, A., 2011. Tertiary stratigraphy. In MF Ridd, AJ Barber and MJ Crow, The Geology of Thailand. The Geological Society, 223-271.

Muffler, P.L.J, Cataldi, R., 1978. Methods for regional assessment of geothermal resources. Geothermics 7, 53-89.

Muffler, L.J.P., Christiansen, R.L., 1978/79. Geothermal Resource Assessment of the United States. Pageoph 177, 160–171.

Mutlu, H., 1998. Chemical geothermometry and fluid-mineral equilibria for the Omer Gecek thermal waters, Afyon area, Turkey. Journal of Volcanology and Geothermal Research 80, 303–321.

Naksuksakul, S., Thaicharoen, C., 2013. Review of Geothermal Potential and Development Plan of Thailand. The 13th Indonesia International Geothermal Convention and Exhibition, Jakarta, Indonesia, 12 – 14 June.

Ngansom, W., Durrast, H., 2016. Saline hot spring in Krabi, Thailand: A unique geothermal system. Society of Exploration Geophysicists, 1949–4645.

Ngansom, W., Pirarai, K., Duerrast, H., 2016 Geothermal Exploration in Phang Nga, Southern Thailand. The 15th World Renewable Energy Congress (WREC), Jakarta, Indonesia, 19–23 September.

Ngansom, W., Pirarai, K., Duerrast, H., 2017. Integrated geoscientific investigations of the Phang Nga geothermal system, southern Thailand. Society of Exploration Geophysicists, 5427– 5431.

Nicholson, K., 1993. Geothermal fluids. Springer-Verlag, Berlin, Heidelberg, New York, 263.

Palmer-Wilson, K., Banks, J, Walsh, W., Robertson, B., 2018. Sedimentary basin geothermal favourability mapping and power generation assessments 127, 1087–1100.

Pasqualetti, M. J., 1981. Geothermal Energy, Site Specificity, and Resource Reserves GeoJoumal Supplementary 3, 49–58.

Paster, A., 2010. Mixing between fresh and salt waters at aquifer regional scale and identification of transverse dispersivity. Journal of Hydrology 380, 36–44.

Polachan, S., Sattayarak, N., 1989. Strike-slip tectonics and the development of Tertiary basins in Thailand, In: International Symposium on Intermontane Basins, Chiang Mai, Thailand, February, p. 243–253.

Polachan, S., Pradidtan, S., Tongtaow, C., Janmaha, S., Intarawijitr, K., Sangsuwan, C., 1991. Development of Cenozoic basins in Thailand. Marine and Petroleum Geology 8(1), 84–97.

Praserdvigai, S. 1986. Geothermal development in Thailand. Geothermics, 15, 5/6, 565-582.

Promprou, S., Jaroensutasinee, M., Jaroensutasinee, K., 2005. Impact of climatic factors on dengue haemorrhagic fever incidence in Southern Thailand. Walailak J Sci Tech 2, 59–70.

Quinao, J.J.D., Zarrouk, S.J., 2018. Geothermal Resource Assessment using Experimental Design and Respons Surface Methods: The Ngatamariki Geothermal Field, New Zealand. Renewable Energy 116 (Part A), 324–334.

Raksaskulwong, M., 2008. Thailand geothermal energy: development history and current status. The 8th Asian Geothermal Symposium, GREEN, Japan, at Hanoi, Vietnam, 11.

Raksaskulwong, M., Thienprasert, A., 1995. Heat flow studies and geothermal energy development in Thailand. Terrestrial Heat flow and geothermal energy in Asia, 129–144

Ramingwong, T., Lertsrimonkol, S., Asnachinda, P., Praserdvigai, S., 2000. Update on Thailand geothermal research and development. In: The World Geothermal Congress, Tohoku, May 28–June 10, 377–386.

Ratanasthien, B., Panjasawatwong, Y., Yaowanoiyothin, W., Lerdthusnee, S., Haraluck, M., 1985. Water qualities of geothermal fluids from San Kamphaeng and Fang geothermal systems. Final Report to Electricity Generating Authority of Thailand, 249.

Ravens, J., 2007. Globe Claritas, Seismic Processing Software Manual-Part1, 5th edition, 250.

Ridd, M.F., Watkinson, I., 2013. The Phuket-Slate Belt terrane: tectonic evolution and strike-slip emplacement of a major terrane on the Sundaland margin of Thailand and Myanmar. Proceedings of the Geologists' Association 124(6), 994 –1010.

Ridd, M.F., 2009. The Phuket Terrane: A Late Palaeozoic rift at the margin of Sibumasu. Journal of Asian Earth Sciences 36(2–3), 238 – 251.

Ridd, M.F., 2012. The role of strike-slip faults in the displacement of the Palaeotethys suture zone in Southeast Thailand. Journal of Asian Earth Sciences 51, 63–84.

Rubio-Maya, C., AmbrízDíaz, V.M., PastorMartínez, E., Belman-Flores, J.M., 2015. Cascade utilization of low and medium enthalpy geothermal resources – A review Renewable and Sustainable Energy Reviews 52, 689–716.

Sanmuang, E., Lohawijarn, W., Duerrast, H., 2007. Gravity Anomaly of Ranong Geothermal Area, Thailand. In: The 7th National Graduate Research Conference, Surat Thani, Thailand, 4–5 April, 244–248.

Schön, J., 1996. Physical properties of rocks. Handbook of geophysical exploration. Vol 18. Pergamon, Oxford, New York.

Shi, X., Liu, S., Fang, X., Qiao, S., Khokiattiwong, S., Kornkanitnan, N., 2015. Distribution of clay minerals in surface sediments of the western Gulf of Thailand: Sources and transport patterns. Journal of Asian Earth Sciences 105, 390–398.

Sholkovitz, E.R., 1993. The geochemistry of rare earth elements in the Amazon River estuary. Geochimica el Cosmochimica Acta 57, 2181–2190.

Shortall, R., Davidsdottir, B., Axelsson, G., 2015. A sustainability assessment framework for geothermal energy projects: Development in Iceland, New Zealand and Kenya, Renewable and Sustainable Energy Reviews 50, 372–407.

Siripunvaraporn, W., Egbert, G., 2009. WSINV3DMT: vertical magnetic field transfer function inversion and parallel implementation. Phys. Earth Planet. Inter. 173, 317– 329.

Siripunvaraporn, W., Egbert, G., Lenbury, Y., Uyeshima, M., Ogawa, Y., Junge, A., Jones, A.G., 2005. Three-dimensional magnetotelluric inversion: data-space method. Phys. Earth Planet. Inter. 150, 3-14.

Spencer, K.L., Harvey, G.L., 2012. Understanding system disturbance and ecosystem services in restored saltmarshes: Integrating physical and biogeochemical processes. Estuarine, Coastal and Shelf Science 106, 23–32.

Stelling, P., Hinz, N.H., Kolker, A., Ohren, M., 2015. Exploration of the Hot Springs Bay Valley (HSBV) geothermal resource area, Akutan, Alaska. Geothermics 57, 127–144.

Stober, I., Bucher, K., 2013. Geothermal energy, from theoretical models to exploration and development, 350. Springer-Verlag, Berlin, Heidelberg.

Subtavewung, P., Raksaskulwong, M., Tulyatid J., 2005. The Characteristics and classification of hot Springs in Thailand. The World Geothermal Congress 2005, Antalya, Turkey, 24-29 April.

Swart, P.K., Burns, S.J., Leder, J.J., 1991. Fractionation of the stable isotopes of oxygen and carbon in carbon dioxide during the reaction of calcite with phosphoric acid as a function of temperature and technique, Chemical Geology: Isotope Geoscience section 86(2), 89–96.

Takashima, I., Jarach, W., 1987. Isotope geochemistry of six geothermal fields in northern Thailand. Bull. Geol. Surv. Japan 38, 33-39.

Tan, B.K., 1992. Seventh Regional Conference on Geology, Mineral and Hydrocarbon Resources of Southeast Asia (GEOSEA VII), Bangkok, 5–8 November 1991. Journal of Southeast Asian Earth Sciences 7(4), 253–285.

Taylor, S.R., McLennan, S.M., 1981. The composition and evolution of the continental-crust-rare-earth element evidence from sedimentary-rocks. Philosophical Transactions of the Royal Society of London 301(1461), 381-399.

Teerarungsigul, N., Raksakulwong, L., Khantaprab, C., 1999. Reconsideration of the lithostratigraphy of non-marine Mesozoic in Thung Yai-Khlong Thom area, Southern Thailand. Proceedings on Symposium on Mineral, Energy, and Water Resources of Thailand: Towards the year 2000. October 28-29, Bangkok, Thailand, 98-114.

TGE, 2013a. Magneto Telluric (MT) Prospecting, Geothermal Power Plant Project, Apas Kiri Geothermal Field, Final Report; Tawau Green Energy Sdn. Bhd., December 2013 (unpublished Report).

TMD, 2015. The climate of Thailand. Climatological Group, Meteorological Development Bureau, Meteorological Department, Thailand. https://tmd.go.th/en/archive/thailand_climate.pdf.

Tonani, F., 1980. Some remarks on the application of geochemical techniques in geothermal exploration, in Proc. Adv. Eur. Geoth. Res., Second Symp. Strasbourg, 428- 443.

Trisurat, Y., Shrestha, R.P., Kjelgren, R., 2011. Plant species vulnerability to climate change in Peninsular Thailand. Applied Geography 31(3), 1106–1114.

Truesdell, A.H., 1976. Summary of section III geochemical techniques in exploration, in Proc. Second United Nations Symposium on the Development and Use of Geothermal Resources. San Francisco, 1915(1): Washington. D.C., U.S. Government Printing Office.

Tsuchiya, N., Yamada, R., 2017. Geological and Geophysical Perspective of Supercritical Geothermal Energy in Subduction Zone, Northeast Japan. Procedia Earth and Planetary Science 17, 193–196.

Turcotte, D.L., Schubert, G., 2002. Geodynamics. 2nd edition, Cambridge, 456

Tütken, T., Eisenhauer, A., Wiegand, B., Hansen, B.T., 2002. Glacial-interglacial cycles in Sr and Nd isotopic composition of Artic marine sediments: changes in sediment provenance triggered by the Barents Sea ice sheet. Marine Geology 182, 351–372.

Wanakasem, S., Takabut, K., 1986. Present status of Fang geothermal project, Thailand. Geothermics, 15, 5/6, 583-587.

Watkinson, I., Elders, C., Hall, R., 2008. The kinematic history of the Khlong Marui and Ranong Faults, southern Thailand. Journal of Structural Geology 30 (12), 1554–1571.

Wiegand, B., Dietzel, M., Bielert, U., Groth, P., Hansen, B.T., 2001. 87Sr/86Sr-Verhältnisse als Tracer für hydrochemische Prozesse in einem Lockergesteinsaquifer (Libenau, NW-Deutschland).

Wood, S.H., Kaewsomwang, P., Singharajwarapan, F.S., 2018. Geologic framework of the Fang Hot Springs area with emphasis on structure, hydrology, and geothermal development, Chiang Mai Province, northern Thailand. Geothermal Energy Science Society Technology 6(3), 1–51.

Xiao, C. H., Wang Q.F., Zhou, X.Z., Yang, L.Q., Zhang, J., 2010. Rare-earth elements in hot spring waters in the Tengchong geothermal area. Acta Petrologica Sinica 26(6), 1938–1944 (in Chinese with English abstract).

Yasukawa, K., Kubota, H., Soma, N., Noda, T., 2018. Integration of natural and social environment in the implementation of geothermal projects. Geothermics 73, 111–123.

Younas, U., Khan, B., Ali, S.M., Arshad, C.M., Farid, U., Zeb, K., Rehman, F., Mehmood, Y., Vaccaro, A., 2016. Pakistan geothermal renewable energy potential for electric power generation: A survey. Renewable and Sustainable Energy Reviews 63, 398–413.

Yuksel, Y. E., Ozturk, M., Dincer, I., 2018. Thermodynamic analysis and assessment of a novel integrated geothermal energy-based system for hydrogen production and storage, International Journal of Hydrogen Energy 43 (9), 4233–4243.

Zarrouk, S. J., Moon, H., 2014. Efficiency of geothermal power plants: A worldwide review, Geothermics 51, 142–153.

APENDICES

Appendix A

List of Publications

I. Ngansom, W. and Duerrast, H., 2018. Positive Attitude Factors Assessing Geothermal Resources related to Hot Springs in Southern Thailand. **Manuscript submission for Chiang Mai Journal of Science**.

II. Ngansom, W. and Duerrast, H., 2018. Integrated geoscientific investigations of the Saline Hot Spring Khlong Thom, Krabi, Thailand: A unique geothermal system. **Manuscript submission for Environmental Earth Sciences**.

III. Ngansom, W., Pirarai, K., Duerrast, H., 2018. Subsurface Characteristics and Geochemistry of the Kapong Non-Volcanic Geothermal Hot Spring Area in Southern Thailand. **Manuscript submission for Geothermics**

IV. Durrast, H., Ngansom, W., 2018. Geochemical Characteristics of Hot Springs in Southern Thailand. The 8th International Conference on Applied Geophysics, Songkhla, Thailand, 8–10 November.

V. Durrast, H., Ngansom, W., 2018. Design Methodology for Assessment and Ranking of Geothermal Resources: A Case Study of Southern Thailand. The 12th Asian Geothermal Symposium, Deajeon, Korea, 10-12 November 2018

VI. Ngansom, W., Durrast, H., 2018. Delineation of Unconventional Groundwater: II. Saline Geothermal Groundwater in Krabi, Thailand. The International Conference on Water Management and Climate Change towards Asia's Water-Energy-Food Nexus and SDGs, Bangkok, Thailand, 23–25 January.

VII. Ngansom, W., Durrast, H., 2017. Phang Nga Geothermal System in Southern Thailand. The European Geothermal PhD Day (EGPD), Bochum, Germany, 28 February– 3 March.

VIII. Ngansom, W., Pirarai, K., Duerrast, H., 2017. Integrated geoscientific investigations of the Phang Nga geothermal system, southern Thailand. Society of Exploration Geophysicists, 5427– 5431.

IX. Duerrast, H., Ngansom, W., Pirarai, K., 2016. Geothermal Exploration in Phang Nga, Southern Thailand. The 11th Asian Geothermal Symposium, Chiang Mai, Thailand, 18–20 November.

X. Ngansom, W., Durrast, H., 2016. Saline hot spring in Krabi, Thailand: A unique geothermal system. Society of Exploration Geophysicists, 1949–4645.

XI. Ngansom, W., Pirarai, K., Duerrast, H., 2016 Geothermal Exploration in Phang Nga, Southern Thailand. The 15th World Renewable Energy Congress (WREC), Jakarta, Indonesia, 19–23 September.

XII. Ngansom, W., Durrast, H., 2016. Characteristics and Potential of Geothermal Resources in Southern Thailand. The 12th Conference on Energy Network of Thailand, Phitsanulok, Thailand, 8–10 June.

XIII. Phalakarn, M., Petrit, K., Ngansom, W., Durrast, H., 2016. Geoscientific Investigations of Geothermal Systems: Case Study Khlong Thom, Krabi. The 12th Conference on Energy Network of Thailand, Phitsanulok, Thailand, 8–10 June.

XIV. Ngansom, W., Durrast, H., 2016. Geochemistry of hot spring waters from Krabi, Southern Thailand. The 7th International Conference on Applied Geophysics, Bangkok, Thailand, 14–15 January.

XV. Ngansom, W., Durrast, H., 2015. Subsurface structure of the saline hot spring in Krabi, Southern Thailand, from an integrated geoscientific investigation. The 6th International Geosciences Student Conference, Prague, 13 – 16 July 2015, 67 – 69.

Appendix B

Authors: Wipada Ngansom, Kriangsak Pirarai and Helmut Dürrast

Title: Integrated geoscientific investigations of the Phang Nga geothermal system, Southern Thailand

Publisher: Society of Exploration Geophysicists

Integrated geoscientific investigations of the Phang Nga geothermal system, Southern Thailand

Wipada Ngansom[1], Kriangsak Pirarai[2] and Helmut Dürrast[1], [1]Geophysics, Prince of Songkla University, Hatyai, Thailand, and [2]Department of Groundwater Resources, Bangkok, Thailand*

Summary

The Phang Nga geothermal area represents a small, moderate temperature, deep circulating geothermal system, apparently typical of those associated to hot springs in southern, central and northern Thailand. An integrated geological, geochemical and geophysical study was carried out and was found to be useful for understanding subsurface flow characteristics and for developing a conceptual model of the system. Resistivity and magnetotellurics (MT) data at a depth of down to 500 m define a low-resistivity layer with shallow hot aquifer water. Residual magnetic intensity from aeromagnetic data indicate that the hot spring area is apparently located at the boundary between two larger igneous bodies, both likely granitic bodies. Partially equilibrated and immature hot spring waters indicate reservoir temperatures between 100 to 120 °C determined with geothermometers. Possibility of the origin of the hot spring is derived from deep circulation of lower resistive meteoric waters, based on MT data down to 2 km, and which is controlled by faults that are associated either with the igneous bodies or larger tectonics. A regional forced convective-circulation model for this geothermal area is suggested, thus reflecting deep structural controls of the fluid pathways in this area, which has limited the degree of mixing.

Introduction

Hot springs are common features in most parts of Thailand, from the north to the south, except in the northeastern part. As some hot springs are in national parks, others are utilized as tourist sites with spa. This particular study is focusing on the understanding of the geothermal system of one of the two Phang Nga hot spring sites located in Kapong district, about 40 km north of Phang Nga City or 100 km north of Phuket in Southern Thailand (Figure 1a and 1b). In the mountainous area six natural hot springs with surface exit temperatures from 73 to 78 °C can be found close to and at the banks of the Pai Phu River, an area of about 1,000 m times 200 m in size and partly bounded by step mountain flanks.

Methodology

Geological surveys were conducted in the study area to assess the main rock units. Aeromagnetic data were provided as maps by the Department of Mineral Resources, Bangkok (Figure 1c). Surface water exit temperatures were measured at the outlet of each hot spring. Chemical parameters of water samples taken at different hot spring sites were studied in detail with different geochemical methods; analysis of the main cation and anions (at Prince of Songkla University) as well as certain isotopes (at TINT, Bangkok; Geochemistry Department, GZG Goettingen, Germany) in order to understand the origin of the hot spring waters (see Table1, Figure 2).

Surface electrical methods are chosen to image hot water pathways and reservoirs at depth, with vertical electrical resistivity sounding (VES) for shallow parts and magnetotelluric (MT) surveys for deeper regions. 50 VES surveys were conducted using Schlumberger configuration with AB/2 distances of up to 150 m. MT measurements have been carried out using 30 stations and covering over 50 km^2 of the larger study area (Figure 3), defined as resistivity parameter integrating all layers from the surface to 2 km depths.

Results and Discussion

Data of the cation and anion concentration measurements of the hot spring waters are shown in Table 1.

Table 1: Chemistry of Phang Nga hot spring waters with pH, major cation and anion concentrations (mg/L)

Site	pH	Mg	Ca	K	Na	Cl	HCO_3
PG1	7.96	0.30	11.23	2.47	27.82	8.25	185.75
PG2	8.07	0.45	8.65	3.07	76.37	37.51	180.80
PG3	8.12	0.12	12.14	3.38	69.64	15.20	183.00
PG4	8.18	0.11	12.14	3.38	68.21	16.20	180.50
PG5	8.03	0.12	12.43	3.42	69.64	14.20	165.50
PG6	8.08	0.12	12.29	3.42	68.57	16.90	155.50

Slightly higher than neutral pH values, around 8.0 (see Table 1), indicate likely the dissolution of a significant part of silica. Na and K are most probable the result of ion exchange of Ca and to a lesser extent of Mg from the source rocks. There is a predominance of Ca and Mg in most of the hot spring waters. Na and K bicarbonates are likely derived from sandstones, which are rich in feldspar and which are likely to be found in recharge areas or along the flow paths. All features indicate that the low salinity Phang Nga hot spring waters are of meteoric origin.

Chemical compositions of the hot waters studied and described in terms of relative concentrations of the major cations and anions illustrate that the hot spring water are Ca–Na–bicarbonate rich waters (see Figure 2a and 2b). Results seem to suggest that the bicarbonate-rich hot water aquifers (see Figure 2b) are like those from the basement and alluvial aquifers, which indicate a meteoric water source as discussed above (see Table 1).

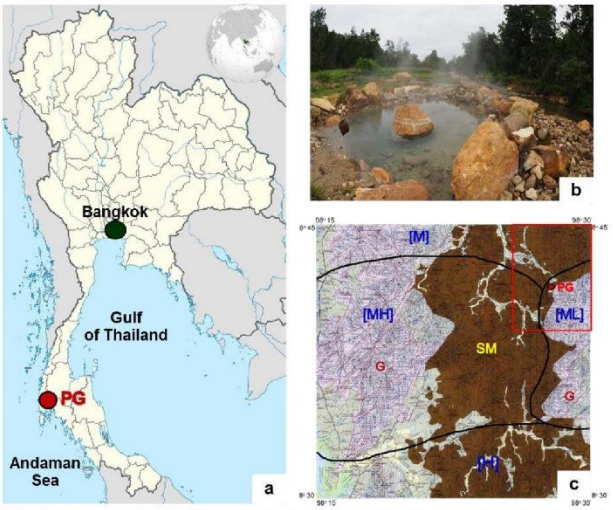

Figure 1: a) Location of the Phang Nga hot spring site (PG) in Thailand, (b) Main pool of the natural hot spring sites at the banks of the Khlong Pai Phu River, and c) Delineated residual magnetic intensity from aeromagnetic data (black lines) combined with the geology map at the Phang Nga hot spring site (PG). Residual magnetic intensity value ranges: [M] = 58-62 nT, [ML] = 43-50 nT, [MH] = 60-65 nT and [H] = 65-75 nT. G=granite and SM=sedimentary and/or metamorphic rocks

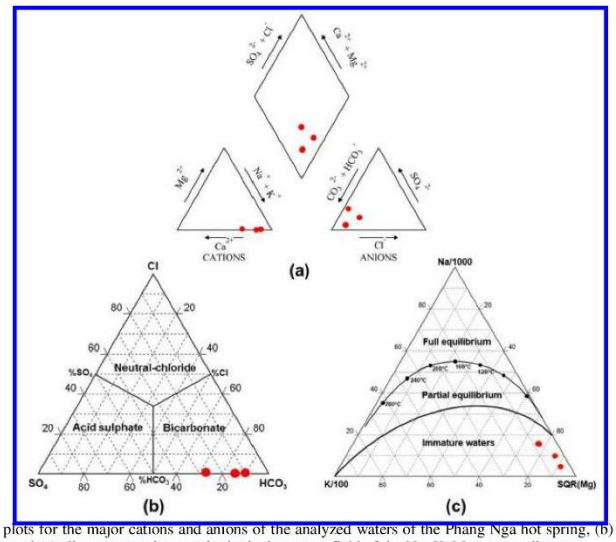

Figure 2: (a) Triangular plots for the major cations and anions of the analyzed waters of the Phang Nga hot spring, (b) Most samples plot in the bicarbonate water region, and (c) all water samples are plot in the immature field of the Na–K–Mg ternary diagram.

Based on these results, these waters can be classified as Ca–Na–K–(Mg)–HCO_3 water, thus reflecting local variations in the geological formations and hydrochemical processes governing the quality of these hot spring waters (see Figure 2c). Results are consistent but more work is needed to establish the underlying processes.
The isotope signature of hydrogen and oxygen (not shown in here) confirms that the hot spring waters at this site are of meteoric origin, which then cycle deep along faults and fractures into the granites. A negative Eu anomaly in the hot spring waters (not shown in here) has been induced by the water-rock interaction between these meteoric waters and the igneous rocks with a negative Eu anomaly at depth.

Reservoir temperatures of the geothermal system are estimated with various cation geothermometers. The Na–K geothermometer values are in agreement with the ones obtained with the Na–K–Ca geothermometers giving an average of about 120-150 °C. The silica geothermometers was used to determine the reservoir temperature of water–rock interaction processes at depth in an uprising fluid before discharge show an average value of 100-120 °C. The silica geothermometer values were generally lower than those obtained with the cation geothermometers. Such differences might be due to disequilibrium between silica and the hot water, probably caused by mixing between waters of different temperature and silica content. Differences in the results between the different geothermometers may indicate shallow conditions of mixing with groundwater (Figure 2c). It is possible that the reservoir depth is deeper than 1-2 km with possible higher reservoir temperatures.

The larger geological setting of the Phang Nga hot springs is affected by the major Khlong Marui (KMF) and Ranong Fault (RF) zones, both with a more or less SW-NE strike direction and apparently intersecting in the northern Gulf of Thailand. Rocks in and around the Phang Nga hot spring site are dominantly granites (Figure 1c), which are distributed in the south eastern part of the study area, and a sedimentary/metamorphic rock units, which cover other parts.

MT data of the 3D surveys are shown in Figure 3, whereas the geoelectric data of the 1D survey (VES) data are not shown here. 1D models of VES surveys revealed that the investigated subsurface comprises of 3-4 geoelectrical layers with a maximum attained depth of less than 100 m. In the shallow surface high resistivity patterns (>9,500 ohm-m) can be characterized as dry topsoil, possibly also dry sandstone. A low resistivity zone (<500 ohm-m) is detected below the high-resistivity top layer and can be well correlated to MT results at 50-100 m depth. The low resistivity layer is extending to a depth of down to 50-100 m, covering an area of over 30 km^2, which can be considered freshwater aquifers.

For zones deeper than 1 km depth and down to 2 km the 3D models of the MT profile (Figure 3) were utilized with horizontal (Figure 3) and vertical (Figure 4) sections. Results show areas of low resistivity values indicate hotter water-rock systems at depth, thus showing the location of the deep reservoir and the possible fluid path from and to the surface of the Phang Nga geothermal system. Such low resistivity sections resemble possible faults at depth within the geothermal system. A high resistivity value shown of several hundreds and up to 2,000 ohm-m is observed in different coherent blocks extending from the low resistivity fault lines.
Deep resistive blocks (Figure 3) are bounded by two conspicuous conductive zones (resistivity lower than 500 ohm-m) that possibly was formed through the upwards movement of hot igneous basement rocks. It is inferred that the basement is fractured below the conductive zone and large heat flow values of the Phang Nga geothermal system are reported; the zone is probably filled with fluids which may have a deep heat source.
Following these results, it can be proposed that the conductivity anomalies presented here could derive from processes of the fault zones in the area. Data suggest that the deeper resistivity values are connected along N-S trending larger vertical faults planes; one they might resemble a boundary between two granitic bodies at depth. Residual magnetic intensities derived from aeromagnetic measurements show different values suggesting such magnetic bodies at depth, likely to be granites (Figure 1c).

Conclusions

Based on the integration of all available data and results a schematic model of the Phang Nga geothermal system is presented in Figure 4, showing the different waters and major faults as their pathways. The subsurface strata were assumed to be four layers: alluvial deposits, mudstone, sandstones, a sedimentary/metamorphic rock unit, and basement rocks (mainly granite).
Data suggest that the heat source of the hot spring is the results of upwards movement of hotter rock material causing deep-fluid circulation of meteoric water through faults down to the top of the basement rock. Such faults allow the formation of discharging conduits for water ascending from depth after being heated and interacted with the rocks. The relatively shallower and hotter basement rock is the site of high heat flow and has probably a limited extension. After heating, the mixed waters rise through vertical fracture that is assumed to come from the intersection of major faults. In the next step a deeper well is required to get more understanding and to assess the electrical power generation potential of this hot spring site.

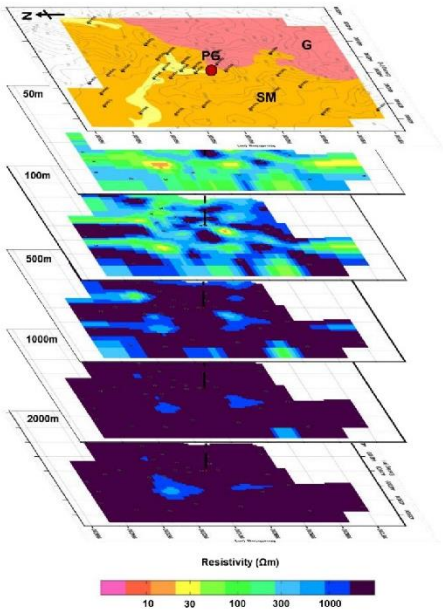

Figure 3: Horizontal depth slices of the resistivity distribution of the Phang Nga hot spring site from 3D inversion of MT surveys. PG=hot spring site. G=granite, SM=sedimentary/metamorphic rock unit. Black dots on the geological map indicate MT measurement locations.

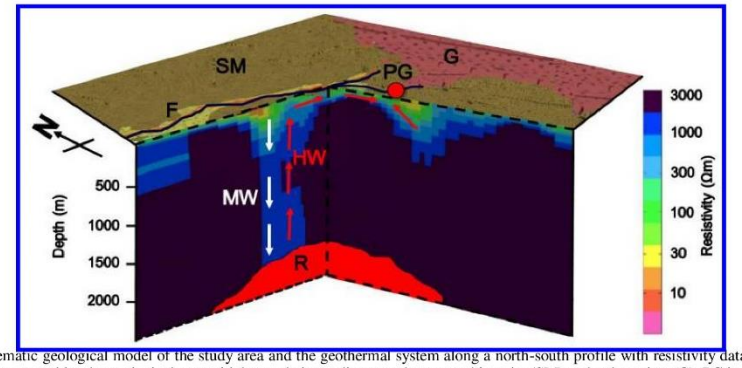

Figure 4: Schematic geological model of the study area and the geothermal system along a north-south profile with resistivity data from the MT surveys; Surface resembles the geological map with brown being sedimentary/metamorphic units (SM) and red granites (G); PG is the Phang Nga hot spring site, MW – cooler meteoric water; HW – hot water; R – geothermal reservoir, and F – fault

EDITED REFERENCES

Note: This reference list is a copyedited version of the reference list submitted by the author. Reference lists for the 2017 SEG Technical Program Expanded Abstracts have been copyedited so that references provided with the online metadata for each paper will achieve a high degree of linking to cited sources that appear on the Web.

REFERENCES

Department of Groundwater Resources, 2015, Geothermal energy in Thailand Project.

Department of Mineral Resources, 2011, Geological map of Thailand 1:50000 sheet 4626II: Amphone Kapong.

Department of Mineral Resources, 2014, Aeromagnetic map (C1S block) residual magnetic intensity.

Durrast, H., W. Ngansom, and K. Pirarai, 2016, Geothermal exploration in Phang Nga, Southern Thailand: 11th Asian Geothermal Symposium.

Appendix C

Authors: Wipada Ngansom and Helmut Dürrast

Title: Saline Hot Spring in Krabi, Thailand: A unique Geothermal System

Publisher: Society of Exploration Geophysicists

Saline hot spring in Krabi, Thailand: a unique geothermal system

*WipadaNgansom*and Helmut Dürrast, Prince of Songkla University, Hatyai, Thailand*

Summary:

An integrated geological, geochemical and geophysical study has shown that the saline hot spring in Krabi in Southern Thailand is quite unique in its occurrence. Hot spring waters from the depth flow upwards and mix with saline groundwater aquifers as the result of seawater intrusion from a nearby estuary and the existence of a salt marsh south and east of the main hot spring site. The estuary is also responsible for seasonal flooding of the area. Geoelectricdata show very low resistivity values in the shallow subsurface which that corresponding to black marine clay and groundwater salinity. Geochemical analysis showed that saline groundwater and hot water from deep aquifers mix while emerging along faults. This results in a saline groundwater layer above a saline hot spring water layer at depth. The depth of the interface of both waters depends on the season, dry and wet, and by this on rainfall and flooding;thus making this area quite unique.

Introduction

Hot springs, the surface manifestation of active geothermal systems in the subsurface, can be found in most regions in Thailand, mainly used for spa and tourism purposes; only in Fang, Northern Thailand, geothermal energy is utilized for electricity production. Most of the hot springs have water exit temperatures of around 40 to 70 °C.

A saline water hot spring can be found inKhlong Thom District of Krabi Province in Southern of Thailand, about 70 km southeast of KrabiCity, at 7° 54.199' N and 99° 6.505' E (Figure 1). The site is located close to one of the tributaries of the PhelaRiver system, which is connected to the Andaman Sea. Altogether 15 natural hot springs can be found in the area that covers about 0.5 km^2 with surface exit temperatures from 41 to 47 °C and a salinity of 21 ppt. Several the hot springs have been developed for tourism (Figure 2) (Ngansom et al., 2015). An integrated study has been carried out in order to understand the unique nature of this hot spring site.

Methodology

Geological surveys including shallow soil borings were carried out to understand the surface geology. For geochemical analysis water samples were collected from natural pools and local wells (Figure 2)with temperature and salinitymeasured in the field. Major cations and anions as well as isotopes (not shown here) were measured in the laboratory. Silica and cation geothermometers, Qz, Na-K, K-Mg and Na-K-Ca,were applied to estimatethe aquifer temperature (Baioumy et al., 2015).

Vertical electrical soundings (VES) at 15 sites, with Schlumberger array anda maximum AB/2 of 150 m,and electrical resistivity tomography (ERT) in dipole-dipole configuration, with an electrode spacing of 25 m, n=8, and an effective depth of 50 m, along two lines have been carried in the larger area (Figure 2). ERT processing was done with RES2DINV software to produces an image of the electrical resistivity distribution in the subsurface.
Further, data from wells in the area and information from related government agencies and local people were used.

Results:

The chemical compositions of five water samples taken natural pools and local wells are presented in Table 1 (see also Figure 2), showing a very high Na and Cl content, as well as Mg, reflecting the higher salinity. The elevated Ca value is indicating that the water might have been interacted with limestone at depth.
The geothermometer calculationsbased on the chemical water analysis found partially equilibrated and immature waters with reservoir temperature values between 55 and 150°C (see Table 2).

Table 1: Temperature, pH, and major element composition (in mg/L) of saline hot springs and well waters.

Parameter	KB4/5	KB4/10	Well01	Well02	Well03
T (°C)	46	45	43	42	41
pH	6.76	6.72	6.54	6.51	6.8
Cl	10,361	7,811	9,086	9,237	7,710
HCO_3	289	228	174	192	203
Ca	948	849	838	838	253
Fe	0.013	0.009	0.010	0.001	0.096
K	183	161	158	166	88
Mg	339	309	316	317	138
Na	5,198	4,778	4,710	4,741	626
SO_4	420	610	582	584	512

The geochemical data of the saline hot spring show that cations, K, Mg, and Na, occur in relatively high contents, while Fe shows very low concentrations. On the other hand, HCO_3 is present in relatively high concentration compared to other anions (SO_4 and Cl).
A comparison of the different geothermometers show that the quartz geothermometer show generally lower values than those of the Na-K geothermometer, whereas the K-Mg and Na-K-Ca geothermometers values are much lower than those of the quartz and Na–K geothermometers.

Saline hot spring in Krabi, Thailand: a unique geothermal system

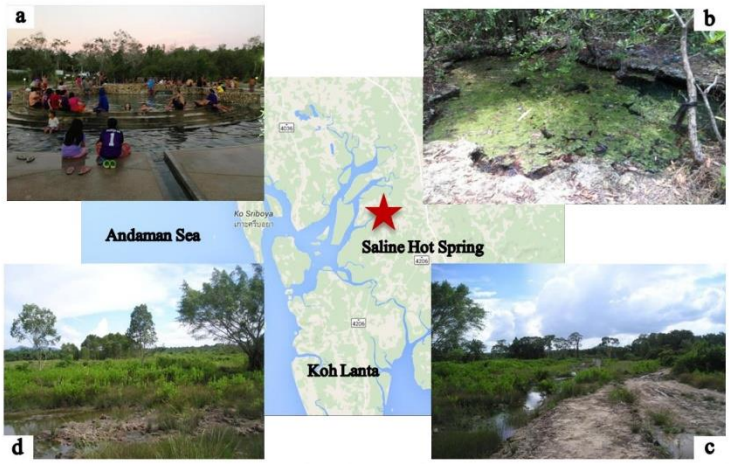

Figure 1: Location of the study area with saline hot spring; a) manmade structures for tourism, b) natural hot spring sites with precipitated carbonate crust around and c) and d) salt marsh area before and after seasonal rainy season (monsoon).

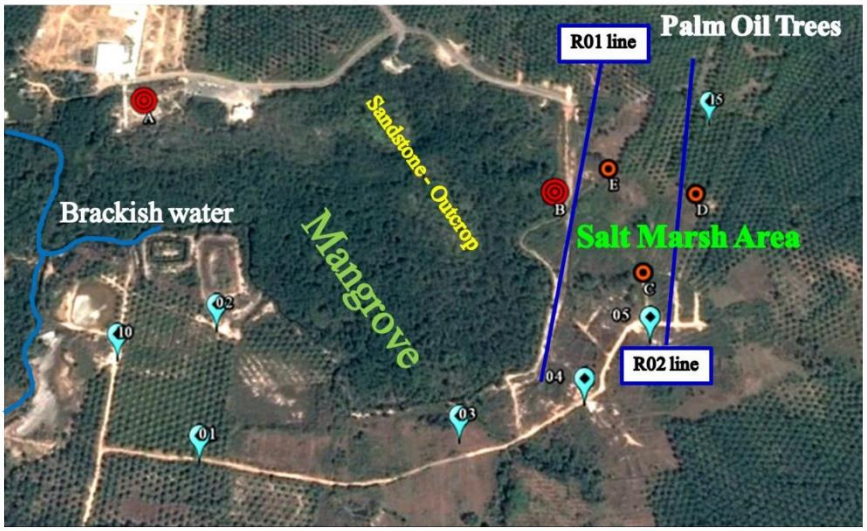

Figure 2: Location of natural hot spring, local wells (A: KB4/5; B: KB4/10; C: Well01; D: Well02; E: Well03) and geophysical survey locations, with number from 1-15 (not all shown on the map) indicate VES points, and R01 and R02indicate ERT lines.

Table 2: Reservoir temperatures calculated withdifferent geothermometers using the data from Table 1.

Location	Temperature (°C)			
	Quartz	Na-K	K-Mg	Na-K-Ca
KB4/5	100	150	60	83
KB4/10	N/A	142	62	80
Well01	110	138	58	81
Well02	100	135	56	79
Well03	102	140	55	75

Differences in the reservoir temperature values suggest that the quartz or Na-K of geothermometer reflect the reservoir temperature, whereas the K-Mg records intermediate temperatures between the reservoir values and the hot spring values as the geothermal waters re-equilibrates upon conductive cooling or mixing with cooler Mg-rich waters, likely marine or brackish water.

For the geoelectricdata one line of the 2D surveys are shown in Figure 3, whereas the 1D survey data are not shown here.

1D models revealed that the investigated subsurface comprises of 4-5 geoelectrical layers with a maximum attained depth of less than 50 m. Detected layers show a wide range of resistivity varying from 1 to 2,100 Ohm-m except for the shallow layer at 5 to 20 m depth which shows very low resistivity values (below 10 Ohm-m) in the southern part of the hot spring site(Figure 3). Very low resistivity values could be attributed to effect of the marine or brackish water intrusion at shallow depth of black marine clay near the surface. Abrupt changes in the depth of the layers at short horizontal distance indicate vertical faults in the area.

2D models show resistivity values ranging from 0.45 to 235 Ohm-m, corresponding to different lithological units and water content. The shallow part of the section shown in Figure 3 is occupied by very low resistivity values corresponding to the black marine clay and groundwater salinity. Dense sandstone with almost no water content which exhibit high to very high resistivity values.The bottom of the clay layer and groundwater salinity at depths is at about 40 m of north of the local well (Figure 3).

Geological surveys in the area showed different geological units belonging to Tertiary and alluvial deposits (Jonjana et al., 2012). The shallow subsurface of alluvial deposits consists of medium to coarse grained sand with plant roots, black marine clay and clay, and covers most parts of the study area (Nilsuwan, 2011).

Sandstone in Tertiary deposits covers all of the study area, and carbonate crusts can found aroundthe natural pools inside the mangrove and near the local wells.The carbonate crusts indicate that the hot water pathway from the depth of the reservoir likely was through a layer of the carbonate rock, e.g. limestone (Figure 1b and 4).

Conclusions:

The integrated geological, geochemical and geophysical study has shown that the saline hot spring is quite unique in its occurrence. Hot water at depth is flowing up along larger faults (not shown here) to the shallower subsurface (depth has still to be evaluated) and mixes there with saline groundwater due to groundwater intrusion from the nearby estuary containing brackish water. South and east of the main hot spring sites are salt marshes indicated older coastal areas with black marine clay and salt crusts on the surface (not shown here). Local people reported that during the annual rainy and monsoon season the water level in river increases causing widespread flooding in the area of the hot springs and salt marsh resulting in an infiltration of saline water in the shallow groundwater layers.

Geoelectrical and geochemical results have shown that the 1D and 2D interpretation were successfully used to outline the groundwater zone at relatively shallow depth. The 2D inversion models clearlyexhibit the effect of salt marsh and seawater intrusion (Figure2, 3 and 4) showing very low resistivity values;it appears at 25m depth in the northern part and it was extended southwards (Figure 3). However, with increasing depth the water is becoming saline hot spring water, which could not be separated by the resistivity surveys, but shown by the well water. After opening the artesian wells the water is first saline with normal temperature (around 25-30 °C, depending on air temperature) and after several minutes the water was getting hotter until reaching the hot spring water temperature. The amount of saline groundwater depends on the season (dry and wet) and therefore in some extent also on the rainfall. Further investigations are currently done.

Geochemistry results obtained show that temperature values in the shallow geothermal reservoir occur due to mixing of fresh meteoric water along pathways. A regional forced convective-circulation model is suggested based on differences interpreted to reflect deep structural controls on fluid pathways in the field, which has limited the degree of mixing between them.

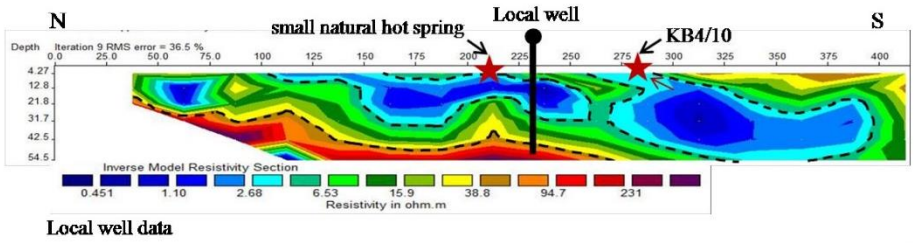

Local well data

Depth (m)	0-10	10-20	20-30	30-40	40-50
Description	black marine clay	soft sand with clay	very coarse clay with traces of sandstone	red light brown sandstone	sandstone

Figure 3:2D section of ERT Line RO1 with the location of hot springs, and well with lithological information from cutting (see also Figure 2).

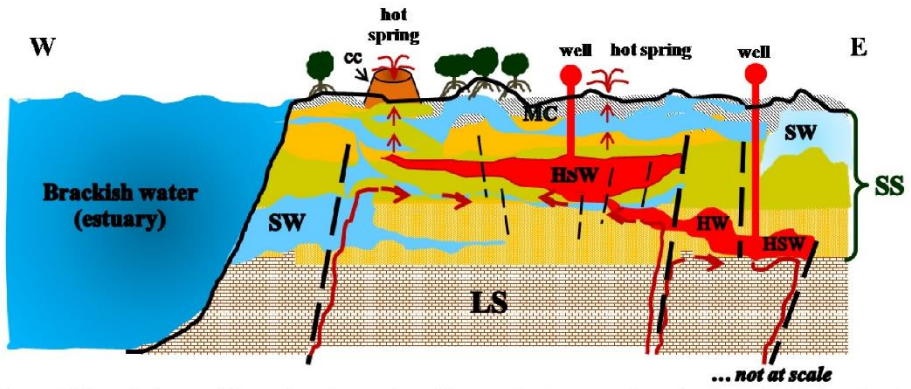

Figure 4: Schematic diagram of the geothermal system in Krabi; cc – carbonate crusts at hot spring sites, MC - black marine clay, HW-hot water, HSW-hot salty water, SW-salty water (not hot), SS - sandstone, and LS – limestone.

EDITED REFERENCES

Note: This reference list is a copyedited version of the reference list submitted by the author. Reference lists for the 2016 SEG Technical Program Expanded Abstracts have been copyedited so that references provided with the online metadata for each paper will achieve a high degree of linking to cited sources that appear on the Web.

REFERENCES

Baioumy, H., M. Nawawi, K. Wagner, and M. H. Arifin, 2015, Geochemistry and geothermometry of non-volcanic hot springs in West Malaysia: Journal of Volcanology and Geothermal Research, **290**, 12–22, http://dx.doi.org/10.1016/j.jvolgeores.2014.11.014.

Jonjana, S., W. Lohawijarn, and H. Dürrast, 2012, Geological structure and origin of the Kaochaison hot spring in Phattalung, Southern Thailand: Songklanakarin Journal of Science and Technology. **34**, 231–239.

Ngansom, W., and H. Dürrast, (2015). Subsurface structure of the saline hot spring in Krabi, Southern Thailand, from an integrated geoscientific investigation, 6th International Geosciences Student Conference, 13–16 July 2015, Prague, 27–29.

Nilsuwan, U., 2011. Gravity and magnetic investigations of the geothermal hot springs in Krabi, Southern Thailand. Master Thesis, Geophysics Program, Faculty of Science, Prince of Songkla University.

Appendix D

Surface temperatures, location, pH, concentrations of cations and anions of hot springs in Southern Thailand

Hot spring	Surface temp. (°C)	UTM		pH	Content (mg/L)									Sources
		East	North		TDS	HCO_3	Na	K	Ca	Mg	SiO_2	Cl	SO_4	
CP1	50	512222	1075014	7.5	580	354	63.5	6.77	89.5	29.8	64.2	112	8	PSU, 2016
RN1	65	462169	1100516	8.3	330	182	48.4	2.8	44.1	0.02	79.3	4.8	19.3	PSU, 2016
RN2	40	460000	1094700	8.3	330	189	46.4	3.2	44.1	0.03	75.5	11	44.9	DMR, 2012
RN3	45	461030	1093400	8.4	330	190	46.9	3	44.3	0.01	72	10	44.9	DMR, 2012
RN5	46	456192	1080300	8.3	240	151	46.1	2.03	17.8	0.05	87	5.9	7	DMR, 2012
RN6	75	470810	1060430	8.1	310	177	51.3	3.48	28.1	0.9	111	13.3	10	DMR, 2012
SR1	45	521107	1034893	7.7	13690	103	3850	132	933	156	65	7020	839	DMR, 2012
SR2	40	520518	1033905	7.8	7180	112	1855	64.2	400	74.8	39	3403	427	DMR, 2012
SR3	65	522412	1031459	7.9	12610	117	3655	115	840	148	58.5	6630	746	PSU, 2016
SR4	41	555129	1009502	8.3	270	181	20.5	2.4	27.8	22.4	37.4	21	26	DMR, 2012
SR5	42	545897	972938	8.4	320	210	55.9	6	20.9	2.47	80.2	14	7	DMR, 2012
SR6	53	503522	979890	8.1	740	132	44.8	5.2	97.1	28	53.6	14	306	DMR, 2012
SR7	70	529417	991895	7.9	1980	117	64.5	13.6	381	75.2	60.7	21	1180	PSU, 2016
SR9	62	524947	977116	8.2	1300	131	12.1	4.61	265	42.5	62	8.9	830	DMR, 2012
PG1	78	441455	960807	8.07	215	180.8	76.37	3.07	8.65	0.45	70.26	37.5	35	PSU, 2016
PG3	45	420496	918037	6.9	5100	62	1250	50.3	515	32.8	77	3097	22	PSU, 2016
KB1	42	499622	900439	7.06	338	329	15.45	2.12	70.46	16.19	20.52	60.01	4.9	PSU, 2016
KB2	43	500183	891731	6.58	11754	105	5188	112.8	632	170.2	18.53	7158	891	PSU, 2016
KB3	45	510462	888220	7.2	3300	229	986	22.1	382	74	25.5	1656	63.8	PSU, 2016
KB4	46	512329	873475	7.8	14910	322.69	4840	352	914.25	352	14.57	9211	650	PSU, 2016
KB5	47	523171	876867	7.26	427	156	6.52	1.23	116.3	30.48	25.66	45.05	205	PSU, 2016
TR1	52	551391	818787	7.1	548	162	69.2	2.36	95.60	26.35	22.62	215.23	60	PSU, 2016
PL1	57	625096	823266	7.7	265	250	39.1	3.67	45.5	10.8	25.5	8.1	4.3	PSU, 2016
PL3	50	604490	816432	8.0	240	125	69.7	3.2	5.13	0.04	73.6	6.3	4.9	PSU, 2016
YL1	80	729730	646758	7.8	330	200	76.6	6.38	16.7	0.45	97.6	5.8	3.1	PSU, 2016

VITAE

Name Miss Wipada Ngansom

Student ID 5610230015

Educational Attainment

Degree	Name of Institution	Year of Graduation
B. Sc (Physics)	Ramkhamhaeng University	2006
M. Sc (Physics)	Ramkhamhaeng University	2009

Scholarship Awards during Enrolment

1. PSU-Ph.D. Scholarship
2. The National Research Council of Thailand (FY2016)

List of Publication and Proceeding

Ngansom, W., Pirarai, K., Duerrast, H., 2017. Integrated geoscientific investigations of the Phang Nga geothermal system, southern Thailand. Society of Exploration Geophysicists, 1949–4645.

Ngansom, W., Durrast, H., 2016. Saline hot spring in Krabi, Thailand: A unique geothermal system. Society of Exploration Geophysicists, 1949–4645.

Ngansom, W., Pirarai, K., Duerrast, H., 2016. Geothermal Exploration in Phang Nga, Southern Thailand. The 15th World Renewable Energy Congress, Jakarta, Indonesia, 19–23 September.

Duerrast, H., Ngansom, W., Pirarai, K., 2016. Geothermal Exploration in Phang Nga, Southern Thailand. In: 11th Asian Geothermal Symposium, Chiang Mai, Thailand, 18–20 November.

Ngansom, W., Durrast, H., 2015. Subsurface structure of the saline hot spring in Krabi, Southern Thailand, from an integrated geoscientific investigation. The 6th International Geosciences Student Conference, Prague, 13 – 16 July.